FERNANDA MAGNO SILVA

ADVANCES IN PROXIMAL SENSING: APPLICATION OF PEDOMETRICS IN TROPICAL SOILS

LAVRAS – MG
2023

FERNANDA MAGNO SILVA

ADVANCES IN PROXIMAL SENSING: APPLICATION OF PEDOMETRICS IN TROPICAL SOILS

Tese apresentada à Universidade Federal de Lavras, como parte das exigências do Programa de Pós-Graduação em Ciência do Solo, área de concentração em Recursos Ambientais e Uso da Terra, para obtenção do título de Doutor.

Prof. Dr. Sérgio Henrique Godinho Silva
Orientador

LAVRAS – MG
2023

Ficha catalográfica elaborada pelo Sistema de Geração de Ficha Catalográfica da Biblioteca Universitária da UFLA, com dados informados pelo(a) próprio(a) autor(a).

Silva, Fernanda Magno.
Advancesin proximal sensing: application of pedometrics in tropical soils / Fernanda Magno Silva. - 2023.
120 p. : il.

Orientador(a): Sérgio Henrique Godinho Silva.

Tese (doutorado) - Universidade Federal de Lavras, 2023.
Bibliografia.

1. Solos tropicais. 2. Gênese do solo. 3. Sensores próximos. I. Godinho Silva, Sérgio Henrique. II. Título.

FERNANDA MAGNO SILVA

ADVANCES IN PROXIMAL SENSING: APPLICATION OF PEDOMETRICS IN TROPICAL SOILS

AVANÇOS NO SENSORIAMENTO PROXIMAL: APLICAÇÃO DA PEDOMETRIA EM SOLOS TROPICAIS

Tese apresentada à Universidade Federal de Lavras, como parte das exigências do Programa de Pós-Graduação em Ciência do Solo, área de concentração em Recursos Ambientais e Uso da Terra, para obtenção do título de Doutor.

Aprovada em 02 de Agosto de 2023.
Dr. Michele Duarte de Menezes, UFLA
Dr. Felipe Haenel Gomes, UFLA
Dr. Tiago Rodrigues Tavares, USP
Dra. Giovana Clarice Poggere, UTFPR

Prof. Dr. Sérgio Henrique Godinho Silva
Orientador

LAVRAS – MG
2023

À minha família e amigos pelo amor incondicional e encorajamento constante.

Dedico

AGRADECIMENTOS

Agradeço a Deus por sempre me mostrar o melhor caminho e que tudo acontece no tempo certo.

Aos meus pais, irmãos e familiares pelo incentivo e paciência, foram fundamentais para minha persistência e sucesso ao longo deste processo.

Aos meus amigos pelo cuidado e amparo nos momentos difíceis.

Ao professor e orientador Sérgio Henrique Godinho Silva e ao professor Nilton Curi pelos ensinamentos, dedicação, compreensão e principalmente pelo acolhimento.

Ao professor Alberto Vasconcelos Inda e a Universidade Federal do Rio Grande do Sul, cujo a contribuição foram fundamentais para a realização desta pesquisa.

Aos meus colegas e técnicos da universidade, agradeço por sua colaboração e apoio mútuo. Suas amizades tornaram essa jornada acadêmica mais simples e prazerosa.

À Universidade Federal de Lavras e ao Departamento de Ciência do Solo pela oportunidade.

O presente trabalho foi realizado com apoio da Coordenação de Aperfeiçoamento de Pessoal de Nível Superior (CAPES).

Ao Conselho Nacional de Desenvolvimento Científico e Tecnológico (CNPq) e a Fundação de Amparo à Pesquisa do Estado de Minas Gerais (FAPEMIG), por outros auxílios financeiros.

A todos aqueles que, de alguma forma, contribuíram para esta tese, meu mais sincero obrigado. Este trabalho não teria sido possível sem o envolvimento e apoio de cada um de vocês.

“O presente é a chave para o passado.”

(James Hutton)

ABSTRACT

Understanding pedogenesis, soil variability, its physical, chemical and mineralogical characterization and its respective parent materials is not always a simple and straightforward task, especially in tropical regions. Technological advances, methodologies and tools, such as portable X-ray fluorescence (pXRF) and diffuse reflectance spectroscopy in the visible and near infrared region (Vis-NIR) associated with X-ray diffraction (XRD) and magnetic susceptibility (MS) were employed to characterize soils, investigating their genesis and reducing costs. This study aims to use proximal sensors pXRF, Vis-NIR and MS associated with and XRD to: 1) characterize soils developed from different parent materials; 2) identify and quantify the mineralogy of sand, silt and clay fractions of different soils derived from different parent materials; and 3) assess the spatial variation of properties within soil profiles. Twenty-seven soil profiles were described in the region of Lavras and Ijaci (MG), with the collection of samples in 85 horizons for analysis. Samples from A, B and C horizons and the sand, silt and clay fractions of the respective horizons were analyzed by pXRF, Vis-NIR and MS. The analysis for mineralogy identification via XRD was performed on the sand, silt and clay fractions. The pXRF and MS revealed the diversity and alterations in the elemental composition of the soil profiles, showing how each parent material imprinted its characteristics on each of them. While Vis-NIR confirmed the mineralogy found through XRD and accurately predicted the contents of minerals present in the clay fraction. Proximal sensors allowed the detection of soil properties variation within and in between soil horizons. The relationship between the data obtained by the sensors allowed a more comprehensive, accurate and rapid assessment of soils and their properties, providing a complete analysis of the pedogenetic processes and the influence of the parent material on the characteristics of the soils studied.

Keywords: Soil genesis. Spatial variation. Prediction models. PXRF. Vis-NIR. X-ray diffraction. Magnetic susceptibility.

RESUMO

Compreender a pedogênese e a variabilidade do solo, assim como a sua caracterização física, química e mineralógica e seu respectivo material de origem nem sempre é uma tarefa simples e direta, especialmente nas regiões tropicais. Avanços tecnológicos, metodologias e ferramentas como a fluorescência de raios-X portátil (pXRF), a espectroscopia de refletância difusa no espectro visível e infravermelho próximo (Vis-NIR DRS), associadas à difração de raios-X (DRX) e à suscetibilidade magnética (SM), estão sendo empregados para caracterizar o solo, investigar sua gênese e reduzir custos. Este estudo tem como objetivo utilizar os sensores próximos pXRF, Vis-NIR e SM associados à DRX para: 1) caracterizar solos desenvolvidos a partir de diferentes materiais de origem; 2) identificar e quantificar a mineralogia das frações areia, silte e argila de diferentes solos derivados de diferentes materiais de origem; e 3) avaliar a variação espacial das propriedades dentro dos perfis de solo. Vinte e sete perfis de solos foram descritos na região de Lavras e Ijaci (MG), com a coleta de amostras em 85 horizontes para análise. As amostras dos horizontes A, B e C e as frações areia, silte e argila dos respectivos horizontes foram analisadas por pXRF, Vis-NIR e SM. A análise para identificação da mineralogia via DRX foi realizada nas frações areia, silte e argila. O pXRF e a SM revelaram a diversidade e alterações na composição elementar dos perfis de solo, mostrando como cada material de origem imprimiu suas características em cada um deles. Enquanto o Vis-NIR confirmou a mineralogia encontrada por meio da DRX e previu com precisão o conteúdo dos minerais presentes na fração de argila. Os sensores próximos permitiram a detecção da variação das propriedades do solo dentro e entre os horizontes do solo. A relação entre os dados obtidos pelos sensores permitiu uma avaliação mais abrangente, precisa e rápida dos solos e de suas propriedades, fornecendo uma análise completa dos processos pedogenéticos e da influência do material de origem nas características dos solos estudados.

Palavras-chave: Gênese do solo. Variação espacial. Modelos de predição. PXRF. Vis-NIR. Difração de raios - X. Susceptibilidade magnética.

SUMÁRIO

PRIMEIRA PARTE

1. INTRODUÇÃO GERAL

O solo é resultado da interação de processos intempéricos no material de origem por longos períodos de tempo (HEUNG et al., 2014), e é justamente esse material que desempenha um papel fundamental em diversos atributos do solo. Entende - se por material de origem a rocha inalterada situada abaixo do solo, sedimentos minerais ou orgânicos, ou ainda materiais alterados provenientes de outras litologias (materiais alóctones) (KER et al., 2012). Diversas pesquisas têm evidenciado que, em condições equiparáveis, diferenças nos materiais de origem acarretam distintas propriedades físicas, químicas e mineralógicas dos solos delas derivados, mesmo naqueles muito intemperizados (ARAÚJO et al., 2014; CURI; FRANZMEIER, 1987; COSTA et al., 2019; MARANHÃO et al., 2020) levando a contrastes na pedogênese (GOZUCA et al., 2021; MANCINE et al., 2023; STOCKMANN et al., 2016) e consequentemente na variabilidade espacial dos solos e seus atributos (GRAUER-GRAY et al., 2018).

As análises convencionais utilizadas na caracterização química, física e mineralógica do solo são demoradas, apresentam alto custo e geram uma grande quantidade de resíduo químico, exigindo cuidados especiais para o descarte adequado. Uma alternativa para essa questão é o uso dos sensores próximos, como o espectrômetro portátil de fluorescência de raios–X (pXRF) e o espectrômetro de refletância difusa do visível e infravermelho próximo (Vis – NIR).

Esses sensores têm sido empregados por pesquisadores devido à sua rapidez, baixo custo, caráter não destrutivo e eficiência operacional. Além disso, essas técnicas não produzem efluentes químicos e podem ser aplicadas tanto em campo quanto em laboratório. Adicionalmente, esses sensores podem ser utilizados de maneira independente ou em conjunto com outras técnicas, como a difração de raios-X e a susceptibilidade magnética.

Na pXRF uma amostra é irradiada por uma fonte de raios-X do equipamento, com isso os elétrons das camadas internas são deslocados para as camadas mais externas. Em sequência, elétrons externos se movem para ocupar o espaço deixado pelos elétrons deslocados, liberando energia na forma de fluorescência. Esta energia é característica de cada elemento, permitindo sua identificação e a intensidade da fluorescência é quantificada pelo equipamento (WEINDORF et al., 2014). Os raios-X emitidos penetram aproximadamente 2 mm na matriz do solo (SHAND et al., 2014), conseguindo detectar

elementos químicos do Mg ao U na tabela periódica. Alguns destes elementos quantificados nos solos podem ser marcadores de outros atributos dos solos. Zhu et al. (2011) observaram estreita relação entre o teor de argila e o de Fe, devido aos óxidos e/ou oxi-hidróxidos de Fe pedogênicos encontrados nessa fração. A literatura também relata a utilização do pXRF, na predição de atributos relacionados à fertilidade do solo (ANDRADE et al., 2020, TEIXEIRA et al., 2022), bem como no estudo da pedogênese (BENEDET et al., 2022; STOCKMAN et al., 2016). Por identificar e quantificar diversos elementos químicos no perfil de solo, o pXRF aumenta a densidade de informações, permitido a avaliação da sua distribuição espacial (MANCINI et al., 2023; SUN et al., 2020).

A espectroscopia de refletância no solo consiste em uma fonte de energia (sol/lâmpada) que incide sobre este, podendo esta energia ser absorvida ou refletida. A energia refletida pode ser captada por sensores que a separa em diferentes comprimentos de onda, medem sua intensidade relativa e geram curvas espectrais (DALMOLIN et al., 2005). A faixa espectral usada para o estudo do solo corresponde ao visível (Vis) 400 - 700 nm, infra vermelho próximo (NIR) 700 - 1100 nm e infravermelho de ondas curtas (SWIR) 1100-2500 nm (DEMATTÊ et al., 2019). No solo a reflectância depende da associação entre seus constituintes: matéria orgânica, umidade, textura, estrutura, mineralogia e material de origem (STONER; BAUMGARDNER, 1986).

A matéria orgânica ou carbono do solo altera a forma da curva espectral em toda sua extensão, pois ocasiona uma alta absorção resultando em uma baixa refletância (DEMATTÊ et al., 2003). Os óxidos de ferro absorvem de forma diferente a energia que incide no solo, onde a hematita e a goethita afetam as regiões de 480 e 850 nm, enquanto óxidos de ferro menos cristalinos interferem na intensidade de toda a curva espectral (400 a 2500 nm) (DEMATTÊ; GARCIA, 1999). Entre os argilominerais, a caulinita, que possui grupos hidroxila (OH) em sua estrutura, apresenta característica de absorção em 2200 nm (DALMOLIN et al., 2005). Por outro lado, a característica de absorção em 2265 nm está associada ao óxido de alumínio gibbsita (DEMATTÊ et al., 2017; VISCARRA ROSSEL, 2011). Conforme Stoner e Baumgardner, (1981), a umidade do solo ocasiona uma diminuição na reflectância, sendo que os comprimentos de onda de 1400 e 1900 nm estão associadas as bandas características de absorção da água (DALMOLIN et al., 2005). Os solos com maior teor de areia exibem uma maior reflectância devido à sua mineralogia rica em quartzo (DEMATTÊ et al., 2012; DEMATTÊ et al., 2017). Por outro lado, à medida que

o teor de argila, matéria orgânica e óxidos de ferro aumenta, ocorre uma diminuição na reflectância do solo (PEREIRA et al., 2019).

Os óxidos de ferro podem ter origem pedogênica, resultando do processo de formação do solo, ou origem litogênica, correspondendo a minerais não intemperizados provenientes do material de origem (VAN DAM et al., 2005). Em solos de regiões tropicais ocorre uma concentração residual de óxidos de ferro devido ao alto grau de intemperismo e lixiviação (CURI et al., 2017; FERREIRA et al., 1994). Entre os óxidos de ferro, a magnetita (Mt) e a maghemita (Mh) apresentam caráter magnético, enquanto outros óxidos de ferro não proporcionam essa característica ou a apresentam em menor intensidade, como a hematita (Hm) e goethita (Gt), que são relevantes na discriminação do material de origem (CURI; FRANZMEIER, 1987; DEARING, 1999). A magnetita, presente na rocha e em frações grosseiras do solo, e a maghemita, presente na fração argila, controlam a suscetibilidade magnética (SM), sendo essa proporcional à concentração desses minerais ferrimagnéticos por unidade de massa (DEARING, 1999).

A identificação dos minerais presentes nas frações granulométricas do solo, seu tamanho, grau de cristalinidade e substituintes isomórficos na estrutura cristalina podem ser acessados através da difratometria de raios-X (DRX) (MOORE; REYNOLDS, 1997; RESENDE et al., 2011). A DRX baseia-se na reflexão da radiação que incide no cristal para cada um dos planos de átomos paralelos (FABRIS et al., 2016). Quando a onda do raios-X incidentes e difratados está em fase nos planos atômicos e a distância e o comprimento de onda seguem a lei de Bragg, ocorre a interferência construtiva, consequentemente aumento da intensidade do sinal e identificação do mineral na forma de picos no difratograma (FABRIS et al., 2016). O tamanho e intensidade dos picos dependem da natureza cristalográfica do mineral: quanto mais largo o pico, menor o tamanho do cristal (baixo grau de cristalinidade) (RESENDE et al., 2011). Tais informações auxiliam na avaliação da influência da rocha de origem em solos com diferentes graus de intemperismo-lixiviação.

A integração dos dados provenientes dos diferentes sensores é uma abordagem promissora. A combinação do Vis-NIR com o pXRF foi aplicada na predição de atributos do solo, como a textura (BENEDET et al., 2020). Além disso, a combinação do Vis-NIR com o susceptibilímetro magnético foi utilizada para o mapeamento de solos em extensas áreas (BAHIA et al., 2017). Também foram relatadas aplicações da combinação do pXRF com o Vis-NIR e DRX na caracterização de Latossolos (BENEDET et al., 2022; MANCINI

et al., 2021; SILVA et al., 2022). Entretanto, poucos trabalhos integraram pXRF, Vis-NIR, susceptibilidade magnética e DRX.

Diante do exposto, o objetivo desta pesquisa é utilizar os sensores próximos pXRF, Vis-NIR aliados à DRX e susceptibilímetro magnético, na caracterização e diferenciação de classes de solos em função de materiais de origem distintos em mesmas condições tropicais.

i) Capítulo um – combinar os dados dos sensores pXRF, Vis-NIR, DRX e SM para a caracterização de Cambissolos e Latossolos derivados de gabro e gnaisse visando uma compreensão mais aprofundada de sua gênese.

ii) Capítulo dois - usar os sensores pXRF e Vis-NIR em associação com a DRX e SM para identificar e quantificar os elementos químicos e a mineralogia nas frações de areia, silte e argila de diferentes perfis de solo derivados de diferentes materiais de origem. Desenvolver modelos de predição para quantificar os minerais presentes nesses solos.

iii) Capítulo três - utilizar o pXRF, Vis-NIR e a DRX para diferenciar Cambissolos e Latossolos de diferentes materiais de origem e indicar descontinuidades nos materiais de origem através da relação Ti/Zr, Si/Al, AF/AG e da mineralogia das frações areia silte e argila.

Nossa hipótese é que os resultados provenientes do pXRF e Vis-NIR associados à susceptibilidade magnética e à DRX evidenciem as diferenças entre os solos de acordo com seus materiais de origem; e que a quantificação da mineralogia da fração argila do solo com base nos dados dos sensores apresentem resultados confiáveis quando comparados à quantificação mineralógica por DRX.

REFERÊNCIAS

ANDRADE, R. et al. Prediction of soil fertility via portable X-ray fluorescence (pXRF) spectrometry and soil texture in the Brazilian Coastal Plains. **Geoderma**, v. 357, 113960, 2020.

ARAÚJO, M.A. et al. Paragênese mineral de solos desenvolvidos de diferentes litologias na região sul de Minas Gerais. **Revista Brasileira de Ciência do Solo**, v. 38, p. 11–25, 2014.

BAHIA, A.S.R. et al. Prediction and Mapping of Soil Attributes using Diffuse Reflectance Spectroscopy and Magnetic Susceptibility. **Soil Science Society of America Journal**, v. 81, n. 6, p. 1450–1462, 2017.

BENEDET, L. et al. Variation of properties of two contrasting Oxisols enhanced by pXRF and Vis-NIR. **Journal of South American Earth Sciences**, v. 115, 103748, 2022.

BENEDET, L. et al. Soil texture prediction using portable X-ray fluorescence spectrometry and visible near-infrared diffuse reflectance spectroscopy**. Geoderma**, v. 376, 114553, 2020.

CURI, N.; FRANZMEIER, D. P. Effect of parent rocks on chemical and mineralogical properties of some Oxisols in Brazil. **Soil Science Society of America Journal**, v. 51, p. 153–158, 1987.

CURI, N. et al. **Mapeamento de Solos e Magnetismo no Campus da UFLA Como Traçadores Ambientais**. Lavras: Editora UFLA, 2017. 147 p.

COSTA, E.U.C. et al. Genesis and classification of nitisols from volcano-sedimentary lithology in Northeastern Brazil. **Revista Brasileira Ciência do Solo**, v. 43, 1–17, 2019. https://doi.org/10.1590/18069657rbcs20180101

DALMOLIN, R.S.D. et al. Relação entre os constituintes do solo e seu comportamento espectral. **Ciência Rural**, v. 35, n. 2, p. 481–489, 2005.

DEARING, J.A. **Environmental magnetic susceptibility**. England: Bartington Instruments, Witney, Oxon, 1999. 43 p.

DEMATTÊ, J.A.M.; EPIPHANIO, J.C.N.; FORMAGGIO, A.R. Influência da matéria orgânica e de formas de ferro na reflectância de solos tropicais. **Bragantia**, v. 62, p. 451–464, 2003.

DEMATTÊ, J.A.M.; GARCIA, G.J. Alteration of Soil Properties through a Weathering Sequence as Evaluated by Spectral Reflectance. **Soil Science Society of America Journal**, v. 63, p. 327–342, 1999.

DEMATTÊ, J.A.M. et al. The Brazilian Soil Spectral Library (BSSL): A general view, application and challenges. **Geoderma**, v. 354, 113793, 2019.

DEMATTÊ, J.A.M. et al. Genesis and properties of wetland soils by VIS-NIR-SWIR as a technique for environmental monitoring. **Journal of Environmental Management**, v. 197, p. 50–62, 2017.

DEMATTÊ, J.A.M. et al. Spectral behavior of some modal soil profiles from São Paulo State, Brazil. **Bragantia**, v. 71, p. 413–423, 2012.

FABRIS, J.D. et al. Métodos físicos de análises em mineralogia do solo. In: MELO, V. de F.; ALLEONI, L. R. F. **Química e Mineralogia do Solo**. Viçosa: Sociedade Brasileira de Ciência do Solo, 2016. p. 573–611.

FERREIRA, S.A.D. et al. Relações entre magnetização, elementos traços e litologia de duas sequências de solos do estado de Minas Gerais. **Revista Brasileira de Ciência do Solo**, v. 18, p. 167–174, 1994.

GOZUKARA, G. et al. Using vis-NIR and pXRF data to distinguish soil parent materials – An example using 136 pedons from Wisconsin, USA. **Geoderma**, v. 396, 2021.

GRAUER-GRAY, J.; HARTEMINK, A.E. Raster sampling of soil profiles. **Geoderma**, v. 318, p. 99–108, 2018.

HEUNG, B.; BULMER, C.E.; SCHMIDT, M.G. Predictive soil parent material mapping at a regional-scale: A Random Forest approach. **Geoderma**, v. 214–215, p. 141–154, 2014.

KER, J. C.; CURI, N.; SCHAEFER, C.E.G.R.; VIDAL-TORRADO, P. **Pedologia: fundamentos**. Viçosa: SBCS, 2012. 343p.

MANCINI, M. et al. Formation and variation of a 4.5 m deep Oxisols in southeastern Brazil. **Catena**, v. 206, 105492, 2021.

MANCINI, M. et al. Digital morphometrics and genesis of soils with buried horizons and lithological discontinuities in southeastern Brazil. **Geoderma**, v. 32, e00612, 2023.

MARANHÃO, D.D.C.et al. Pedogenesis in a karst environment in the Cerrado biome, northern Brazil. **Geoderma**, v. 365, 2020.

MOORE, D.M.; REYNOLDS R.C.JR. X-rayDiffraction and the Identification and Analysis of Clay Minerals. 2nd ed. Oxford University Press, 1997. 378p.

PEREIRA, G.E. et al. VIS-NIR spectral reflectance for discretization of soils with high sand content. **Semina: Ciências Agrarias**, v. 40, n. 1, p. 99–112, 2019.

RESENDE, M. et al. **Mineralogia dos solos brasileiros: interpretação e aplicações**. 2nd ed. Re ed. Lavras: Editora UFLA, 2011. 192 p.

SHAND, C.A.; WENDLER, R. Portable X-ray fluorescence analysis of mineral and organic soils and the influence of organic matter. **Journal of Geochemical Exploration,** v. 143, p. 31–42, 2014.

SILVA, F.M. et al., Using proximal sensors to assess pedogenetic development of Inceptisols and Oxisols in Brazil. **Geoderma Regional**, v. 28, p. 1–10. 2022,

STOCKMANN, U. et al. Utilizing portable X-ray fluorescence spectrometry for in-field investigation of pedogenesis. **Catena**, v. 139, p. 220–231, 2016.

STONER, E.R.; BAUMGARDNER, M.F. Characteristic Variations in Reflectance of Surface Soils. **Science Society of America Journal**, v. 45, p. 1161-1165, 1986.

SUN, F. et al. Enhanced soil profile visualization using portable X-ray fluorescence (PXRF) spectrometry. **Geoderma**, v. 358, 113997, 2020.

TEIXEIRA, A.F. et al. 2022. Proximal sensor data fusion for tropical soil property prediction: Soil fertility properties. **Science Society of America Journal**, v. 116, 103873, 2022. https://doi.org/10.1016/j.jsames.2022.103873

VAN DAM, R. L. et al. Conceptual model for prediction of magnetic properties in tropical soils. **Proceedings of spie**, v. 5794, p. 177-187. 2005.

VISCARRA ROSSEL, R.A.; CHEN, C. Digitally mapping the information content of visible-near infrared spectra of surficial Australian soils. **Remote Sensing of Environment**, v. 115, p. 1443–1455, 2011.

WEINDORF, D.C.; BAKR, N.; ZHU, Y. Advances in Portable X-ray Fluorescence (PXRF) for Environmental, Pedological, and Agronomic Applications. **Advances in Agronomy**, v.128, p. 1–45, 2014.

ZHU, Y.; WEINDORF, D. C.; ZHANG, W. Characterizing soils using a portable X-ray fluorescence spectrometer: 1. Soil texture. **Geoderma**, v. 167–168, p. 167–177, 2011.

SEGUNDA PARTE – ARTIGOS

Artigo publicado na Geoderma Regional, v. 28, e00465, 2022
(https://doi.org/10.1016/j.geodrs.2021.e00465)

ARTIGO 1 - Using proximal sensors to assess pedogenetic development of Inceptisols and Oxisols in Brazil.

Fernanda Magno Silva [a], Sérgio Henrique Godinho Silva [a], Anita Fernanda dos Santos Teixeira [a], Alberto Vasconcellos Inda [b], Tatiele Fruett [b], David C. Weindorf [c], Luiz Roberto Guimarães Guilherme [a], Nilton Curi [a]

[a] Federal University of Lavras, Department of Soil Science, Lavras, Minas Gerais, Brazil
[b] Department t of Agronomy, Federal University of Rio Grande do Sul, Porto Alegre, Rio Grande do Sul, Brazil
[c] Department of Earth and Atmospheric Sciences, Central Michigan University, Mount Pleasant, USA

Abstract

Proximal sensors like portable the X-ray fluorescence (pXRF) spectrometer, visible and near-infrared spectrometer (Vis-NIR) and magnetic susceptibilimeter have been increasingly used for the acquisition of complementary data to investigate chemical, physical and mineralogical properties of soils. Through the association between these sensors, this study aims to differentiate classes of soils with similar pedogenetic development, but developed from different parent materials. Four soil profiles were described and sampled in Lavras, Minas Gerais, Brazil: Oxic Dystrustept and Anionic Acrudox, developed from gabbro and Typic Dystrustept and Rhodic Hapludox, developed from gneiss. Samples from the A, B and C horizons were subjected to analyses by pXRF, Vis- NIR, and magnetic susceptibility, in addition to their physicochemical characterization and determination of their mineralogy via X-ray diffraction (XRD). The contents of Si, Fe and Ti obtained by pXRF as well as the MS values were decisive in distinguishing soil classes according to the parent material. The spectral curves generated by Vis- NIR showed different spectral responses for the same soil class due to their differential mineralogical constitution. Soils developed from gabbro had higher contents of iron oxides and a low reflectance in relation to the soils developed from gneiss. The proximal sensors contributed to the differentiation of soil properties both within soils developed from the same parent material, mainly expressing their different weathering

degrees, and within soils of the same taxonomic order, but developed from distinct parent materials. These proximal sensors can improve the characterization of soils and evaluations about their genesis at reduced time and costs.

Keywords: pXRF, Vis-NIR, Ferralsols, Oxisols, Cambisols, Inceptisols, Tropical soils

1. Introduction

Soil properties are derived from the factors and processes acting during soil formation (Jenny, 1941; Schaetzl and Anderson, 2005). The formation of deep, old and low natural fertility soils like Oxisols occurs due to intense desilification of easily weathered primary minerals (EWPM) such as olivine, augite (pyroxene), hornblende (amphibole), anorthite (plagioclase-Ca), biotite and feldspars, causing the residual concentration of iron and aluminum oxides (ferralization). Generally, Oxisols are formed in more stable and smooth portions of the landscape, under both free draining and humid tropical climate (Kämpf and Curi, 2012).

Although Oxisols are the most common soils in Brazil and more adequate for **intensive** uses, Inceptisols are fragile soils found in all the regions of Brazil and also widely used for agriculture and livestock. Recent studies have indicated that even Inceptisols with low natural fertility and located in areas with steep relief may promote high productivity of crops when correctly managed (Oliveira et al., 2017), which demands more specific studies to avoid their degradation. Inceptisols do not have a dominant pedogenic process (Buol et al., 2011). Most of these young soils present little effective depth and are extremely and highly variable in almost all of their properties (Resende et al., 2014). They often have morphological and even chemical properties similar to Oxisols (Skorupa et al., 2017), differing from those highly-weathered soils by presenting high contents of silt in relation to clay and/or a higher proportion of EWPM (Resende et al., 2014).

These two soil classes can be derived from variable lithologies, which result in different physical, chemical and mineralogical properties of the soils derived from them, even in very old ones (Curi and Franzmeier, 1987; Araujo et al., 2014), under comparable environmental conditions. This fact generates contrasts in pedogenesis (Silva et al., 2018; Stockmann et al., 2016) and consequently in the spatial variability of these soils and their properties (Grauer-Gray and Hartemink, 2018). Moreover, in Brazil, Oxisols and Inceptisols are often associated in the landscape, occupying a large territorial extension (Pereira et al.,

2010; Resende et al., 2014), where various forming factors and processes act differently, justifying more detailed studies, including modern and fast techniques, without generating chemical effluents.

For a quick and accurate characterization of the soil, proximal sensors such as the portable X-ray fluorescence spectrometer (pXRF), visible and near-infrared spectrometer (Vis-NIR) and magnetic susceptibilimeter have been successfully used by several researchers worldwide (Araujo et al., 2014; Bahia et al., 2017; Silva et al., 2016; Tatyanchenko et al., 2013). In addition to the speed and low cost of these analyses, they are non-destructive, do not generate chemical effluents, allow operational gains and have an environmental appeal (Weindorf et al., 2014; Silva et al., 2021).

PXRF data can be obtained in the laboratory and used to accurately predict soil properties and classes (Silva et al., 2018; Silva et al., 2019; Silva et al., 2020a; Andrade et al., 2020b). Under a soil genesis scope, Stockmann et al. (2016) determined the parent material of three soil profiles based on their elemental similarities via pXRF analyses in Australia. In Brazil, Silva et al. (2018) used pXRF for investigations of chemical differences caused by weathering of minerals present in the sand, silt and clay fractions and also determined within horizon variations of soil properties.

Visible and near-infrared spectroscopy (Vis-NIR) has also been used in studies related to clay minerals and iron oxide minerals in the soil (Shi et al., 2015; Demattê et al., 2003), as well as in the prediction of Cr (Xu et al., 2019) and other metals (Piccolo and Stevenson, 1982). Vis-NIR data have been correlated to the presence of minerals in soils (Demattê et al., 2017). Moreover, the set of data obtained by pXRF and Vis-NIR has been used in studies for the prediction of soil classes (Benedet et al., 2020), in the evaluation of pH for risks of environmental contamination with heavy metals (Wan et al., 2019), and the prediction of physical and chemical soil properties (Zhang and Hartemink, 2019; Demattê et al., 2019; O'Rourke et al., 2016).

Magnetic susceptibility, which is the measurement of the magnetism of materials, has been widely used for complementing soil characterization and for predictions of related properties, e.g., soil mineralogy, texture, organic carbon content, heavy metals content, etc. (Maher, 1986; Wang, 2013; Cervi et al., 2014; Bahia et al., 2017; Söderström et al., 2016). In soils, magnetism is mostly related to the presence of Fe-bearing magnetic minerals, e.g., maghemite, magnetite, hematite, etc., which are also related to soil parent material (Poggere et al., 2018). Magnetic susceptibility has been used along with other proximal sensor data,

such as pXRF and Vis-NIR to infer soil properties and to help studies on soil genesis (Magiera et al., 2019; Barbosa et al., 2021; Curi and Franzmeier, 1987; Andrade et al., 2020a; Silva et al., 2018).

Thus, the objective of this research was to use pXRF, Vis-NIR and magnetic susceptibility to differentiate soils classes with a similar degree of pedogenetic development primarily due to rocks of different origin (gabbro and gneiss), under the same tropical conditions. Specifically, Inceptisols and Oxisols derived from either gabbro or gneiss will be systematically characterized via a combination of proximal sensors and X-ray diffraction (XRD) to provide better comprehension of their genesis under the same environmental conditions.

2. Material and methods

2.1. Characterization of the study area

The study was conducted in the municipality of Lavras, Minas Gerais state, Brazil (Fig. 1a). The region's climate is Cwa, according to the Köppen classification, characterized by dry winters and rainy summers, an average annual temperature of 20.4 ◦C and average annual precipitation of 1460 mm (Dantas et al., 2007; Alvares et al., 2013). The average altitude is 918 m above sea level (Curi et al., 2020). Geologically, the study region is in Southeastern Brazil, located on the south edge of the São Francisco Craton (Queméneur et al., 2002). Bueno et al. (1990) mapping the lithological units within this region identified granites, gneisses, colluvial materials, gabbro, granulite, migmatites, mica-schists and quartzites (Fig. 1b). Oxisols and Inceptisols represent 56% of the soils in this region and the native vegetation is sub-perennial rainforest (Silva et al., 2018; Curi et al., 2020).

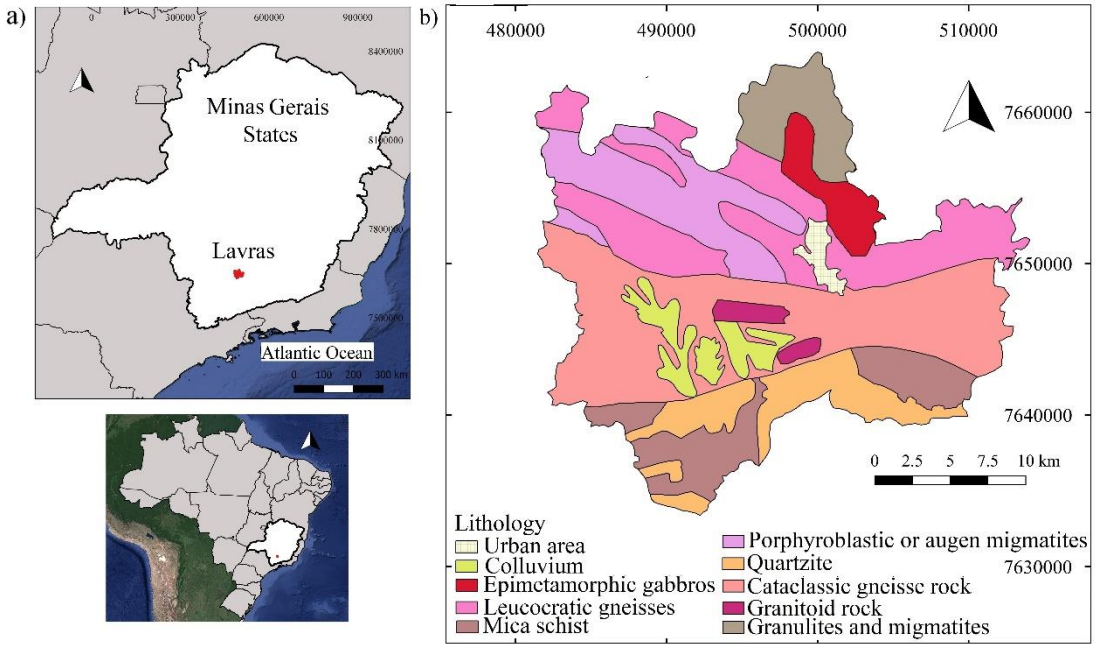

Fig. 1. a) Location of the municipality of Lavras in Minas Gerais, Brazil; and b) lithological map of the municipality of Lavras (MG) (adapted from Bueno et al., 1990).

2.2 Soils and laboratory analysis

Four soil profiles representative of the region were selected: Oxic Dystrustept and Anionic Acrudox, developed from gabbro and Typic Dystrustept and Rhodic Hapludox, developed from gneiss (Fig. 2). In each soil profile a morphological description was performed and composite samples of the main horizons were collected. The samples were air-dried, passed through a 2 mm sieve (air-dried fine earth - ADFE) and subjected to the following laboratory analyses: texture by the pipette method (Gee and Bauder, 1986); exchangeable $Ca2^{+}$, Mg^{2+} and Al^{3+} extracted with KCl 1 mol L^{-1} (McLean et al., 1958), Ca^{2+} and Mg^{2+} determined by an atomic absorption spectrometer, Al^{3+} by titration with NaOH 0.025 mol L^{-1}, available K and P were extracted with Mehlich-1 solution (Mehlich, 1953), with K determined by flame photometer and P by the blue molybdate colorimetry; soil organic matter (SOM) content was determined per Walkley and Black, 1934 and remaining P (P-rem.) as proposed by Alvarez and Fonseca (1990).

Fig. 2. Soil profiles evaluated in this study from Lavras, Minas Gerais, Brazil.

Magnetic susceptibility (MS) per unit of mass (χlf,10-8 m3 kg-1) was determined at low frequency (χlf = 0.47 kHz) in triplicate in ADFE and in the sand, silt and clay fractions separately using a Bartington MS2B susceptibilimeter according to the methodology described by Dearing (1999) and Poggere et al. (2018). Calculations were made via the expression χlf = (10× k) m-1, where k is dimensionless, and m is the mass of the used sample.

2.3. Elementary analysis by pXRF

Analyses of the content of the chemical elements were performed on air-dried fine earth (composite samples) using a Bruker pXRF, model S1 Titan LE. This equipment contains a Rh tube of X-rays of 50 keV and 100 μA, and a silicon drift detector with resolution of <145 eV. To assure the quality of pXRF analyses, some samples certified by the manufacturer of the pXRF (check sample) and samples certified by the National Institute of Standards and Technology (NIST) (2710a and 2711) were scanned and the results were compared with the certified contents. The recovery values (content obtained by

pXRF/certified content) for the check sample, 2710a and 2711, respectively, were Al: 0.91/1.34/0.49; Si: 0.91/1.53/0.85; Fe: 0.91/0.44/1.09; K: 0.88/0.66/0.68; Ca: –/1.62/ 0.44; Ti: –/0.74/0.95; Zr: –/1.31/–. The "–" symbol corresponds to either the absence of a certified value in the reference sample or absence of results by the equipment for that element. Each soil sample (ADFE previously mentioned) was analyzed for 60 s in triplicate using Geochem software in Trace mode (dual soil) (Weindorf and Chakraborty, 2016).

2.4. Spectral analysis by Vis-NIR

Soil samples were collected in each horizon of the studied soil profiles. The soil samples were air-dried, passed through a 2 mm sieve (ADFE) and homogeneously distributed into Petri dishes for analyses via Vis-NIR. Then, a portable Vis-NIR DRS PSR-3500 spectrometer (Spectral Evolution, Haverhill, MA, USA) with a spectral range of 350 to 2500 nm and a sampling interval of 2 nm was used to scan the ADFE samples. The digitalization of the data was performed using a contact probe with an integrated 5 W halogen light source coupled with a metal-clad PSR-3500 fiber optic cable. The analyses were performed in the laboratory at room temperature, where the probe for digitization was placed vertically on the samples. The samples were scanned three times, with each sample rotated 90º between scans. The spectral curve was obtained by the average of the three scans, where each individual scan presents an average of 10 internal scans for 1.5 s. A 12.7 by 12.7 cm NIST traceable radiation calibration panel was used after digitizing each five samples.

2.5. Mineralogical analysis by X-ray diffraction

The mineralogical composition of sand, silt and clay fractions was determined by X-ray diffraction (XRD) on a Bruker D2 Phaser diffractometer equipped with a fast linear detector Lynxeye™ and software Diffrac.Suite™. CuKα radiation (λ = 0.15418 nm), Ni filter, current intensity of 10 mA and power of 30 kVA were used. Samples were analyzed as pressed powder and irradiated over the 2–50◦ 2θ at a speed of 2º 2θ $minute^{-1}$. The positions of the peaks in the XRD were acquired through the Diffrac.SuiteTM Eva software Eva software and interpreted with the aid of tables by Brindley and Brown (1980).

2.6. Statistical analyses

The elemental data obtained by pXRF, spectral data (Vis-NIR), physical and chemical properties from wet-chemistry analyses and magnetic susceptibility of the soils were used for calculations of Pearson's correlation and for Principal Component Analysis

(PCA). Both statistical procedures were performed in the R environment (R Core Team, 2020) using RStudio (RStudio Team, 2016). From Pearson's correlation, correlograms were created for the soil classes and for the parent materials through the corrplot package (Wei et al., 2017), while the PCA was performed to differentiate the soil classes, properties and the parent materials through the vegan package (Oksanen et al., 2019).

3. Results and discussion

3.1. Soil physical and chemical properties

The values of the physical and chemical properties of the studied soils are presented in Table 1. The Oxic Dystrustept exhibits clay content 10% greater than the Typic Dystrustept in the superficial horizons, indicating greater clay formation due to the greater presence of EWPM in gabbro than in gneiss. The greater sand contents in all three horizons of the Typic Dystrustept, derived from gneiss, support the previous statement. Moreover, the higher content of silt in the Typic Dystrustept C horizon compared to the Oxic Dystrustept reflects a higher concentration of silt-sized kaolinite pseudomorphs in that (Resende et al., 2019; Pinto, 1971) in association with the remaining gneiss structures identified in that horizon during field work. The high clay content in the C horizon of the Oxic Dystrustept also indicates faster weathering of minerals of this soil due to its lower resistance to weathering in comparison with the minerals of the Typic Dystrustept. Among the Oxisols, Rhodic Hapludox present higher sand contents in relation to Anionic Acrudox, a consequence of the higher quartz content in gneiss, a mineral resistant to weathering in this size fraction (and Curi, 2012).

The lowest values of sum of bases (SB) and base saturation (BS) observed in the Bo horizon of Anionic Acrudox compared to Rhodic Hapludox reflect its higher degree of weathering-leaching, in association with its lower cation exchangeable capacity (CEC) and freer drainage. Among the Inceptisols, there are higher values of available K in the Typic Dystrustept, probably due to the weathering of muscovite inherited from gneiss (Resende et al., 2019).

The Anionic Acrudox has the lowest available P values among the Oxisols, possibly due to the greater P fixation caused by its more oxidic mineralogy and higher clay content (Resende et al., 2020). The lower values of the SiO_2/Al_2O_3 molar ratio in the gabbro-derived Oxisol indicate its greater degree of weathering-leaching compared to the Oxisol derived

from gneiss (Silva et al., 2020b). The lower proportion of quartz in gabbro that originated the Anionic Acrudox helps to explain these results.

The most smoothed position in the landscape favors greater water infiltration in the soil profile and the formation of more pedogenically developed soils such as Oxisols (Dortzbach et al., 2016). Even exhibiting a more advanced degree of weathering-leaching and presenting deep profiles, Oxisols still reflect properties of their parent rock (Curi, 1983; Curi and Franzmeier, 1987).

The differences in texture, SB and BS between Anionic Acrudox and Rhodic Hapludox demonstrate the more accentuated degree of weathering-leaching of the former, since gabbro is more easily weathered than gneiss under comparable conditions (Resende et al., 2019). The remaining P values are consistently higher in both soils derived from gneiss. Recall that the lower the remaining P, the greater the potential P adsorption of the soil, which is increased with the presence of oxide minerals in soils. Thus, these results explain the more kaolinitic and less oxidic mineralogy (Kämpf and Curi, 2012) as well as the lower clay contents (Table 1) of those soils derived from gneiss.

Table 1. Chemical and physical properties of the studied soils.

Soil	Parent material	Depth	Hor.	pH	K	P	Ca^{+2}	Mg^{2+}	Al^{3+}	$H+Al^{3+}$	SB	t	T	BS	m	SOM	P-Rem	Clay	Silt	Sand	SiO_2/Al_2O_3
		cm			mg dm^{-3}		$cmol_c$ dm^{-3}							%		dag kg^{-1}	mg L^{-1}	%			
Oxic Dystrustept	Gabbro	0-5	A	6.2	81.4	1.5	4.8	2.2	0.0	3.3	7.2	7.2	10.5	68.5	0.4	5.5	21.7	53	29	18	-
		05-26	Bw	5.9	38.5	0.9	2.8	0.9	0.1	4.4	3.8	3.9	8.2	46.4	1.8	3.8	16.2	53	27	20	1.5
		26-47	C	5.8	15.1	0.5	1.3	0.3	0.0	2.4	1.7	1.7	4.1	42.2	1.2	1.7	14.7	47	26	27	-
Typic Dystrustept	Gneiss	0-22	A	4.9	130.8	4.7	2.2	0.4	0.4	5.9	3	3.4	8.9	33.5	12.1	2.7	33.8	43	16	31	-
		22-50	Bw	4.8	82.9	1.3	0.4	0.1	0.9	4.5	0.7	1.5	5.2	13.1	55.8	1.3	31.4	43	21	36	1.4
		72-140	C	4.8	92.3	1	0.3	0.1	0.9	2.1	0.6	1.5	2.7	22.1	60.8	0.3	56	11	46	33	-
Anionic Acrudox	Gabbro	0-20	A	5.2	82	0.3	1.7	1.3	0.2	4.9	3.2	3.2	8.1	40	6	3.7	4.9	70	11	19	-
		80-100	Bo	5.5	16	0	0.2	0.3	0.0	1.4	0.5	0.5	1.9	28	0	0.8	0.6	69	16	15	0.7
Rhodic Hapludox	Gneiss	0-20	A	6	118	2.6	4.5	0.8	0.0	1.9	5.6	5.6	7.5	75	0	3.1	16.9	55	9	36	-
		60-80	Bo	7.4	8	0.8	5.9	0.1	0.0	0.9	6	6	6.9	87	0	2.4	8.2	71	5	24	1.3

SB – sum of bases; T – potential cation exchangeable capacity; t – effective cation exchangeable capacity; BS – bases saturation; m –Al^{3+} saturation; SOM – soil organic matter; P-Rem – remaining P; SiO_2/Al_2O_3 – molar relation.

3.2. Chemical elements obtained by pXRF

The highest concentrations of Si were found in Typic Dystrustept and Rhodic Hapludox (Fig. 3), fundamentally reflecting the mineralogical constitution of gneiss (higher quartz content). The differences are smaller between Oxisols, possibly due to the longer exposure time to bioclimatic agents and their homogenizing effect (Birkeland, 1999). Al contents are substantially higher in the C horizon of the Oxic Dystrustept compared to the Typic Dystrustept, possibly due to the higher gibbsite content of the former, reflecting a relatively higher degree of weathering-leaching.

The higher Fe content in soils developed from gabbro, which presents a chemical composition similar to basalt, is a consequence of the higher concentration of ferromagnesian minerals in this parent rock in comparison with gneiss, causing greater Fe contents in Anionic Acrudox than in Rhodic Hapludox (Fig. 4). Ti contents are markedly lower in the Typic Dystrustept, following lower Fe contents. The higher concentration of Ca in the A horizon of the Oxic Dystrustept and Rhodic Hapludox must be related to the contribution of colluvial material from soils located in upper landscape positions.

The Inceptisol derived from gneiss has higher K contents due to the higher concentration of mica and feldspars in relation to the Inceptisol derived from gabbro. This trend remains the same in the Oxisols, however it is more tenuous in relation to Oxisols due to the greater intensity of weathering-leaching.

The contents of Zr are due to the presence of zircon or rutile (in this case after isomorphic substitution), minerals highly resistant to weathering, as they tend to residually accumulate in older soils (Stockmann et al., 2016; Marques et al., 2004). The highest relative concentration was found only in the Rhodic Hapludox, and the gneisses in the study region have zircon as a mineral (Bueno et al., 1990).

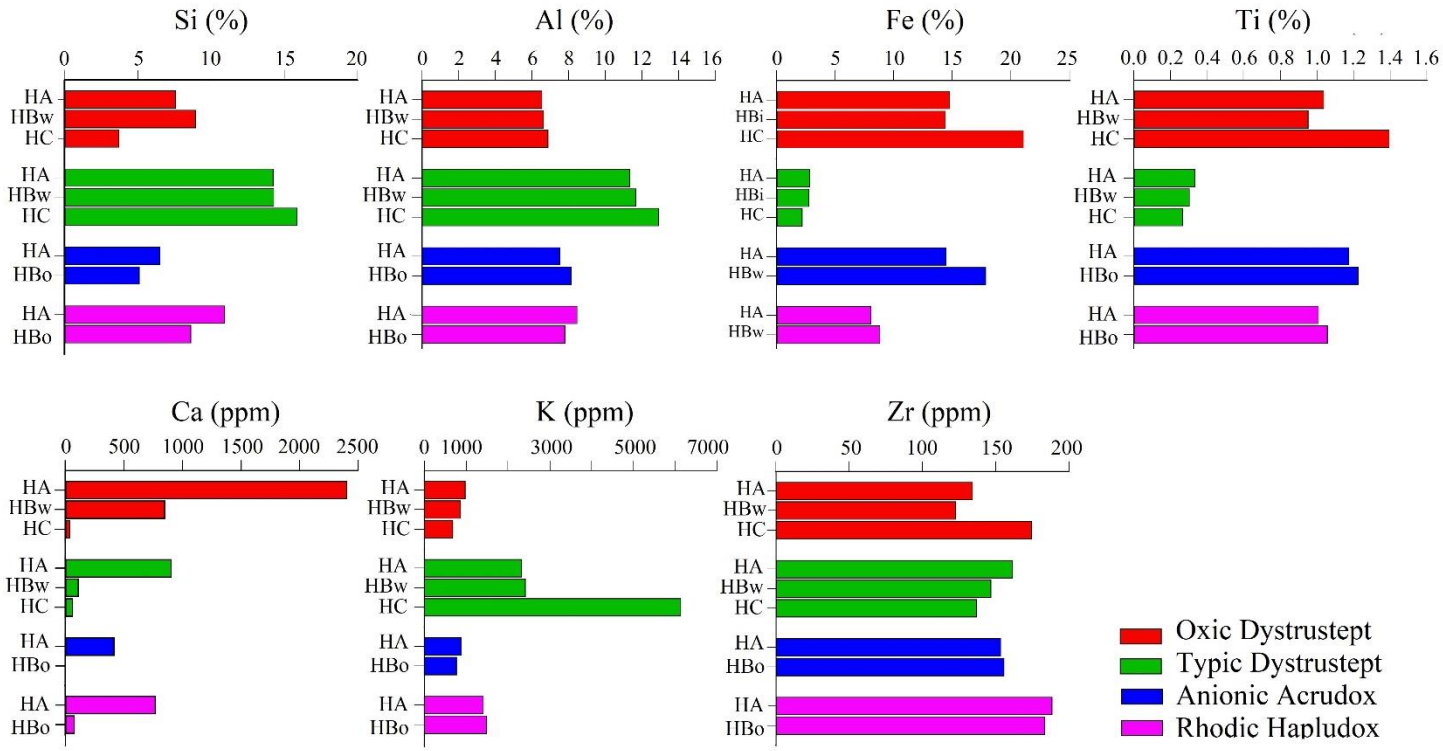

Fig. 3. Average levels of chemical elements obtained by portable X-ray fluorescence spectrometry (pXRF) at air-dried fine earth, for the soil classes studied.

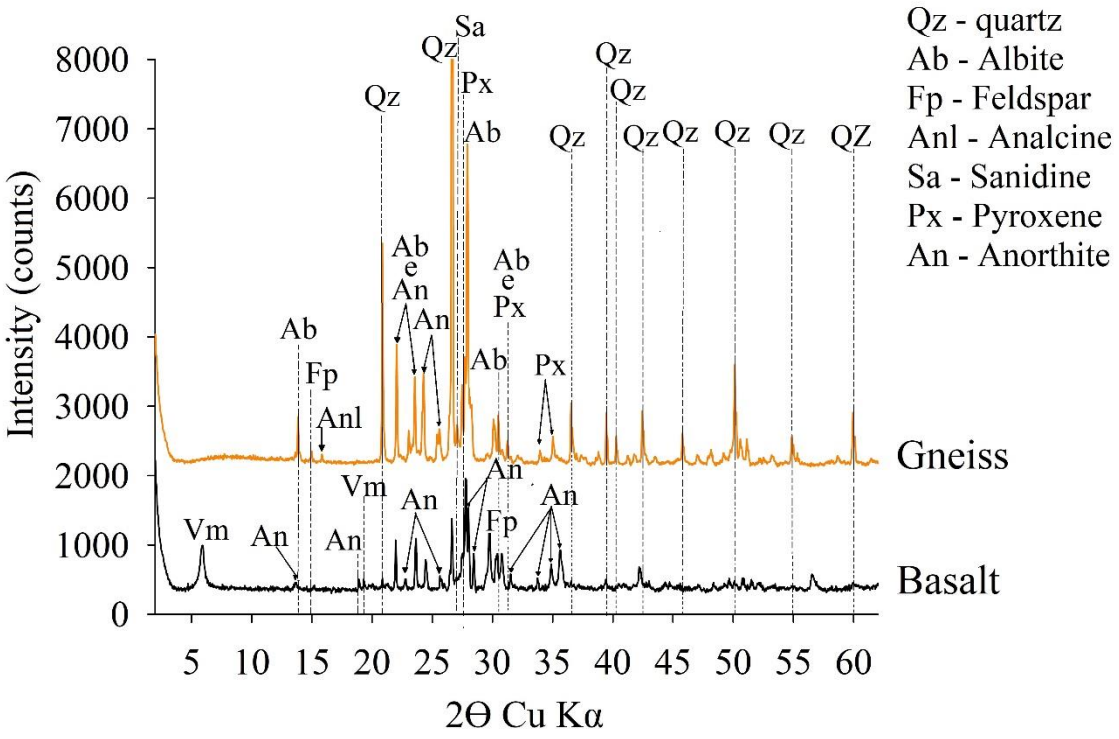

Fig. 4. X-ray diffractograms of the Gneiss and Basalt, Qz – quartz; Ab – Albite; Fp – feldspar; Anl – Analcine; Sa – Sanidine, Px – Pyroxene, An - Anorthite

3.3. Magnetic susceptibility

The values of magnetic susceptibility in ADFE and in soil size fractions are shown in Table 2. In ADFE, MS varied from 0.3 to 18 × 10^{-7} m^3 kg^{-1} for soils developed from gneiss and from 82.8 to 235 × 10^{-7} m^3 kg^{-1} for soils developed from gabbro. The much higher MS values of soils derived from gabbro compared to gneiss (Lima et al., 2020) are in agreement with the above values. According to Kämpf and Curi (2000), in the sand and silt fractions magnetite prevails while maghemite, a secondary iron oxide formed by its oxidation, is found in the clay fraction. These ferrimagnetic minerals are responsible for the expression of the magnetization of tropical soils (Poggere et al., 2018).

The low MS values presented in the Rhodic Hapludox and Typic Dystrustept refer to the magnetite poverty in the gneisses and consequently lower concentrations of magnetite and maghemite in the soils derived from them. It is noteworthy that the higher the degree of weathering-leaching, the higher the MS, even among Oxisols. A positive correlation between maghemite concentration, Fe content, clay content and more mafic parent material has already been found (Poggere et al., 2018; Fontes and Weed, 1991).

In relation to the MS of the different granulometric fractions of the soils, the sand and silt fractions of the soils developed from gabbro present much higher values, in agreement with the higher levels of magnetite in this parent rock (Caner et al., 2014) and its maintenance in the coarser fractions of the soils, here better expressed in the XRDs of the silt fraction (Fig. 5b). The highest MS values observed for the clay fraction of gabbro-derived soils occur due to the higher concentration of maghemite in this fraction (Fig. 5c). Among Oxisols, XRD indicates higher levels of maghemite, particularly in the Bo horizon, corroborating the MS data in Table 2.

Table 2. Magnetic susceptibility in air-dried fine earth (ADFE) and in the clay, silt and sand fractions of soils.

Soil Classes	Parent Material	Depth	Horizon	Magnetic Susceptibility ($10^{-7}m^3\ kg^{-1}$)			
		Cm		ADFE	Clay	Silt	Sand
Oxic Dystrustept	Gabbro	0-5	A	112.1	133.7	157.8	69.4
		5-26	Bw	122.8	139.5	167.6	60.3
		26-47	C	82.8	142.6	106.0	20.4
Typic Dystrustept	Gneiss	0-22	A	2.6	3.0	4.2	3.4
		22-50	Bw	2.2	1.9	3.0	3.0
		72-140	C	0.3	1.9	0.2	0.1
Anionic Acrudox	Gabbro	0-20	A	235.0	246.0	251.7	100.4
		60-80	Bo	232.3	240.0	278.3	94.1
Rhodic Hapludox	Gneiss	0-20	A	18.6	37.9	39.8	14.7
		60-80	Bo	16.0	18.9	24.6	17.0

3.4. Mineralogy

3.4.1. Sand fraction

In the sand fraction of the evaluated soils, quartz stands out as the dominant mineral (Fig. 5a). Kaolinite appears in the C horizon of the Typic Dystrustept, while gibbsite occurs in the C horizon of the Oxic Dystrustept. The most conspicuous occurrence of gibbsite in this horizon compared to the Bo horizon of the Anionic Acrudox is associated with the colluvial contribution of soils located at upper landscape positions.

Among Oxisols, higher levels of kaolinite, gibbsite, hematite, goethite and maghemite are observed in the Anionic Acrudox (Fig. 5a). The presence of higher levels of iron oxide minerals in this soil is related to the parent rock richer in Fe with a higher degree

of pedogenetic development of this soil compared to the Rhodic Hapludox (Marques et al., 1992).

3.4.2. Silt fraction

With the exception of Rhodic Hapludox, the mineralogy of the silt fraction shows a reduction in quartz in all soils compared to the sand fraction (Fig. 5.b). Micas still persist in this fraction, particularly in the Typic Dystrustept, where goethite stands out in relation to the Oxic Dystrustept. Conversely, gibbsite contents are higher in this soil compared to Typic Dystrustept. This reflects that gabbro is weathered more quickly than gneiss in comparable conditions. Also, hematite, goethite and magnetite were found in all horizons of the Oxic Dystrustept.

Among the Oxisols, kaolinite is higher in Rhodic Hapludox and gibbsite is higher in Anionic Acrudox, in line with the higher degree of pedogenetic development of the latter. Fe oxide minerals are also higher in this soil.

3.4.3. Clay fraction

The clay fraction of the Typic Dystrustept has more kaolinite and gibbsite (with the exception of the C horizon) than the Oxic Dystrustept (Fig. 5.c). Fe oxide minerals remain higher in the latter.

Higher concentrations of kaolinite were observed in Rhodic Hapludox among the Oxisols, while gibbsite has equivalent levels in both soils. Iron oxide minerals tend to be higher in the Bo horizon of the Anionic Acrudox, in accordance with the more mafic material in gabbro and a higher degree of weathering-leaching of this soil (Kämpf and Curi, 2000).

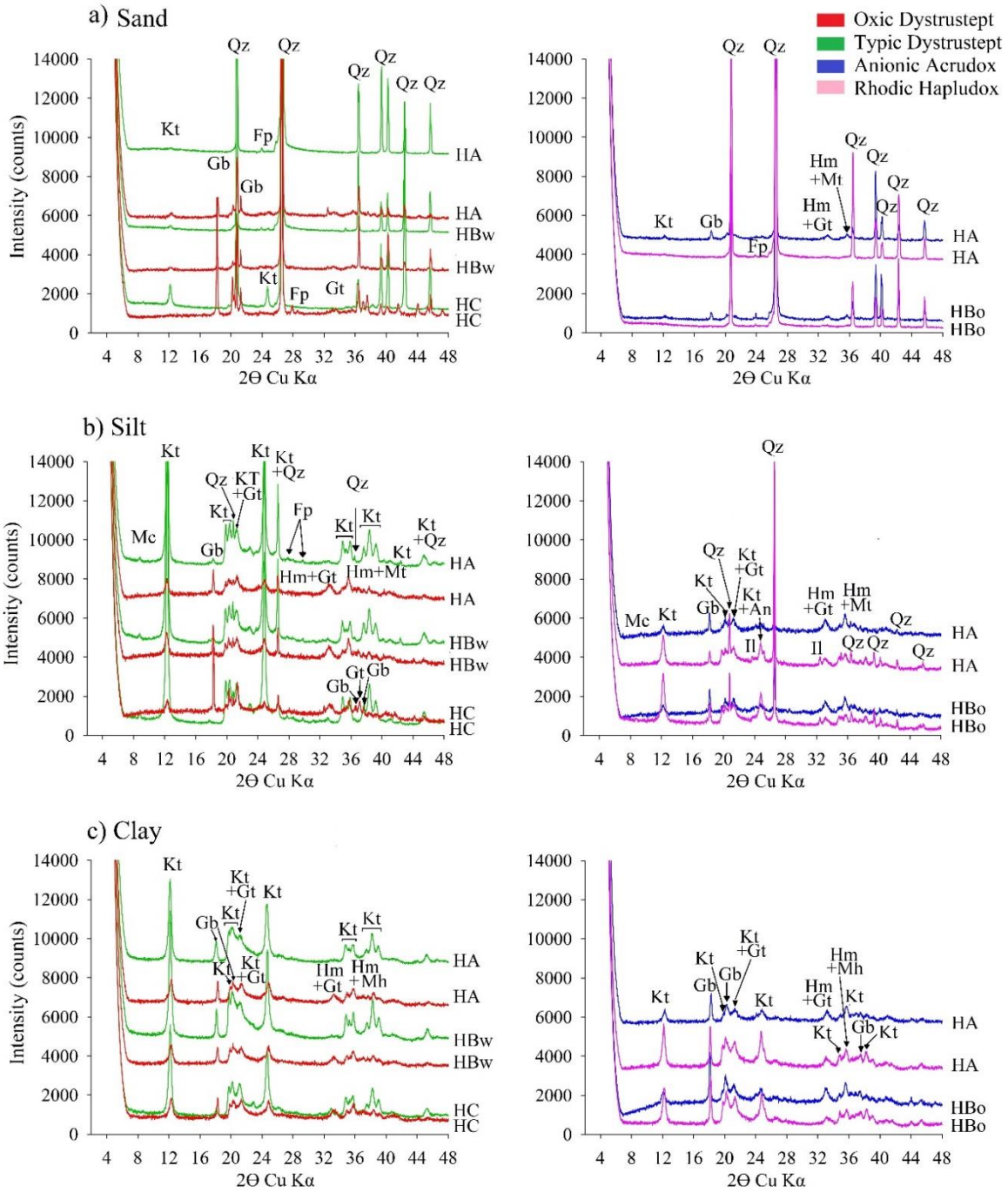

Fig. 5. X-ray diffractograms of the sand (a), silt (b) and clay (c) fractions of the Inceptisols and Oxisols. Kt-kaolinite; Hm - hematite; Mt - magnetite; Mh - maghemite; Gb - gibbsite; Gt - goethite; Qz - quartz; An - anatase; Il - ilmenite; Fp - feldspar.

3.5. Spectral data

The spectral curves observed in the soils developed from gabbro have a lower reflectance factor when compared to the soils developed from gneiss (Fig. 6), due to higher

concentrations of opaque minerals and a greater absorption of light emitted by the Vis-NIR equipment. The Typic Dystrustept shows the highest reflectance, particularly in the C horizon. Among the evaluated soils, it exhibits the highest levels of sand with quartz as the main mineral in this fraction; the reflectance of quartz is high and, therefore, greater reflectance intensity found for that horizon (White et al., 1997). The lower intensities of the reflectance curves for the Oxic Dystrustept when compared to the Typic Dystrustept, reflect higher levels of clay, Fe oxides, mainly hematite, and SOM, causing a darker color and, thus, greater absorbance of light.

The main difference between the spectral curves of Oxisols is related to the levels of Fe and clay, where the Anionic Acrudox has less reflectance, due to the greater absorption caused by iron oxide minerals and higher clay content. The water strongly adsorbed on the clay particles also promotes this absorption, particularly at wavelengths of 1400, 1900 and 2200 nm (Montgomery, 1976), causing a decrease in reflectance.

In the Oxic Dystrustept, Anionic Acrudox and Rhodic Hapludox, the absorption bands of 400 to 600 nm and 800 to 900 nm are more accentuated Galvão and Vitorello (1996) identified these bands as being characteristic of iron oxide minerals, which indicates higher levels of these minerals in these soils. In addition, the greater reflectance and the narrower concavity at 480 nm suggest that the Rhodic Hapludox has a greater amount of goethite, while the Anionic Acrudox presents more hematite.

Water molecules in the clay minerals are identified by bands at 1400 and 1900 nm, more evident in the soils developed from gneiss, especially the Typic Dystrustept. Demattê and Garcia (1999) found that the band at 850 nm indicates the presence of iron oxide minerals with a higher degree of crystallinity (more common in Oxisols) such as hematite and goethite. The Typic Dystrustept must have iron oxides with a lower degree of crystallinity since it is a younger soil.

The 2200 nm band has a more prominent “step”, indicating a higher concentration of kaolinite in the Typic Dystrustept and Rhodic Hapludox derived from gneiss compared to the Oxic Dystrustept and Anionic Acrudox derived from gabbro (Lindberg and Snyder, 1972; Mathews et al., 1973; Demattê et al., 2015).

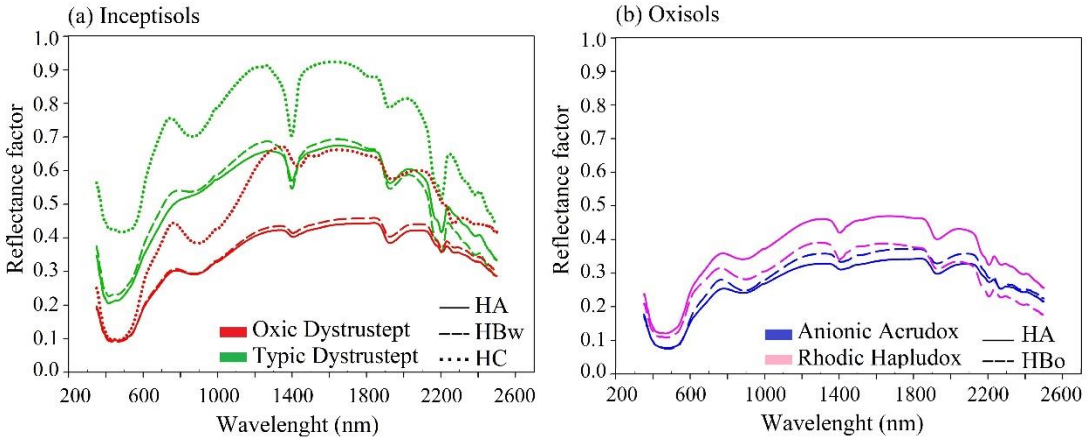

Fig. 6. Spectral curves corresponding to the Inceptisols (a) and Oxisols (b).

3.6. Correlations between elements, texture and MS

In Inceptisols, Si shows a strong and positive correlation with K (r = 0.78) and Al (r = 0.92), as observed in Fig. 7a, due to the occurrence of these elements in the structure of primary minerals such as feldspars, plagioclases and micas, and in secondary minerals such as kaolinite, respectively. Si also shows a strong and negative correlation with Fe (r = - 0.99) and Ti (r = - 0.99). Among the granulometric fractions, the highest correlation of Si occurs with the sand fraction (r = 0.68), since quartz predominates in the sand fraction of tropical soils (Araujo et al., 2014).

Strong and positive correlations are observed between Al and K (r = 0.85) and sand (r = 0.89) due to the presence of mica and feldspar in this fraction. The negative correlation between Ca and the coarse fractions of the Oxisols results from the release of Ca from the structure of easily weathered primary minerals (EWPM) associated with its ease of being leached and/or eroded. However, as the Inceptisols are less weathered soils, Ca can remain in their coarse fractions.

There is a very strong correlation between Fe and Ti (r = 1), and both show a positive correlation with clay and MS (r = 0.68). According to Curi et al. (2017), the high correlation between Fe and MS content is greatly influenced by the soil parent material and the pedogenetic processes during soil formation. The clay fraction tends to concentrate elements such as Fe and Ti with the increase of the degree of weathering of the soils. Zr has a positive correlation with the sand fraction (r = 0.41) and negative one with Si (r = - 0.28), in association with zirconite ($ZrSiO_4$), a mineral very resistant to weathering.

In Fig. 7b (Oxisols), Si shows a high and positive correlation with K (r = 0.89), Ca (r = 0.73) and Zr (r = 0.87). In addition, these elements show high and positive correlations with the sand fraction (r = 0.79; r = 0.81; 0.87, respectively) and with each other (K and Ca, r = 0.34; K and Zr, r = 0.96; Ca and Zr, r = 0.42). Fe and Ti show a high and positive correlation with each other (r = 0.99). The correlations involving Fe and Ti are higher in the silt fraction (r = 0.89; r = 0.81, respectively) and lower in the clay fraction (r = 0.52; r = 0.64, respectively), in line with a higher correlation between silt and MS (r = 0.82).

The negative correlation between Si and Al (r = - 0.46) for soils developed from gabbro (Fig. 7c) indicates a greater ease of desilification, resulting in an accumulation of Al in the form of kaolinite and gibbsite. Fe has a positive correlation with Ti (r = 0.89), Zr (r = 0.84) and both correlate with the sand fraction. Clemente and Marconi (1994) identified magnetite and ilmenite in the sand fraction of soils developed from diabase; anatase was found in the sand fraction of Oxisols developed from diabase and basalt. The presence of maghemite in the clay fraction was indicated by the high correlation between clay and MS (r = 1).

For soils developed from gneiss (Fig. 7d), Si has a positive correlation with Al (r = 0.98), K (r = 0.75), silt (r = 0.84) and sand (r = 0.58). Fe shows a positive correlation with Ti (r = 1), Zr (r = 0.93) and the clay fraction (r = 0.82), indicating the residual accumulation of these elements with the highest degree of weathering-leaching of the soil. In the soils developed from gabbro, there is a positive correlation between the clay fraction and MS. According to Poggere et al. (2018), the presence of maghemite in the clay fraction helps explain this trend.

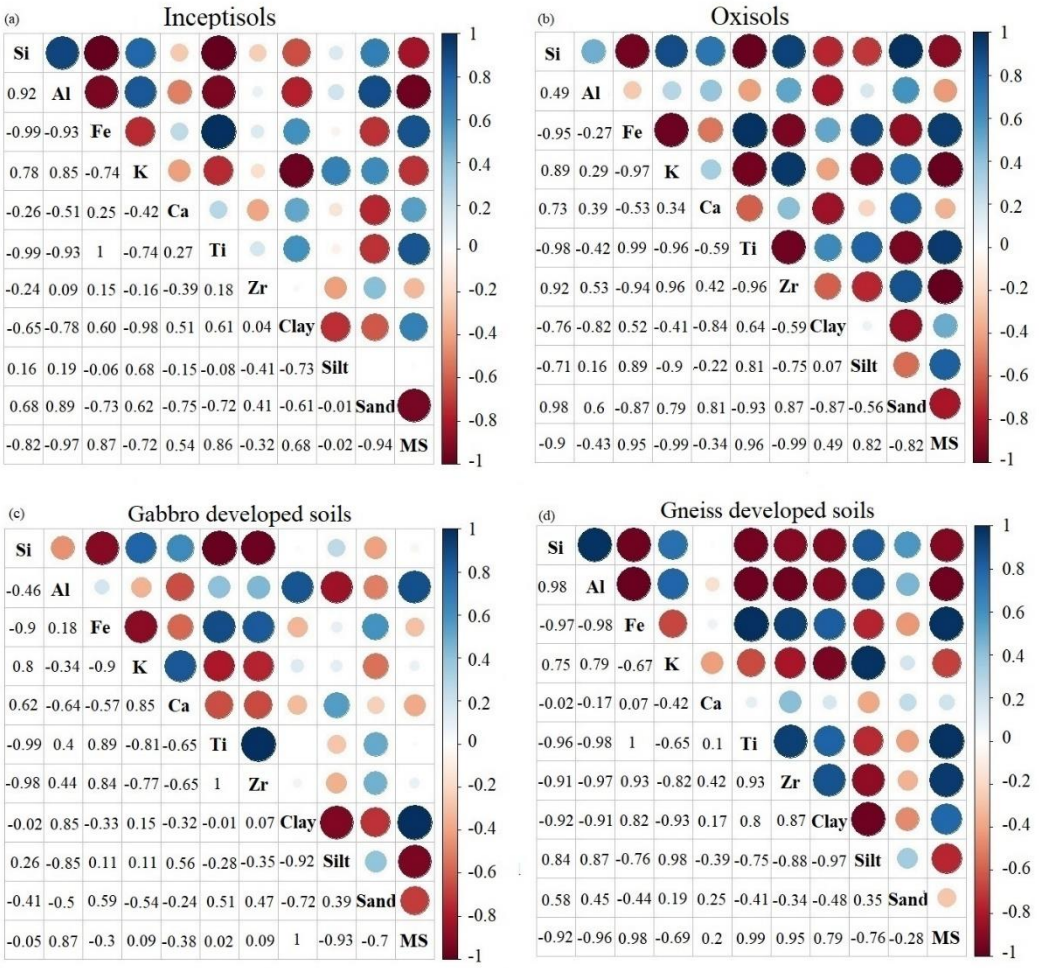

Fig. 7. Correlograms of the contents of the elements obtained by pXRF, texture and MS: Inceptisols (a), Oxisols (b), gabbro developed soils (c) and gneiss developed soils (d). The bluer the circle, the greater the positive correlation; the redder the circle, the greater the negative correlation.

3.7. Principal component analysis of elements, texture and MS values

The differences in the pattern of the elements obtained by pXRF, texture and MS are observed in the analysis of PCA (Fig. 8). The data variability explained by PC1 (38.8%) and PC2 (32.8%), total 71.6%. Si, Al, K and the sand fraction are negatively correlated mainly with Ti, Fe, clay fraction and MS, while Zr was opposed to Ca and the silt fraction.

Due to the differences between the soil classes grouped by a similar degree of pedogenetic development and developed from different parent materials, the horizons of the evaluated soils were distinctly positioned in the PCA, even those belonging to the same soil profile. A and Bo Horizons are influenced by Zr for Rhodic Hapludox, while Fe, Ti, clay fraction and MS directly influence these horizons in the Anionic Acrudox.

The A and Bw horizons of the Oxic Dystrustept were directly influenced by Ca, while the C horizon was influenced by Ti, Fe and clay fraction. For the Typic Dystrustept, these horizons were strongly influenced by Al, Si, K and the sand fraction. Both the Typic Dystrustept and Oxic Dystrustept horizons were distinguished from the other horizons.

The PCA shows a distinct pattern between the soil classes separated by a similar degree of weathering-leaching and their respective horizons, which was already expected, since these soils originate from different parent materials. The differences represented by the PCA show the variation between the parent materials with respect to the content of the elements obtained by pXRF, texture and MS, especially the soils derived from gabbro being more influenced by Fe, Ti, clay content and MS.

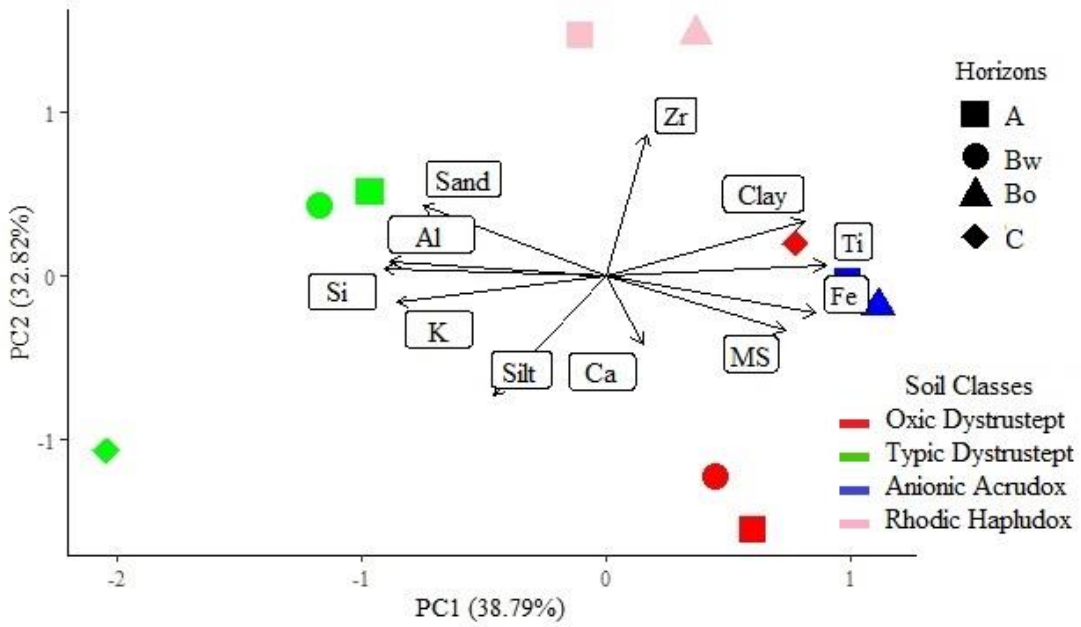

Fig. 8. Principal component analysis of the elementary levels obtained by portable X-ray fluorencence spectrometry, texture and soil magnetic susceptibility.

3.8. Advantages of using proximal sensors on investigations of soil genesis

Through the data provided by pXRF, Vis-NIR and MS, specific correlations and detailed understanding of soil genesis and related properties are possible. PXRF provided insights on the concentration of elements in the sand, silt and clay fractions, which correlate with soil mineralogy of such particle size fractions. Moreover, pXRF and MS support the calculation of correlations between their data and soil texture, besides demonstrating their variability caused by weathering of minerals and, hence, variation of elemental contents in

the sand, silt and clay fractions of different soil horizons. Even in morphologically homogeneous soil profiles (e.g., Oxisols), soil horizons presented variations easily detected by Vis-NIR spectra, MS and differential elemental contents by pXRF (including in the particle size fractions), showing proximal sensors can contribute to in-depth evaluations of soil genesis (Zhang et al., 2021; Mancini et al., 2021). Finally, this study also showed analyses of proximal sensors on the sand, silt and clay fraction in addition to analyses on bulk soil can elucidate their physical, chemical and mineralogical changes due to weathering.

4. Conclusions

The elemental contents obtained by pXRF showed that the soils derived from gneiss have a higher concentration of Si, which decreases with depth, while the soils developed from gabbro have higher contents of Fe and Ti. Moreover, these latter also present higher MS resulting from the higher concentration of magnetite and maghemite. Inceptsols, younger soils, have EWPM in their composition, such as feldspars in Typic Dystrustept, in addition to hematite, gibbsite and kaolinite. The high contents of gibbsite in the silt fraction of Oxic Dystrustept indicate that under the same environmental conditions, gabbro weathered more quickly than gneiss.

Both Oxisols presented striking differences caused by the two parent materials, which influenced their contrasting properties. Their spectral curves distinguished Fe oxides, in the form of goethite and hematite, and the largest presence of kaolinite in Rhodic Hapludox. The mineral composition of Anionic Acrudox demonstrates its greatest pedogenetic development.

Thus, the use of pXRF, VIS-Nir as well as magnetic susceptibility were efficient in differentiating the physical, chemical and mineralogical properties of the evaluated soils in greater detail, according to their respective parent materials and similar degree of weathering-leaching.

5. Acknowledgements

The authors would like to acknowledge the Brazilian National Council for Scientific and Technological Development (CNPq), Coordination for the Improvement of Higher Education Personnel (CAPES) and Research Support Foundation of the State of Minas

Gerais (FAPEMIG) for the financial support of research funds and fellowships associated with the research groups involved.

References

Alvares, C.A., Stape, J.L., Sentelhas, P.C., de Moraes, G., Leonardo, J., Sparovek, G., 2013. Köppen's climate classification map for Brazil. Meteorol. Z. 22 (6), 711–728. https://doi.org/10.1127/0941-2948/2013/0507.

Alvarez, V.H., Fonseca, D.M., 1990. Definitions of doses of phosphorus to determine the maximum phosphate adsorption capacity and to aid greenhouse experiments. (In Portuguese.) Rev. Bras. Cienc. do Solo. 14, 49-55.

Alves, M.J.F., Melo, V. de F., Reissmann, C.B., Kaseker, J.F., 2013. Reserva mineral de potássio em Latossolo cultivado com Pinus taeda L. Rev. Bras. Ciência do Solo 37, 1599–1610. https://doi.org/10.1590/S0100-06832013000600016.

Andrade, R., Silva, S.H.G., Weindorf, D.C., Chakraborty, S., Faria, W.M., Guilherme, L.R.G., Curi, N., 2021. Micronutrients prediction via pXRF spectrometry in Brazil: Influence of weathering degree. Geoderma Reg. 27, e00431. https://doi.org/10.1016/j.geodrs.2021.e00431.

Araújo, M.A., Pedroso, A.V., Amaral, D.C., Zinn, Y.L., 2014. Paragnese mineral de solos desenvolvidos de diferentes litologias na região sul de Minas Gerais. Rev Bras Cienc do Solo 38, 11–25. https://doi.org/10.1590/S0100-06832014000100002.

Bahia, A.S.R.d.S., Marques, J., Siqueira, D.S., 2015. Procedures using diffuse reflectance spectroscopy for estimating hematite and goethite in Oxisols of São Paulo, Brazil. Geoderma Reg. 5, 150–156. https://doi.org/10.1016/j.geodrs.2015.04.006.

Barbosa, J.Z., Poggere, G., Silva, S.H.G., Mancini, M., Motta, A.C.V., Marques, J.J.G. de S. e. M., Curi, N., 2021. National-scale spatial variations of soil magnetic susceptibility in Brazil. J. South Am. Earth Sci. 108. https://doi.org/10.1016/j.jsames.2021.103191.

Benedet, L., Faria, W.M., Silva, S.H.G., Mancini, M., Demattê, J.A.M., Guilherme, L.R.G., Curi, N., 2020. Soil texture prediction using portable X-ray fluorescence spectrometry and visible near-infrared diffuse reflectance spectroscopy. Geoderma 376, 114553. https://doi.org/10.1016/j.geoderma.2020.114553.

Birkeland, P.W., 1999. Soils and geomorhology, Third ed. Oxford University Press, New York.

Bigham, J.M., Fitzpatrick, R.W., Schulze, D.G., 2002. Iron Oxides. In: Soil Mineralogy with Environmental Applications. Madison, pp. 323–366. https://doi.org/10.1515/9783110289039.351.

Brindley, G.W., Brown, G., 1980. Crystal structures of clay minerals and their X-ray identification. Mineralogical Society of Great Britain and Ireland, London. https://doi.org/10.1180/mono-5.

Bueno, C.R.P., Bahia, V.G., Curi, N., Dias Junior, M.S., 1990. Unidades litológicas do município de Lavras (MG). Ciência e Prática 14, 352–365.

Buol, S.W., Southard, R.J., Graham, R.C., McDaniel, P.A., 2011. Soil Genesis and Classification, sixth ed. A John Wiley & Sons Ltd, Chichester.

Caner, L., Radtke, L.M., Vignol-Lelarge, M.L., Inda, A.V., Bortoluzzi, E.C., Mexias, A.S., 2014. Basalt and rhyo-dacite weathering and soil clay formation under subtropical climate in southern Brazil. Geoderma. 235-236, 100-112. https://doi.org/10.1016/j.geoderma.2014.06.024.

Cervi, E.C., Maher, B., Poliseli, P.C., Souza Junior, I.G., da Costa, A.C.S., 2019. Magnetic susceptibility as a pedogenic proxy for grouping of geochemical transects in landscapes. J. Appl. Geophys. 169, 109–117. https://doi.org/10.1016/j.jappgeo.2019.06.017.

Clemente, C.A., Marconi, A., 1994. Mineralogia e mobilidade de cátions de uma alteração intempérica de diabásio. Scientia Agricola. 51, 335-344. https://doi.org/10.1590/S0103-90161994000200021.

Curi, N., 1983. Lithosequence and Toposequence of Oxisols from Goias and Minas Gerais States, Brazil (Ph.D. dissertation) Purdue University, West Lafayette.

Curi, N., Franzmeier, D. P., 1987. Effect of Parent Rocks on Chemical and Mineralogical Properties of Some Oxisols in Brazil. Soil Sci. Soc. Am. J. 51, 153-158.

Curi, N., Silva, E., Gomes, F.H., Menezes, M.D., Silva, S.H.G., Teixeira, A.F. dos S., 2020. Mapeamento de solos, aptidão agrícola e taxa de adequação do uso das terras do município de Lavras (MG), 1st ed. Editora UFLA, Lavras.

Curi, N., Silva, S.H.G., Poggere, G.C., Menezes, M.D., 2017. Mapeamento de solos e magnetismo no campus da UFLA. Editora UFLA, Lavras.

Da Costa, A.C.S., Bigham, J.M., Rhoton, F.E., Traina, S.J., 1999. Quantification and characterization of maghemite in soils derived from volcanic rocks in southern Brazil. Clays Clay Miner. 47, 466–473. https://doi.org/10.1346/CCMN.1999.0470408

Dalmolin, R.S.D., Gonçalves, C.N., Klamt, E., Dick, D.P., 2005. Relação entre os constituintes do solo e seu comportamento espectral. Ciência Rural 35, 481–489. https://doi.org/10.1590/s0103-84782005000200042.

Dantas, A.A.A., Carvalho, L.G. de, Ferreira, E., 2007. Classificação e tendências climáticas em Lavras, MG. Ciência e Agrotecnologia 31, 1862–1866. https://doi.org/10.1590/S1413-70542007000600039.

Dearing, J., 1999. Environmental Magnetic Susceptibility: Using the Bartington MS2 System, second ed. Chi Publishing, Kenilworth.

Demattê, J.A.M., Garcia, G.J. 1999. Alteration of Soil Properties through a Weathering Sequence as Evaluated by Spectral Reflectance. Soil Sci. Soc. Am. J. 63, 327-342. https://doi.org/10.2136/sssaj1999.03615995006300020010x.

Demattê, J.A.M., Epiphanio, J.C.N., Formaggio, A.R., 2003. Influência da matéria orgânica e de formas de ferro na reflectância de solos tropicais. Bragantia. 62, 451-464. https://doi.org/10.1590/s0006-87052003000300012.

Demattê, J.A.M., Araújo, S.R., Fiorio, P.R., Fongaro, C.T., Nanni, M.R., 2015. Espectroscopia VIS-NIR-SWIR na avaliação de solos ao longo de uma topossequência em Piracicaba (SP). Revista Ciencia Agronomica. 46, 679-688. https://doi.org/10.5935/1806-6690.20150054.

Demattê, J.A.M., Horák-Terra, I., Beirigo, R.M., Terra, F. da S., Marques, K.P.P., Fongaro, C.T., Silva, A.C., Vidal-Torrado, P., 2017. Genesis and properties of wetland soils by VIS-NIR-SWIR as a technique for environmental monitoring. J. Environ. Manage. 197, 50-62. https://doi.org/10.1016/j.jenvman.2017.03.014.

Demattê, J.A.M., Carnieletto, A., Paiva, A.F.S., Sato, M.V, Dalmolin, R.S.D., Araújo, S.B.de, Elisângela, B., Nanni, M.R., Noronha, N.C., Lacerda, M.P.C., Coelho, J., Filho, D.A., Rizzo, R., Bellinaso, H., Francelino, M.R., Schaefer, C.E.G.R., Vicente, L.E., Uemeson, J., Sá, E.V.de, Sampaio, B., Menezes, R.S.C., João, J., Souza, L.L.de, Abrahão, W.A.P., Coelho, R.M., Grego, C.R., Lani, J.L., Fernandes, A.R., Gonçalves, D.A.M., Silva, S.H.G., Menezes, M.D.de, Curi, N., Couto, E.G., Lúcia, H.C., Ceddia, M.B., Pinheiro, É.F.M., Grunwald, S., Vasques, G.M., Marques, J., Airon, J., Vasconcelos, M.C.de, Nóbrega, G.N., Marcelo, Z., Souza, S.F.de, Valladares, G.S., Herbert, J., Viana, M., Terra, S., Horák-terra, I., Fiorio, P.R., Rafael, C., Frade, E.F., Lima, R.H.C., Filippini, J.M., SouzaV.S.deLourdesM.deSantos, M., Lourdes, M.de, Ruivo, P., Ferreira, T.O., Brait, M.A., Caetano, N.R., Bringhenti, I., SousaW.deSafanelli, J.L., Guimarães, C.C.B., Poppiel, R.R., Barros, A., Quesada, C.A., Zarate, H.T., 2019. The Brazilian Soil Spectral Library (BSSL): A general view, application and challenges. Geoderma 354, 113793. https://doi.org/10.1016/j.geoderma.2019.05.043.

Dortzbach, D., Pereira, M.G., dos Anjos, L.H.C., Fontana, A., Silva Neto, E. de C., 2016. Genesis and classification of soils from subtropical mountain regions of Southern Brazil. Rev. Bras. Cienc. do Solo. 40, 1–15. https://doi.org/10.1590/18069657rbcs20150503.

Fontes, M.P.F., Weed, S.B., 1991. Iron oxides in selected Brazilian Oxisoil: I. Mineralogy. Soil Sci. Soc. Am. J. 55, 1143–1149. https://doi.org/10.2136/sssaj1991.03615995005500040040x.

Gee, G.W., Bauder, J.W., 1986. Particle-size analysis, in: Klut, A. (Ed.), Methods of Soil Analysis. American Society of Agronomy, Madison, pp. 383–412.

Grauer-Gray, J., Hartemink, A.E., 2018. Raster sampling of soil profiles. Geoderma 318, 99-108. https://doi.org/10.1016/j.geoderma.2017.12.029.

Jenny, H., 1941. Factors of Soil Formation: A System of Quantitative Pedology, Soil Science, McGraw Hill book company, New York.

Kämpf, N., Curi, N., 2000. Óxidos de ferro: indicadores de ambientes pedogênicos e geoquímicos. In: Novais, R.F., Alvarez V.V.H., Schaefer, C.E.G.R. (Ed.), Tópicos em Ciência do Solo Viçosa. Sociedade Brasileira de Ciência do Solo, Viçosa, pp. 107-138.

Kämpf, N., Curi, N., 2012. Formação e evolução do solo (pedogênese). In: Ker, J.C., Curi, N., Schaefer, C.E.G.R., Vidal-Torrado, P. (Eds.), Pedologia - Fundamentos. SBCS, Viçosa, pp. 207-309.

Lima, P.L.T., Silva, M.L.N., Quinton, J.N., Armstrong, A., Inda, A.V., Batista, P.V.G., Poggere, G. C., Curi, N., 2020. Tracing the origin of reservoir sediments using magnetic properties in Southeastern Brazil. Semina. Ciências Agrárias. 41, 847-864. http://dx.doi.org/10.5433/1679-0359.2020v41n3p847.

Lindberg, J. D.; Snyder, D. G., 1972. Diffuse Reflectance Spectra of Several Clay Minerals. American Mineralogist. 57, 485-493.

Magiera, T., Łukasik, A., Zawadzki, J., Rösler, W., 2019. Magnetic susceptibility as indicator of anthropogenic disturbances in forest topsoil: A review of magnetic studies carried out in Central European forests. Ecol. Indic. 106. https://doi.org/10.1016/j.ecolind.2019.105518. Liu, L., Zhang, K., Fu, S., Liu, B., Huang, M., Zhang, Z., Zhang, F., Yu, Y., 2019. Rapid magnetic susceptibility measurement for obtaining superficial soil layer thickness and its erosion monitoring implications.Geoderma 351, 163–173.

Maher, B.A., 1986. Characterisation of soils by mineral magnetic measurements. Phys Earth Planet Inter 42, 76–92. https://doi.org/10.1016/S0031-9201(86)80010-3.

Mancini, M., Silva, S.H.G., Hartemink, A.E., Zhang, Y., de Faria, Á.J.G., Silva, F.M., Inda, A.V., Demattê, J.A.M., Curi, N., 2021. Formation and variation of a 4.5 m deep Oxisol in southeastern Brazil. Catena 206, 105492. https://doi.org/10.1016/j.catena.2021.105492.

Marques, J.J., Schulze, D.G., Curi, N., Mertzman, S.A., 2004. Trace element geochemistry in Brazilian Cerrado soils. Geoderma. 121, 31-43. doi:10.1016/j. geoderma.2003.10.003.

Marques Jr., J., Curi, N., Lima, J.M., 1992. Evolução diferenciada de Latossolo Vermelho-Amarelo e Latossolo Vermelho em função da litologia gnáissica na região de Lavras (MG). Rev. Bras. Cienc. do Solo. 16, 235-240.

Mathews, H. L., Cunningham, R. L., Petersen, G. W., 1973. Spectral Reflectance of Selected Pennsylvania. Soils. Soil Sci. Soc. Am. J. 37, 421-424.

https://doi.org/10.2136/sssaj1973.03615995003700030031x. Melo, V.F., Castilho, R.M.V., Pinto, L.F.S., 2016. Reserva Mineral do Solo, in: Melo, V.F., Alleoni, L.R.F. (Eds.), Química e mineralogia do solo. Viçosa, pp. 251–332.

McLean, E.O., Heddleson, M.R., Bartlett, R.J., Holowaychuk, N., 1958. Aluminum in soils: I. Extraction methods and magnitudes in clays and Ohio soils. Soil Sci. Soc. Am. J. 22 (5), 382-38 https://doi.org/10.2136/sssaj1958.03615995002200050005x.

Mehlich, A., 1953. Determination of P, Ca, Mg, K, Na and NH4. North Carolina Soil Testing Laboratories (Raleigh, NC). Raleigh, NC.

Montgomery, O.L., 1976. An investigation of the relationship between spectral reflectance and the chemical, physical and genetic characteristics of soils. West Lafayette, Purdue University, (Ph.D. dissertation). In: Epiphanio, J.C.N., Formaggio, A.R., Valeriano, M.M., Oliveira, J.B. Comportamento espectral de solos do Estado de São Paulo. INPE, São José dos Campos, pp. 131. Poggere, G.C., Inda, A.V., Barrón, V., Kämpf, N., de Brito, A.D.B., Barbosa, J.Z., Curi, N., 2018. Maghemite quantification and magnetic signature of Brazilian soils with contrasting parent materials. Appl. Clay Sci. 161, 385–394. https://doi.org/10.1016/j.clay.2018.05.014.

Oksanen J., Blanchet F.G., Friendly M., Kindt R., Legendre P., McGlinn D., Minchin P.R., O'Hara R.B., Simpson G.L., Solymos P., Stevens M.H.H., Szoecs E., Wagner H., 2019. Package “vegan”. https://cran.r-project.org/web/packages/vegan/vegan. pdf

Oliveira, V.A., Jacomine, P.T.K., Couto, E.G., 2017. Solos do bioma Cerrado. In: Curi, N., Ker, J.C., Novais, R.F., Vidal-Torrado, P., Schaefer, C.E.G.R. (Eds.), Pedologia - solos dos biomas brasileiros. Sociedade Brasileira de Ciência do Solo, Viçosa, pp. 177-226.

O'Rourke, S.M., Stockmann, U., Holden, N.M., Mcbratney, A.B., Minasny, B., 2016a. An assessment of model averaging to improve predictive power of portable vis-NIR and XRF for the determination of agronomic soil properties. Geoderma. 279, 31-44. https://doi.org/10.1016/j.geoderma.2016.05.005.

Piccolo, A., Stevenson, F. J., 1982. Infrared-spectra of Cu2+, Pb2+ and Ca2+ complexes of soil humic substances. In: Xu, D., Chen, S., Viscarra Rossel, R.A., Biswas, A., Li, S., Zhou, Y., Shi, Z., 2019. X-ray fluorescence and visible near infrared sensor fusion for predicting soil chromium content. Geoderma. 35, 61-69. https://doi.org/10.1016/j.geoderma.2019.05.036.

Pinto, O.C.B., 1971. Formation of a kaolinite from a biotite feldspar gneiss in four strongly weathered soil profiles from Minas Gerais, Brazil. (M.Sc. dissertation) Purdue University, West Lafayette.

Pereira, T.T.C., Ker, J.C., Schaefer, C.E.G.R., de Barros, N.F., Neves, J.C.L., Almeida, C.C., 2010. Gênese de Latossolos e Cambissolo desenvolvidos de rochas pelíticas do grupo bambuí - Minas Gerais. Rev. Bras. Cienc. do Solo. 34, 1283-1295. https://doi.org/10.1590/S0100-06832010000400026.

Poggere, G.C., Inda, A.V., Barrón, V., Kämpf, N., de Brito, A.D.B., Barbosa, J.Z., Curi, N., 2018. Maghemite quantification and magnetic signature of Brazilian soils with contrasting parent materials. Appl. Clay Sci. 161, 385-394. https://doi.org/10.1016/j.clay.2018.05.014.

Quemenéur, J.J.G., Ribeiro, A., Trow, R.A.J., Paciullo, F.V.P., Helibron, M., 2002. Geology of Lavras Sheet, South of Minas Project, Phase I. COMIG-UFMG-UFRJ-UERJ.Belo Horizonte.

R Core Team, 2020. R: A language and environment for statistical computing. R Foundation for Statistical Computing, Vienna, Austria.

Resende, M., Curi, N., Resende, S.B., Corrêia, G.F., Ker, J.C., 2014. Pedologia: Base para a distinção de ambientes, sixth ed. Editora UFLA, Lavras.

Resende, M., Curi, N., Rezende, S.B., Silva, S.H.G., 2019. Da rocha ao solo: enfoque ambiental, first ed. Editora UFLA, Lavras.

Resende, M., Curi, N., Poggere, G.C., Barbosa, J.Z., Pozza, A.A.A., Teixeira, A.F.S. 2020. Pedologia, fertilidade água e planta: inter-relações e aplicações, 2nd ed. Editora UFLA, Lavras.

RStudio Team. 2016. RStudio: Integrated development environment for R. RStudio, Inc. www.rstudio.com (accessed 16 Mar. 2018).

Schaetzl, R.J., Anderson, S., 2005. Soils: Genesis and Geomorphology. Cambrige University Press, New York.

Silva, S.H.G., Poggere, G.C., de Menezes, M.D., Carvalho, G.S., Guilherme, L.R.G., Curi, N., 2016. Proximal sensing and digital terrain models applied to digital soil mapping and modeling of Brazilian Latosols (Oxisols). Remote Sens. 8, 614-635. https://doi.org/10.3390/rs8080614.

Silva, S.H.G., Hartemink, A.E., Teixeira, A.F. dos S., Inda, A.V., Guilherme, L.R.G., Curi, N., 2018. Soil weathering analysis using a portable X-ray fluorescence (PXRF) spectrometer in an Inceptisol from the Brazilian Cerrado. Appl. Clay Sci. 162, 27-37. https://doi.org/10.1016/j.clay.2018.05.028.

Silva, F.M., Weindorf, D.C., Silva, S.H.G., Silva, E.A., Ribeiro, B.T., Guilherme, L.R.G., Curi, N., 2019. Tropical soil toposequence characterization via pXRF spectrometry. Soil Sci. Soc. Am. 83, 1153-1166. https://doi.org/10.2136/sssaj2018.12.0498.

Silva, S.H.G., Weindorf, D.C., Pinto, L.C., Faria, W.M., Acerbi Junior, F.W., Gomide, L.R.,de Mello, J.M., de Pádua Junior, A.L., de Souza, I.A., Teixeira, A.F.dos S., Guilherme L.R.G., Curi, N., 2020a. Soil texture prediction in tropical soils: a portable X-ray fluorescence spectrometry approach. Geoderma. 362, 114136. https://doi.org/10.1016/j.geoderma.2019.114136.

Silva, S. H. G., Silva, E. A., Poggere, G. C., Pádua Junior, A. L., Gonçalves, M. G. M., Guilherme, L. R. G., Curi, N., 2020b. Modeling and prediction of sulfuric acid digestion analyses data from PXRF spectrometry in tropical soils. Sci. agric. 77, https://doi.org/10.1590/1678-992x-2018-0132.

Silva, S.H.G., Weindorf, D.C., Faria, W.M., Pinto, L.C., Menezes, M.D., Guilherme, L.R.G., Curi, N., 2021. Proximal sensor-enhanced soil mapping in complex soil-landscape areas of Brazil. Pedosphere. 31, 615–626. https://doi.org/10.1016/S1002-0160(21)60007-3.

Soil Survey Staff, 2014. Keys to soil taxonomy, 12th ed. USDA-NRCS.

Skorupa, A.L.A., Silva, S.H.G., Poggere, G.C., Tassinari, D., Pinto, L.C., Zinn, Y.L., Curi, N., 2017. Similar soils but different soil-forming factors: converging evolution of Inceptisols in Brazil. Pedosphere. 27, 747-757. https://doi.org/10.1016/S1002-0160(17)60443-0.

Stockmann, U., Cattle, S.R., Minasny, B., McBratney, A.B., 2016. Utilizing portable X-ray fluorescence spectrometry for in-field investigation of pedogenesis. Catena. 139, 220-231. https://doi.org/10.1016/j.catena.2016.01.007.

Tatyanchenko, T. V., Alekseeva, T. V., Kalinin, P.I., 2013. Mineralogical and chemical compositions of the paleosols of different ages buried under kurgans in the southern Ergeni region and their paleoclimatic interpretation. Eurasian Soil Sci. 46, 341-354. https://doi.org/10.1134/S1064229313040145.

Vitorello, I., Galvão, L. S., 1996. Spectral properties of geologic materials in the 400 to 2.500 nm range: review for applications to mineral exploration and lithologic mapping. In: Comportamento espectral de materiais de solos e de estruturas biogênicas associadas. Photo Interpret. 34 , 77-99.

Walkley, A., Black, I.A., 1934. An examination of the Degtjareffmethod for determinig soil organic matter, and a proposed modification of the chromic acid titration method. Soil Sci. 37, 29–38. https://doi.org/10.1097/00010694-193401000-00003.

Wan, M., Qu, M., Hu, W., Li, W., Zhang, C., Cheng, H., Huang, B., 2019. Estimation of soil pH using PXRF spectrometry and Vis-NIR spectroscopy for rapid environmental risk assessment of soil heavy metals. Process Saf. Environ. 132, 73-81. https://doi.org/ 10.1016/j.psep.2019.09.025.

Wei, T., Simko, V., Levy, M., Xie, Y., Jin, Y., Zemla., J., 2017 Package “corrplot”. https://cran.r-project.org/web/packages/corrplot/corrplot.pdf.

Weindorf, D.C., Bakr, N., Zhu, Y., 2014. Advances in portable X-ray fluorescence (PXRF) for environmental, pedological, and agronomic applications. Adv. Agron. 128, 1-45. https://doi.org/10.1016/B978-0-12-802139-2.00001-9.

Weindorf, D.C., Chakraborty, S., 2016. Portable X-ray fluorescence spectrometry analysis of soils. In: Hirmas, D. (Ed.), Methods of Soil Analysis. Soil Science Society America, Madison, pp. 1-8.

White, K., Walden, J., Drake, N., Eckardt, F., Settle, J., 1997. Mapping the iron oxide content of dune sands, Namib Sand Sea, Namibia, using Landsat thematic mapper data. Remote Sens Environment 62, 30–39. https://doi.org/10.1016/S0034-4257(97)00068-0.

Xu, D., Chen, S., Viscarra Rossel, R.A., Biswas, A., Li, S., Zhou, Y., Shi, Z., 2019. X-ray fluorescence and visible near infrared sensor fusion for predicting soil chromium content. Geoderma. 352, 61-69. https://doi.org/10.1016/j.geoderma.2019.05.036.

Zhang, Y., Hartemink, A.E., 2019. Soil horizon delineation using vis-NIR and pXRF data. Catena. 180, 298–308. https://doi.org/10.1016/j.catena.2019.05.001.

^

Artigo elaborado de acordo com as normas do periódico Catena.

ARTIGO 2 - Proximal sensors for the prediction of clay mineralogy contents and characterization of textural fractions of soils developed from different parent materials

Fernanda Magno Silva[a], Sérgio Henrique Godinho Silva[a], Renata Andrade[a], João Augusto Coblinski[b], Alberto Vasconcellos Inda[b], Gustavo Frosi[b], Suane de Souza Franco Lima[b], Luiz Roberto Guimarães Guilherme[a], David C. Weindorf[c], Nilton Curi[a]

[a]Federal University of Lavras, Department of Soil Science, Lavras, Minas Gerais, Brazil
[b]Department of Agronomy, Federal University of Rio Grande do Sul, Porto Alegre, Rio Grande do Sul, Brazil
[c]Department of Earth and Atmospheric Sciences, Central Michigan University, Mount Pleasant, USA

Abstract

Soil parent material and weathering-leaching degree directly influences soils' physical, chemical, and mineralogical properties. Proximal sensors combined with X-ray diffraction (XRD) have optimized soil characterization, but scarce studies have focused on predicting the contents of minerals under this scope. The objectives here in were to: a) use the portable X-ray fluorescence (pXRF) spectrometry, diffuse reflectance spectroscopy in the range of visible and near-infrared (Vis-NIR), magnetic susceptibility (χ) and XRD to characterize the mineralogy of soils derived from representative Brazilian soil parent materials, and b) create predictive models to quantify the minerals obtained via XRD based on the pXRF, Vis-NIR and MS data. Twenty-two soil profiles developed from gabbro, gneiss, quartzite, mineral and organic sediments, were described, and 53 soil horizons were sampled. Each sample had the sand, silt and clay fractions separated and analyzed with XRD, pXRF, χ, and Vis-NIR. Prediction models were created using the Random Forest (RF) algorithm permuting the following predictor variables (separately and combined): pXRF, parent material (PM), χ, soil texture (sand, silt, and clay content), and Vis-NIR second derivative amplitude. Cross-validation was performed on the entire dataset using the leave-one-out method to assess accuracy of predictive models. Si, Al, Fe, Ca, K, and Ti contents obtained by pXRF and the χ discriminated the soil particle size fractions according to the parent material. XRD analysis

allowed the evaluation of the pedogenetic development of soils and their relation to the respective parent material. Due to their varying mineralogical constitution, the Vis-NIR spectral features of the particle size fractions differentiated the soil classes and their parent materials... The best predictions of mineral contents were found for hematite (Hm) (104)+(Gt) (130) (R^2 = 0.83), Hm (110)+Mh (131) (R^2 = 0.74), kaolinite (Kt) (001) (R^2= 0.73), Kt (002) (R^2 = 0.79), mica (Mc) (001) (R^2 = 0.71) and Mc (020)+Kt (020) (R^2 = 0.79). Clay mineralogy content could be accurately predicted using only pXRF and parent material data. This approach can facilitate and speed up detailed soil mineralogy characterization. Further studies are encouraged to assess the prediction of the content of minerals found in the sand and silt fractions of soils with diverse mineralogy via proximal sensors.

Abbreviations: pXRF, portable X-ray fluorescence spectrometer; Vis-NIR, visible and near-infrared spectrometer; XRD, X-ray diffraction; EWPM, easily weathered primary minerals; ADFE, air-dried fine earth; SOM, soil organic matter; χ, magnetic susceptibility; parent material, PM; NIST, National Institute of Standards and Technology; Qz, quartz; Kt, kaolinite; Hm, hematite; Mh, maghemite; Gb, gibbsite; Gt, goethite; Ft, feldspar; An, anatase; Mc, Muscovite.

1. Introduction

In Brazil, a country with a large territorial extension, there are different types of parent materials at distinct topography conditions in combination with variations of climate and organisms, which originate different types of soil (Jenny, 1941). It is common knowledge that the parent material directly influences the chemical, physical and mineralogical properties of the resulting soil. For instance, quartzite, which is rich in quartz and muscovite, derives soils of low fertility, coarse texture, low concentration of Fe oxides, and so forth, conversely to soils derived from basalt or gabbro (Silva et al., 2019; Poggere et al., 2018; Silva et al., 2022). Although the characteristics of the parent material are more easily recognized in lesser-weathered soils, even highly-weathered soils present some properties still related to parent materials (Kämpf and Curi, 2012).

Recent investigations of soil genesis and characterization have been improving due to technological advancement, especially the use of proximal sensors as portable X-ray fluorescence spectrometry (pXRF) and visible near-infrared diffuse reflectance spectrometer

(Vis-NIR) either separately or associated with other techniques such as X-ray diffraction (Barros and Souza et. al., 2021; Mancini et al., 2021; Silva et al., 2022). These sensors have enabled the identification and quantification of chemical elements (pXRF) and correlations with soil mineralogy (Vis-NIR) quickly, with minimal sample preparation, low cost, and without generating chemical waste (Silva et al., 2021; Viscarra Rossel et al., 2016). Such results have contributed to better understanding of pedogenesis under different conditions Bócoli et al. (2021), Grauer-Gray and Hartemink (2018), and Stockman et al. (2016).

Specifically, regarding Vis-NIR, its spectral features reflect the soil matrix. For instance, while soil organic matter (SOM) reduces the reflectance in the entire spectrum, crystalline Fe oxides such as hematite and goethite, decrease the reflectance in the visible range and cause a concavity at 400 and 850 nm (Ramos et al., 2020; Scheinost et al., 1998). Moreover, kaolinitic soils exhibit a strong absorption feature in the 2200 nm region due to the influence of hydroxyl in the kaolinite structure, while absorption features at 2265 are attributed to gibbsite (Madeira Neto et al., 2000).

Another proximal sensor that provides data related to soil mineralogy is the magnetic susceptibilimeter. This equipment quantifies the magnetic susceptibility per unit mass of soil (χ), provided by ferrimagnetic minerals such as magnetite and maghemite (Ramos et al., 2020; Souza Junior et al., 2010). This has been used for assessing relations with soil formation factors (Cervi et al., 2019), tracing the source of sediments (Liu et al., 2019; Lima et al., 2023), and for soil characterization and mapping (Silva et al., 2022; Barbosa et al., 2021).

Despite these new tools, the primary technique for identifying and quantifying soil mineralogy is X-ray diffraction (XRD). However, XRD analysis is costly, time-consuming, and generates chemical residues, which makes its use constrained in large-scale projects (Mendes et al., 2021). As pXRF and Vis-NIR, XRD also has some limitations; e.g., hematite can only be detected by XRD in contents greater than 1% by weight (Balsam et al., 2014). Other examples are the pretreatments conducted to concentrate silicates or oxides to facilitate their identification.

Given the recent successful applications of proximal sensors to multiple branches of science, a few studies have been conducted employing Vis-NIR spectra to estimate the contents of minerals (Coblinski et al., 2021; Hu et al., 2016; Poppiel et al., 2019). This new

approach uses bands of the spectra defined by minimum and maximum reflectance values at certain wavelength intervals, which correspond to minerals in soils (Szalai et al., 2013). The sensitivity of this mathematical procedure was proven by Scheinost et al. (1998), who observed that the addition of 0.05% of any of these Fe oxides to a sample of iron-free soil promoted a significant modification that could be detected and measured in the curves obtained via Vis-NIR. Deaton and Balsan (1991) concluded that Fe oxides (hematite and goethite) can be detected at concentrations lower than 0.03% by Vis-NIR. Bahia et al., (2015) reached a correlation of 0.99 between Vis-NIR and XRD data. More recently, similar results were achieved for clay minerals (Coblinski et al., 2021; Canton et al., 2021). Although studies have identified and quantified the soil mineralogy by Vis-NIR and pXRF (Jones et al., 2019), the association of Vis-NIR, pXRF and magnetic susceptibility (χ) associated with XRD to that end still require investigations.

Thus, the objective of this study was to use the pXRF, Vis-NIR, and χ in association with XRD to: a) identify the mineralogy of the sand, silt, and clay fractions of different soil profiles derived from different parent materials; b) develop prediction models to quantify the minerals present in such soils; and c) identify the best sensor data for such predictions. Our hypothesis is that: a) the quantification of elements from pXRF will determine the chemical traits between minerals of different soil particle size fractions and their change according to the degree of weathering and parent material; b) the identification and quantification of the mineralogy of the soil clay fraction based on sensor data will deliver accurate results, when compared to mineralogical quantification via XRD.

2. Material and methods

2.1 Location and soil sampling

The study area is situated between latitudes 7650808 and 7651674 mS and longitudes 500031 and 492189 mW, Zone 23K, in Lavras municipality, Minas Gerais State, Brazil. According to the Köppen classification system, the climate is categorized as Cwa (dry winter and rainy and hot summer), with an average annual temperature and precipitation of 20.4 ºC and 1,460 mm, respectively (Dantas et al., 2007).

The most common parent materials of the region consist of gneiss (leucocratic and mesocratic), gabbro, present in the form of intrusions, quartzite that predominate in the

higher altitude areas, and organic and mineral sediments found in lowlands. Soils derived from them were collected, totaling 22 soil profiles with 53 sampled horizons. Sampling was conducted in the masters soil horizons (Table 1). Then, the soils were classified at the second taxonomic level according to the US Soil Taxonomy (Soil Survey Staff, 2014) (Table 1).

Table 1 - Soils and their respective horizons and parent materials in the Lavras region, Minas Gerais, Brazil.

Parent Material	Soil Class USST[1]	Depth (cm)	Hor.	SOM[2] (dag/kg)	Parent Material	Soil Class USST*	Depth (cm)	Hor.	SOM (dag/kg)
Gneiss	Typic Dystrustept (TD1)	0 - 17	A	2.27	Mineral Sediments	Typic Endoaquent (TE)	0 - 20	A	1.41
		29 - 50	Bw	0.6			60 - 80	Cg	0.65
		50 - 70	C	0.49	Gabbro	Typic Ustorthent (TU4)	0 - 63	A	4.47
	Typic Dystrustept (TD2)	0 - 22	A	2.72			80 - 100	B	0.62
		22 - 50	Bw	1.28			100 +	C	0.56
		72 - 140	C	0.34		Anionic Acrudox (AA)	0 - 20	A	3.7
	Typic Hapludult (TH1)	0 - 8	A	4.6			60 - 80	Bo	1
		24 - 60	Bt	0.9		Rhodic Kandiudult (RK)	0 - 63	A	2.1
		79 +	C	0.39			80 - 100	Bt	0.8
	Typic Hapludox (TH2)	0 - 20	A	2		Oxic Dystrustept (OD)	0 - 5	A	0.42
		60 - 80	Bo	0.3			5 - 26	Bw	1.82
		80 +	C	0.11			26 - 47	C	1.15
	Inceptic Hapludult (IH)	0 - 20	A	2.36	Quartzite	Typic Ustorthent (TU5)	0 - 20	A	2.52
		60 - 80	B	0.44			20 - 40	C	1.19
	Xanthic Hapludox (XH1)	0 - 20	A	6.0		Xanthic Haplustox (XH2)	0 - 10	A	2.16
		40 - 60	Bo	2.0			20 - 80	Bo	0.89
	Typic Hapludult (TH3)	0 - 20	A	2.7			110 +	CB	0.45
		32 - 54	Bt	0.7		Typic Dystrustept (TD3)	0 - 18	A	1.03
		60 - 80	C	0.18			18 - 40	Bw	0.71
	Rhodic Hapludox (RH)	0 - 20	A	0.65			77 +	CB	0.12
		60 - 80	Bo	0.54		Typic Ustorthent (TU6)	0 - 22	A	1.07
	Typic Ustorthent (TU1)	0 - 7	A	7.1			22 - 43	C	0.49
		40 - 60	B	1			43 +	CR	0.09
	Lithic Ustorthent (LU1)	0 - 12	A	3.27		Lithic Ustorthent (LU2)	0 - 5	A	1.46
Organic Sediments	Typic Udifolist (TU2)	0 - 10	O	14.1			5 - 15	C	0.6
		21 - 108 +	H						
	Typic	0 - 5	A	2.65					

Organic Sediments	Ustifolist (TU3)	30 - 60	H	1.96

[1]USST- Unites States Soil Taxonomy; [2]SOM – Soil organic matter.

The soil samples were air-dried and passed through a 2 mm sieve (air-dried fine earth - ADFE), then subjected to particle size analysis by the pipette method (Gee and Bauder, 1986). To disperse the sand, silt, and clay fractions, 100 mL of NaOH 0.1 mol L^{-1} were added to 50 g of ADFE following by shaking for 16 hours. After full dispersion, the solution was passed through a 53 µm sieve to retain the sand fraction, while the clay fraction was obtained after sedimentation of the silt fraction according to Stokes' law (Gee and Bauder, 1986). After removal of the entire clay fraction by sinfonation, only the silt fraction remained. Each fraction was dried separately in an oven at 40 °C. Soil organic matter was determined via titration (Walkley and Black, 1934).

2.2 Soil analyses via pXRF

The sand, silt, and clay fractions of each horizon of the soil profiles were analyzed by pXRF to determine their chemical element contents according to Weindorf and Chakraborty (2016). For that, we used a pXRF S1 Titan 800 model (Bruker® Nano Analytics, Kennewick, WA, USA), containing a 50 kV X-ray tube, with a 20 mm^2 active area, and typical resolution <145 eV. Measurements were made in triplicate in Geoexploration mode for 60s. To verify pXRF accuracy a check sample (CS) from Bruker and two reference materials certified by the National Institute of Standards and Technology (NIST 2710a and 2711a) were analyzed. The recovery values (100 x elemental content determined via pXRF/certified content) of the elements used in this study were (CS/2710a/2711a): Al_2O_3 101/166/183; SiO_2 --/269/197; Fe 98/91/93; K_2O 100/101/107; CaO --/116/136; Ti --/81/91; Zr --/--/--. The dashes indicate that either the pXRF could not detect the element or it was not present in the certified material.

2.3 Soil analysis via Vis-NIR

The samples of the sand, silt and clay fractions for each horizon were evenly distributed into Petri dishes and scanned via a portable Vis-NIR DRS PSR-3500 spectrometer (Spectral Evolution, USA) with a spectral range of 350 to 2500 nm and

sampling interval of 2 nm. The data acquisition was performed using a contact probe with an integrated halogen light source of 5W coupled with a PSR-3500 optic fiber cable coated with metal. After analysis of five samples, the equipment was calibrated using a 12.7 by 12.7 cm white spectral on panel.

The analyses were performed in the laboratory at room temperature, where the probe for the scanning was placed vertically on the sample. The samples were scanned three times each, rotating 90° the samples at every scan. The spectral curve per sample results from the average of the three scans, and each scan averages 10 internal scans over 1.5s.

2.4 Magnetic susceptibility of soil fractions

Magnetic susceptibility (χ) per unit of mass (χlf,10^{-7} m^3 kg^{-1}) was determined at low frequency (χlf = 0.47 kHz) in triplicate in the sand, silt, and clay fractions separately using the Bartington MS2B susceptibilimeter according to the methodology described by Dearing (1999) and Poggere et al. (2018). Calculations were made via the expression χlf = (10 x k) m^{-1}, where k is dimensionless, and m is the mass of the used sample**.**

2.5 Soil X-ray diffraction (XRD) analysis

A Bruker D2 PHASER diffractometer, equipped with a LYNXEYE^{TM} fast linear module, operated with Diffract Suite ™ software was used to analyze the mineralogy of the sand, silt, and clay fractions of the samples from each horizon. The equipment emits CuKα radiation (λ = 1.541838 Å), containing a Ni filter and a 30 kV X-ray generator with 10 mA. The analyses were performed with the samples unoriented from 4 to 50° 2θ, in angle steps of 0.02° 2θ and dwelling time of 0.5 s. The positions of the reflection peaks in the grain size fractions and the reflection areas of the minerals in the clay fraction were acquired through the Diffrac.Suite^{TM} Eva software and interpreted with the aid of tables by Brindley and Brown (1980).

2.6 Spectral preprocessing of Vis-NIR data

The minerals identified via XRD for quantification were: goethite (Gt), hematite (Hm), gibbsite (Gb), kaolinite (Kt) and muscovite (Mc). Since each mineral has spectral signatures in the Vis-NIR spectrum, the pure spectra of the minerals were obtained from the spectral library of the United States Geological Survey (USGS; https:

//www.usgs.gov/labs/spec-lab). Continuous removal (CR) algorithm contributes to identifying the minerals present in soils as it normalizes the reflectance spectra by highlighting the absorption features typic of each mineral (Fang, 2018; Clark and Roush, 1984). The CR algorithm was executed with R software (R Central Development Team, Vienna, Austria) as per the Prospectr package (Stevens and Ramirez-Lopez, 2014). The absorption features of the minerals present in each soil fraction were identified by comparing the spectral absorption between the pure minerals and the average absorption spectra of the soil particle size fractions of each parent material.

The Kubelka-Munk (KM) function (Fig. 1b) that describes how the reflectance at each wavelength is determined was applied to the raw spectra of the samples (Fig. 1a):

$$f(R\infty) = \frac{k}{s} = \frac{(1 - \mathrm{R}\infty)^2}{2\mathrm{R}\infty}$$

Where K is part of the incident light absorbed (absorption coefficient), S is the part of the light scattered in the opposite direction (reflection coefficients), and R is the reflectance. Then, the second derivative of the spectrum (Scheinost et al., 1998) was calculated on the data obtained by the KM function considering the wavelength, resulting in maximum and minimum light absorption. The higher the peak of intensity, the higher the mineral concentration (Rodriguez and Fernandez, 2005).

An algorithm developed by Savitzky and Golay (1964), using 27 points, was applied to smooth the spectral curve without modifying its original shape (Fig. 1c). The Unscrambler® from CAMO Software, Inc. (Montclair, NJ, USA) software was used to process the KM function and perform the second derivative and its smoothing. Through the specific bands of the minerals in the spectral curve of the second derivative, the maximum and minimum reflectance values of goethite (Fig. 1d), hematite, kaolinite, gibbsite, and mica were identified, and the amplitude of each of these features was calculated (Sellitto et al., 2009). Each mineral's amplitude (difference between the maximum and minimum) refers to its relative quantification in the soil sample.

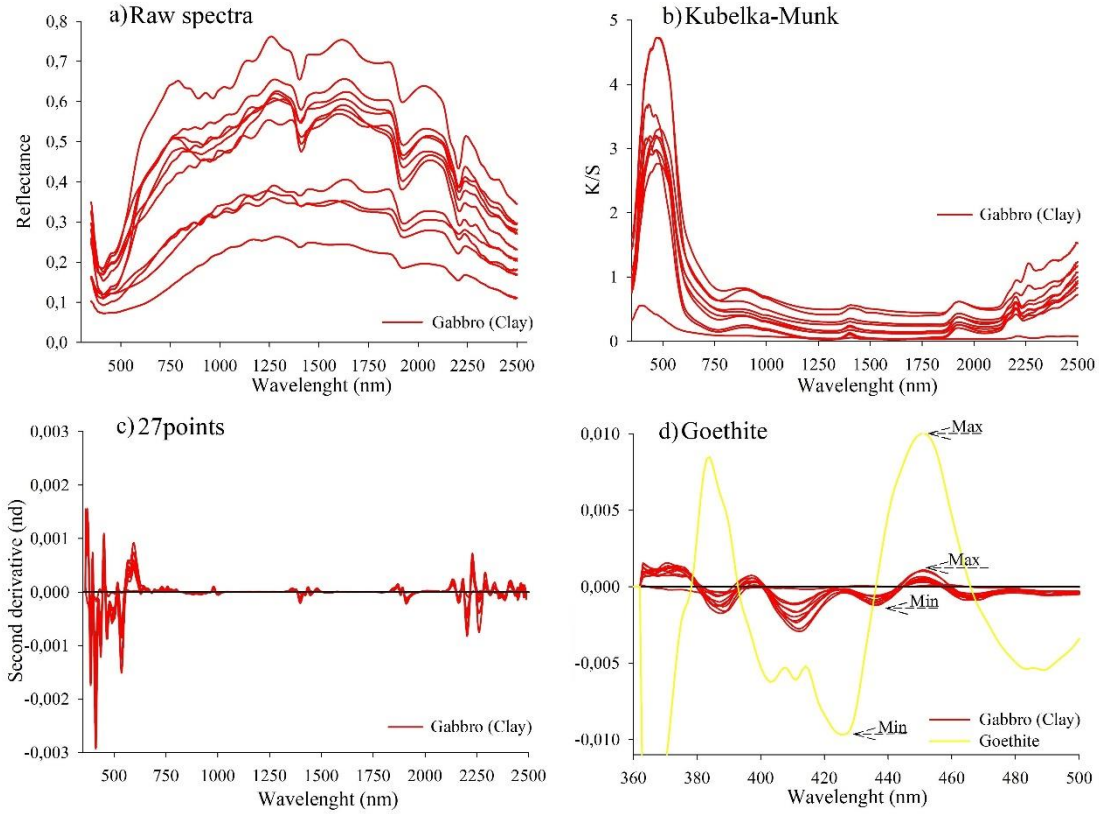

Fig. 1 - Processes performed on the raw spectra to obtain the maximum and minimum values of the second derivative. (a) Raw spectra; (b) Kubelka-Munk; c) Smoothing with 27 points; d) Identification of the maximum and minimum values in the second derivative comparing the minerals of the spectral library with the samples of the clay fraction of the soil for goethite.

2.7 Mineral prediction models

The 51 samples from clay size fraction (<0.002 mm) were used to build the prediction models for the following minerals with their respective reflection planes (hkl): Kt (001), Kt (002), Gb (002), Hm (012), Gt (110), Gt (111), Hm (110)+Mh (313), Hm (104)+Gt (130), Mc (001), Mc (020)+Kt (020) and Qz (100). Prior to the modeling, all pXRF results were centralized (centralized elemental content=(x−mean(x)) / std. dev. (x), where x is the original elemental content) and scaled (scaled elemental content=(x–mean(x)), where x is the original elemental content). Besides scaling and centralizing, there was no other transformation in the data.

The prediction of mineral contents was based on proximal sensors data (pXRF, Vis-NIR and χ), parent material information (PM), and soil texture (sand, silt, and clay contents). Regarding Vis-NIR data, the amplitude of the second derivative of Vis-NIR spectra was used: Gt (~ 410 nm), Hm (~535 nm), Gb (~2260 nm), Kt (~2160 and ~2200 nm), Mc (~2350 nm) and Mc-Kt (~1400nm). Predictions were conducted by combinations of the predictor variables, totaling 27 different prediction models. These models were created through the random forest (RF) algorithm (*ntrees* = 500, *nodesize* and *mtry* were set to default) in R software (version 4.2.1) (R Development Core Team, 2018) and the "caret" package (Kuhn, 2008). Cross-validation was performed in the entire dataset using the leave-one-out method. The prediction models were created using the following explanatory variables and their respective combinations: In order to verify the best Kt amplitude for the mineral content predictions, models with Kt (~2160 nm) and Kt (~2200 nm) were created separately, since both wavelengths are reported in the literature.

The most accurate prediction model per mineral was chosen based on the lowest root mean squared error (RMSE) (Eq. 1) and the highest coefficient of determination (R^2) values.

$$RMSE = \sqrt{\frac{1}{n}\sum_{i=1}^{n}(y_i - m_i)^2} \quad (1)$$

Where, n: number of observations, y_i: estimated value by the model, m_i: measured value by the chemical analysis.

2.8 Statistical analyses

Pearson correlation between the reflection areas of the minerals of the clay fraction obtained from XRD and the amplitude of the second derivative of the Vis-NIR spectra were calculated. The statistical procedure was performed using the R environment with RStudio (RStudio Team, 2018). For the Pearson correlation, a correlogram was generated using the corrplot package (Wei et al., 2017).

3. Results and discussion

3.1 Soil texture

The soils studied presented high variability of texture (Fig. 2) as a consequence of their parent material and degree of weathering. The clayey texture in soils developed from

gabbro was expected due to the weathering of easily weatherable primary minerals (EWPM), such as olivine, pyroxene, amphiboles, and plagioclases that constitute this rock. Similarly, some soils (A and B horizons) derived from gneiss presented predominantly clayey texture, but some of them were classified in other textural classes according to the degree of weathering and horizon.

The texture of soils developed from quartzite ranged from sandy loam to silty loam mainly due to the dominance of quartz and lower amounts of muscovite in quartzite composition. These minerals are resistant to weathering, especially in the sand fraction (Kämpf et al., 2012). The C horizon of Lithic Ustorthent and Typic Ustorthent developed from quartzite presented higher content of silt followed by sand fraction due to its proximity to the parent material. For the C horizon samples, of soils developed from gneiss, texture ranged from sandy loam to loam texture.

Regarding the soils formed from the accumulation of organic sediments, the A horizon samples presented a great variation of sand contents (up to 30%), since the profile with the highest sand content is surrounded by quartzites. For the soils developed from mineral sediments, the granulometric fractions indicated a predominance of clay for the A horizon and sand for the Cg horizon, suggesting contrasting sediment sources for the formation of this soil profile (Typic Endoaquent).

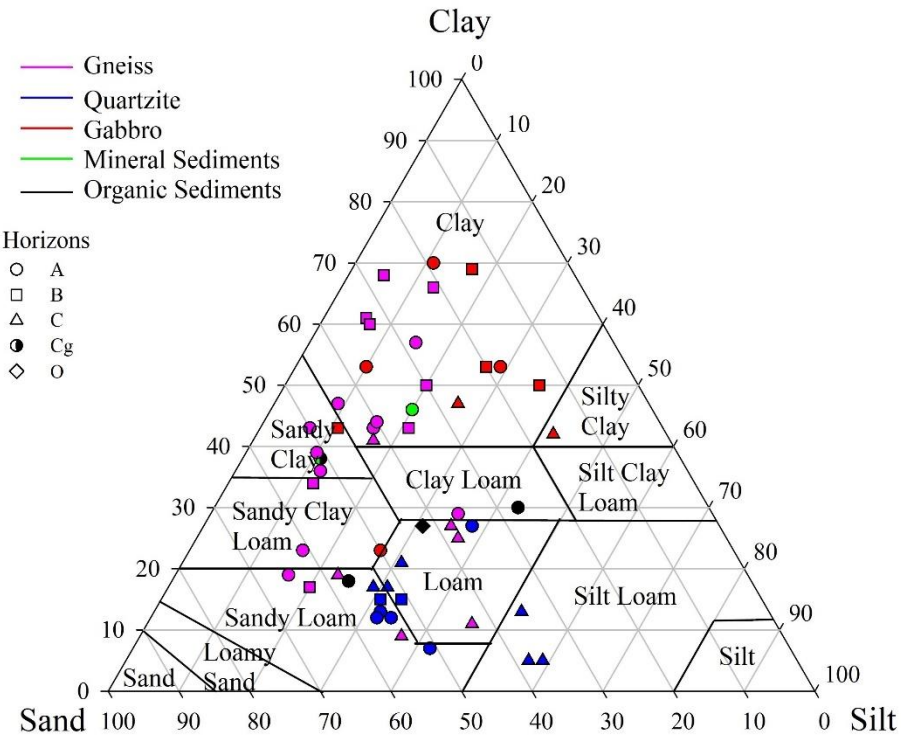

Fig. 2 - Texture of the soil samples per horizon plotted according to the USDA texture classification.

3.2 Chemical and mineralogical relations

The variation of the Si, Al, Fe, Ca, K, and Ti contents are presented in Fig. 3 per soil particle size fraction and parent material. Such variation occurs mainly due to the degree of weathering of the soil classes, parent materials and land use. These latter factors may influence the contents of elements in the soil fractions due to the application of fertilizers in cultivated areas (Andrade et al., 2021; Benedet et al., 2020).

In general, there is a decrease of the Si and Ca contents with the reduction of the size of the soil fraction. The opposite occurs for Al, Fe and K, which exhibited lower content in the coarsest fraction (sand). Ti follows the same trend with the lowest content identified in the sand fraction, except for soils developed from gabbro and gneiss.

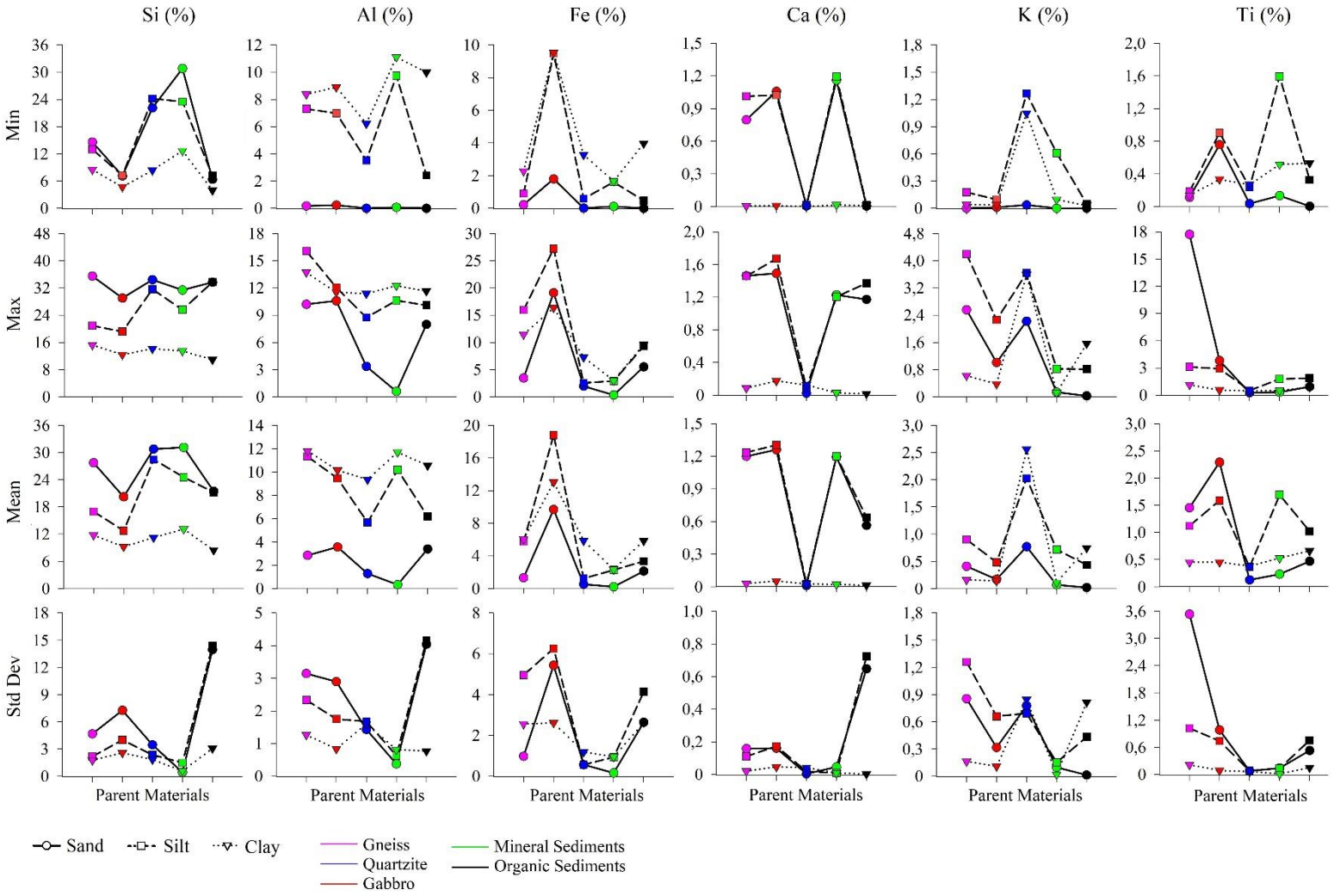
Si (%)
Al (%)
Fe (%)
Ca (%)
K (%)
Ti (%)
Min
Max
Mean
Std Dev
Parent Materials
Sand
Silt
Clay
Gneiss
Quartzite
Gabbro
Mineral Sediments
Organic Sediments

Fig. 3 - Mean, maximum, minimum, and standard deviation (Std Dev) for Si, Al, Fe, Ca, K, and Ti in the sand, silt, and clay fractions of the soils derived from gneiss, gabbro, quartzite, mineral sediments, and organic sediments.

In general, the Si content decreases from silt to clay; in this case, chemical weathering causes partial desilication of primary minerals and neoformation and concentration of secondary minerals. The silt fraction exhibits primary and secondary minerals and Fe and Al oxides. Thus, the presence of Si in this fraction is due to the neoformation of kaolinite and the persistence of quartz and muscovite that still resist in this particle size. According to Schaefer et al. (2007), kaolinite formation demands silica in solution, free drainage, humid climate, and low pH. In addition, the parent material must have feldspars and micas. The dissolution of 2:1 minerals also contributes to the formation of kaolinite.

Quartz and muscovite still persist in the clay fraction of the soils developed from quartzite, but exhibit low-intensity peaks (Fig. 4). Kaolinite can be found in the coarse fractions of younger soils derived from these parent materials and they also exhibit mica interstratification in which K retention occurs (Alves et al., 2013; Melo et al., 2002).

For the soils developed from mineral sediments, the Si in the sand and clay fractions (Fig. 3) are related to quartz and kaolinite (Fig. 4), respectively. The silt fraction of this soil exhibits a range of primary minerals such as quartz, muscovite and feldspar, in which Si is present in the crystalline structure. This mineralogy suggests that the mineral sediments are derived from the gneisses of the surrounding region.

As a result of the difference of the soil parent materials, the Si present in the sand and silt fractions of the Typic Ustifolist located in the quartzite area (Fig. 3) are quartz, mica and kaolinite in the silt fraction and only quartz in the sand fraction (Fig. 4). Conversely, for the Typic Udifolist (derived from organic sediments), kaolinite and quartz dominate the sand and silt fractions Kaolinite is the only Si-bearing mineral in the clay fraction in these two Histosols.

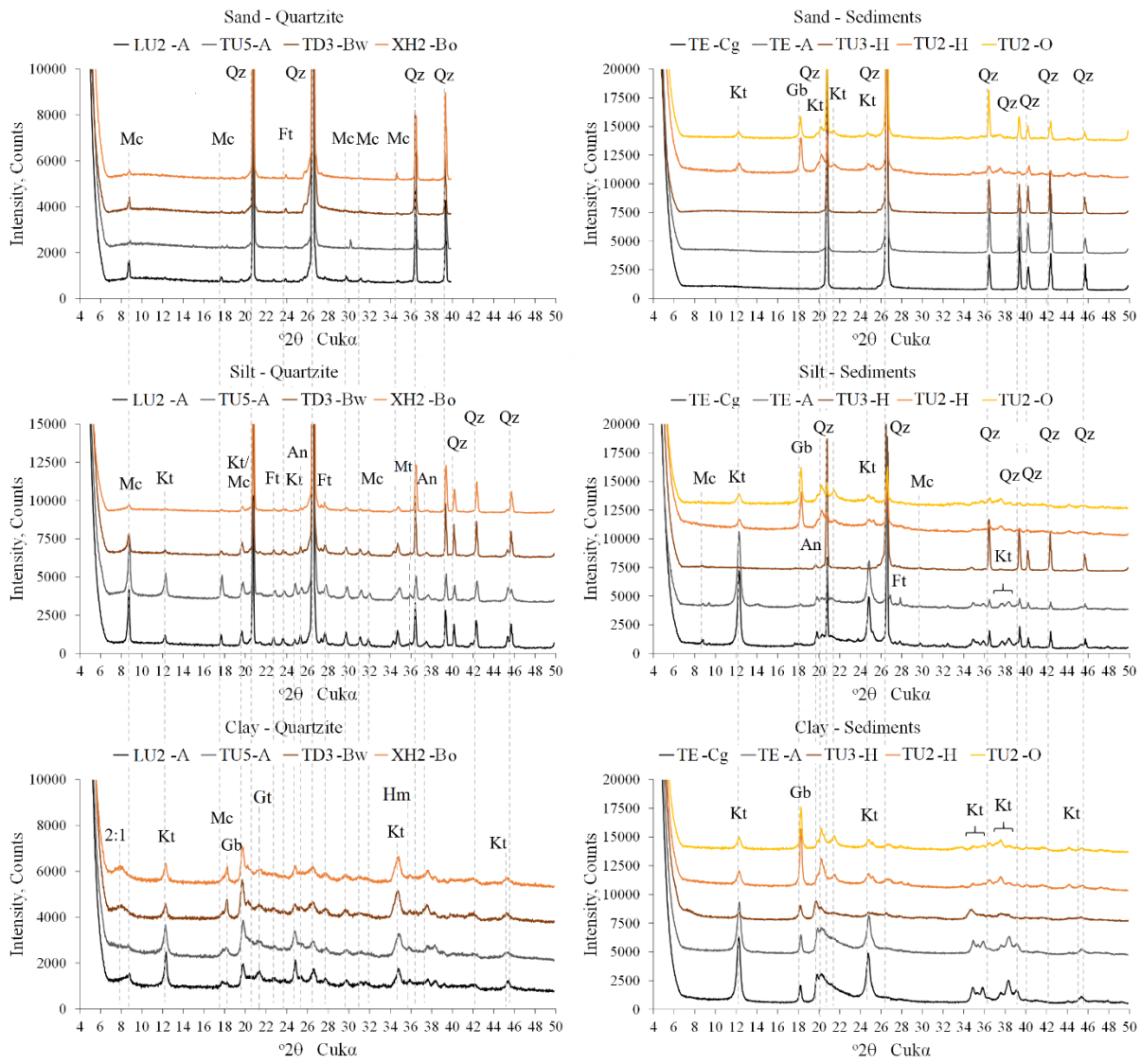

Fig. 4 - X-ray diffractogram of the sand, silt, and clay fractions of Lithic Ustorthent (LU2), Typic Ustorthent (TU5), Typic Dystrustept (TD3) and Xanthic Haplustox (XH2) derived from quartzite; Typic Endoaquent (TE) derived from mineral sediment; Typic Udifolist (TU2) and Typic Ustifolist (TU3) derived from organic sediments. Kt – Kaolinite; Mc – muscovite; Gb - gibbsite; Ft - feldspar; An - anatase; 2:1 - 2:1 minerals; Qz - quartz.

Al is mainly concentrated in kaolinite and gibbsite in the clay fraction of the soils. Its content decreases with the increase in the particle size. The highest average Al contents were observed in the soils developed from gneiss, gabbro, and mineral sediment, which present greater contents of clay. Gneiss and gabbro are rich in feldspars, which contain Al, in addition to muscovite, biotite, and neoformed kaolinite (Melo et al., 2016). In the silt and sand fractions of these soils, feldspars, muscovite, kaolinite, and gibbsite were observed in

most soils, except for the sand fraction of the gabbro-developed soils (absence of muscovite) (Fig. 5).

Total desilication caused by intense weathering, leaching of the bases, and Si cations from solution favors the formation of gibbsite, an Al oxide observed in high concentration in highly weathered soils such as Oxisols (Kämpf et al., 2016a). The formation of gibbsite can occur directly from the total desilication of primary minerals, mainly feldspars, or it can result from kaolinite weathering, both in a free-draining environment (Kämpf et al., 2016b).

Quartz is the only mineral observed in the sand fraction of the Typic Endoaquent, so the Al present in the silt and clay fractions is related to kaolinite, gibbsite, and muscovite (Fig. 4). Although quartz and muscovite are observed in the silt fraction, their proportion is low in relation to the other granulometric fractions in this soil class. This fact in addition to the presence of only quartz in the sand fraction, and kaolinite and gibbsite in the clay fraction, confirms the advanced chemical weathering of these mineral sediments. Guimarães et al. (2013) found that the presence of 2:1 clay such as vermiculite, illite, and montimorilonite associated which kaolinite 1:1 in soils developed from mineral sediments suggests a less advanced degree of pedogenetic development.

In the soils developed from quartzite and mineral sediments, the low average contents of Fe in the coarse fractions indicate the low concentration of Fe-bearing primary minerals. In the sand fraction of the Typic Endoaquent, Fe was not detected, and the average contents of the clay and silt fractions are low and very similar. This soil is formed under prolonged or periodic water saturation conditions, causing the reduction of Fe^{3+} in the structure of the oxide to Fe^{2+} under an anaerobic environment coupled with microbial activity (Vidal-Torrado and Ferreira, 2017). The absence of Fe oxides in the diffractograms of the particle size fractions is due to their removal due to the anaerobic environment (Kämpf et al., 2012).

In the quartzite developed soils, no Fe - oxide was found in the sand fraction, while in the silt fraction, a discrete peak of magnetite is observed (Fig. 4). In the clay fraction, goethite and hematite are present. The low Fe oxide reflections observed in the clay fraction are a consequence of the low Fe concentration in the quartzite.

The low Fe oxides content of the Histosols results from their complexation of organic matter. Furthermore, the high concentration of organic compounds and the poorly drained environment forms Fe oxides of low crystallinity (Benites et al., 2007; Bigham and Fitzpatrick, 2002). This fact explains the absence of Fe oxide in the diffractogram of the Typic Udifolist from the native forest area; however, discrete peaks of goethite are observed

only in the clay fraction of the Typic Ustifolist in the quartzite area, also reported by Araújo et al. (2014).

In the clay fraction, although hematite and goethite predominate in the silt and clay fractions (Fig. 5), it is also possible to observe the presence of maghemite, a secondary Fe oxide derived from the oxidation of magnetite. Some soils derived from gneiss conserved primary and secondary Fe-bearing minerals in the silt fraction.

The Ca content in the clay fraction is low in all the studied soils. The increase of Ca in the coarse fractions in the developed soils of gabbro and gneiss occurs due to the presence of Ca in the structure of feldspar, pyroxenes and amphiboles (Melo et al., 2016).

The high content of Ti found in the soil developed from gneiss, mainly in the Inceptic Hapludult, may be a consequence of isomorphic substitution besides inclusions of rutile and ilmenite (Taboada et al., 2006). The highest average Ti contents were found in soils developed from gabbro due to the likely presence of biotite, titanite and other accessory minerals in its constitution (Queméneur et al., 2002). In addition, Ti shows a high correlation with Fe ($r = 0.93$) (Taboada et al., 2006). Based on the results, the parent materials of soils derived from mineral sediments are also poor in Ti-bearing minerals.

The highest averages of Ti contents were found in the silt fraction of both Typic Ustifolist and Typic Udifolist. It refers to the presence of anatase (Fig. 4) and the fact that Ti may replace Al in the structure of kaolinite (Malengreau et al., 1995). The absence of anatase in the diffractograms can occur since the peaks of this mineral and kaolinite overlap (Malengreau et al., 1995).

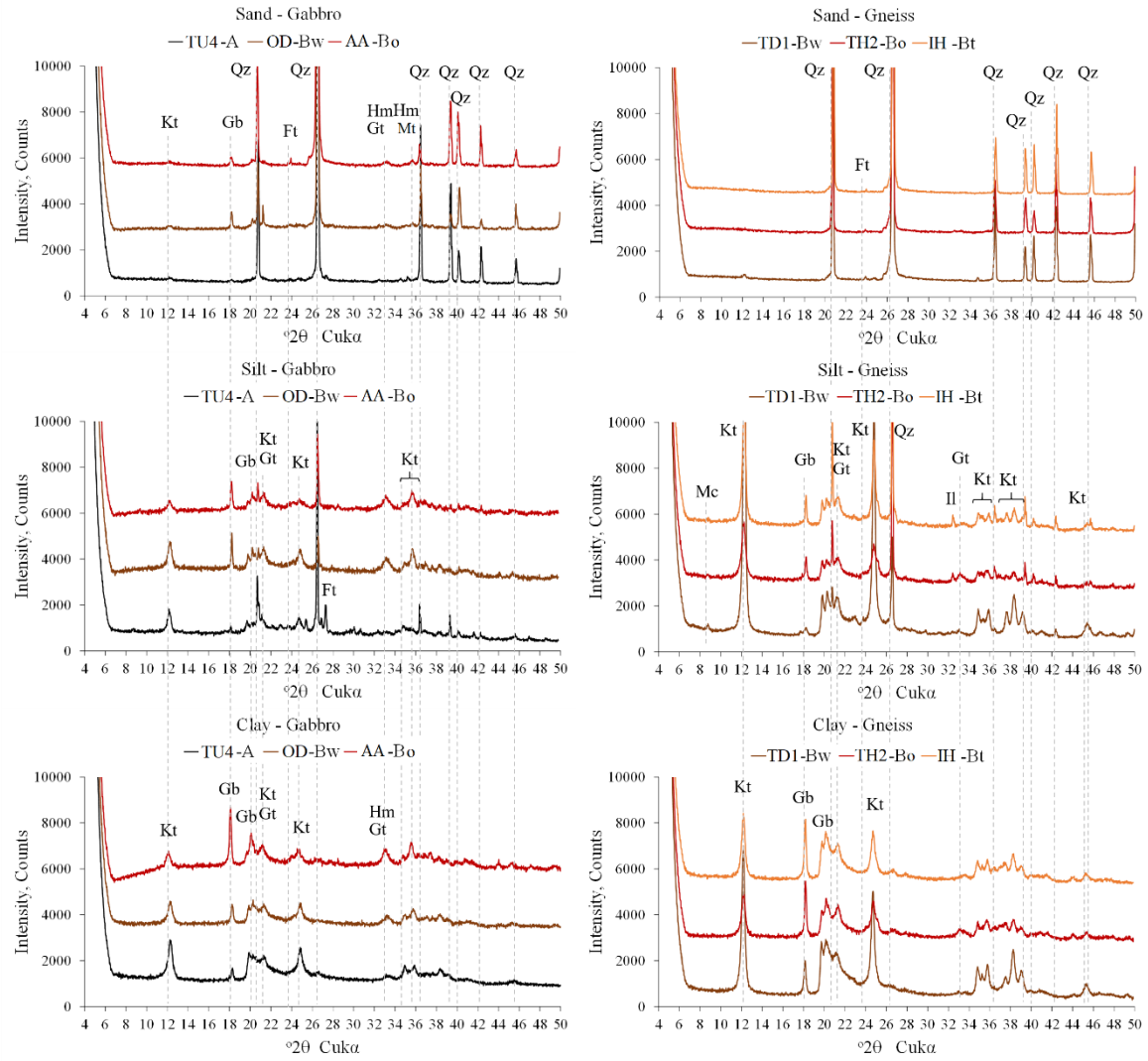

Fig. 5. Diffractogram of sand, silt and clay fractions of the studied soils. TU4 - Typic Ustorthent, OD - Oxic Dystrustept and AA - Anionic Acrudox derived from gabbro; TD1 - Typic Dystrustept, IH - Inceptic Hapludult and TH2 - Typic Hapludox derived from gneiss; Kt - Kaolinite, Mc - muscovite, Gb - gibbsite, Gt - goethite, Hm - hematite, Fp - feldspar, Qz - quartz, Mh - maghemite, Il - Ilita.

3.2 Magnetic susceptibility of soil granulometric fractions

The statistical analyses of the magnetic susceptibility (χ) of the soil fractions are shown in Table 2, and considerable differences can be observed. Among the soils studied, the χ values obtained for those derived from quartzite and organic and mineral sediments were considerably lower. In contrast the average χ value obtained in the sand, silt and clay fractions of the soils developed from gabbro was approximately 10 times greater than the average value for the soils derived from gneiss. This disparity is related to the differences in

the concentration of ferrimagnetic minerals in the parent material and, consequently, in the soil particle size fractions.

Soils derived from gabbro presented maghemite in the clay fraction (Fig. 5) and may present magnetite in the sand fraction (Mello et al., 2020), generating high values of χ. Studies carried out in soils developed from basalt, a rock with the same mineralogical constitution as gabbro, but with fine texture, found the dominance of magnetite in the coarse fractions (Da Costa et al., 1999; Curi and Franzmeier, 1987). However, the sand and silt fractions of the soils developed from the other parent materials showed low χlf; magnetite was not detected by XRD, which demonstrates the ability of χ to complement XRD analysis regarding the presence of ferrimagnetic minerals.

The clay fraction of soils developed from gneiss and gabbro also exhibits the highest values for χlf (9.60 and 107.62 x 10^{-7} m^3 kg^{-3} respectively) when compared to the other soils. Camelo et al. (2017) found a strong correlation between clay and χ for soils derived from parent materials rich in Fe and the opposite trend for soils developed from quartzite, similar to our study.

Table 2 - Mean, maximum, minimum and standard deviation of the magnetic susceptibility at low frequency (χ) of the sand-silt and clay fractions of the studied soils.

		χ (10^{-7} m^3 kg^{-3})		
Parent Material	Statistics	Sand	Silt	Clay
Gneiss	Min	0.10	0.17	0.44
	Max	17.01	40.38	74.67
	Mean	4.76	11.05	9.60
	Std Dev	5.05	13.31	16.15
Gabro	Min	5.62	2.53	7.53
	Max	100.41	278.27	245.98
	Mean	41.68	115.38	107.62
	Std Dev	36.37	97.61	87.20

Quartzite	Min	0.10	0.10	0.51
	Max	5.79	2.00	5.12
	Mean	2.86	0.84	2.43
	Std Dev	1.92	0.56	1.40
Organic Sediments	Min	0.44	0.30	0.26
	Max	12.97	12.14	0.62
	Mean	4.76	3.44	0.44
	Std Dev	7.11	5.81	0.26
Mineral Sediments	Min	0.09	1.20	0.82
	Max	0.19	1.21	2.23
	Mean	0.14	1.21	1.41
	Std Dev	0.07	0.01	0.69

3.3 Spectral behavior of soil sand, silt and clay fractions via Vis-NIR

3.3.1 Sand Fraction

The spectral curves of the sand, silt, and clay fractions of the studied soils showed different behaviors relatable to their parent materials (Fig. 6). This difference is due to each parent material causing different soil physical, chemical, and mineralogical properties that are reflected on the Vis-NIR spectra (Demattê et al., 2004). The reflection intensity of the sand fraction spectra increases in the following order of parent materials: organic sediments < gabbro < gneiss < mineral sediments < quartzite. This happens because quartz stands out as the main mineral in quartzite-derived soils, increasing the reflectance intensity of the spectral curve (White et al., 1997; Demattê et al., 2002).

The curves exhibit a concave and ascending behavior in the visible region (350 - 750 nm). According to Viscarra Rossel et al., (2011), in the region between 400 and 1000 nm, the features related to Fe oxides are observed, while in the region between 1000 and 2500 nm, the absorption features of water and clay minerals are noticed; conversely, organic matter influences the absorption of light in the whole spectrum.

Among the developed quartzite soils, the Typic Dystrustept and Xanthic Haplustox samples presented a flatter spectrum between the wavelengths 700 and 1900 nm, which can

also be observed for the Typic Endoaquent and Typic Ustifolist. According to Formaggio et al. (1996), soils with texture varying from sandy to loam, with low Fe oxides and SOM content, present spectral curves in this shape.

The difference in absorption features can be observed mainly between the spectra of quartzite and gneiss soils, where more developed soils have a smaller valley at 1400 and 1900 nm compared to younger soils with larger mica crystals.

The variation in Fe oxides and organic matter content delivered different shapes to the spectral curves, as seen in gabbro and gneiss-derived soils (greater Fe content). The lower reflectance observed in the sand fraction of developed gabbro soils results from the presence of opaque minerals that resisted to weathering (Demattê et al., 2015; Demattê et al., 2003).

3.2.2 Silt fraction

The spectral curves of the silt fraction for quartzite developed soils present the highest reflectance (Fig. 6). The absorption feature at 850 nm is evident only for the C and CR horizons of the Typic Ustorthentand in gabbro- and gneiss-derived soils due to the higher Fe oxides content. Still, in the Typic Ustorthent derived from quartzite, it is possible to verify the presence of a smooth concavity between 600 and 700 nm, referring to goethite. According to Scheinost and Schwertmann, (1999) goethite exhibits a weak concavity between 600 and 750 nm.

The characteristic of kaolinite absorption in 1400 nm was observed in most of the studied soils. However, the presence of mica explains the greater depth of the absorption feature in the C horizon of the Typic Hapludult, Typic Dystrustept, Typic Hapludox, B horizon of the Inceptic Hapludult derived from gneiss, and the C and CR horizons of the Typic Ustorthent developed from quartzite. These two parent materials have muscovite in their constitution, which make it to remain in the silt fraction even in more weathered soils.

For soils developed from gneiss, gabbro, and mineral sediments, the kaolinite contents in the silt fraction in relation to the sand fraction, results in a profound and defined absorption feature. As in the sand fraction, in the silt fraction, the mica absorption feature stands out at 2200 nm in the quartzite-derived soils due to the absence of the typical kaolinite step.

3.2.3 Clay fraction

In the clay fraction, soils derived from organic sediments have lower reflectance (Fig. 6). The SOM interferes with the shape and reflectance along the entire spectral curve and can hide features related to other soil constituents, such as Fe oxides (Pearlshtien and Ben-Dor, 2020). In this fraction, the absorption features referring to Fe oxides between 350 and 1000 nm are absent in soils developed from organic sediments. The spectral curve assumes an ascending concave shape different from the other soils studied up to 1370 and 1820 nm for the Typic Ustifolist in the quartzite area and the Typic Udifolist. The Typic Udifolist in the forest area contains 141 g kg^{-1} of SOM, while the quartzite area presents 26.5 g kg^{-1} of SOM. High levels of SOM cause the disappearance or attenuation of kaolinite features, as observed at 2200 nm, and when higher than 20 g kg^{-1}, they mask the characteristics of Fe oxides (Dalmolin et al., 2005; Demattê et al., 1998).

The spectral curves for the gabbro- and gneiss-derived soils reveal absorption corresponding to Fe oxides between 400 and 600 nm and 700 and 900 nm. In gneiss-derived soils, there is a decrease in absorption related to goethite around 420 nm. However, the wavelengths around 900 nm in gabbro-derived soils are more intense due to the higher Fe oxides content.

The kaolinite promoted absorption features at 1400 and 2200 nm in the soils derived from gabbro and gneiss, which were more intense in the latter. The more intense desilification in soils derived from gabbro causes the formation of gibbsite (Kämpf et al., 2016b), which is confirmed by the more intense absorption feature at 2260 nm corresponding to gibbsite.

The spectral curve of the clay fraction of the Typic Endoaquent presents a different shape than the curves of the sand and silt fractions. This curve presents an ascending form up to 1200 nm, and the Fe oxides absorption features between 700 and 900 nm do not appear. This corroborates the lowest Fe contents of Typic Endoaquent among the soils studied.

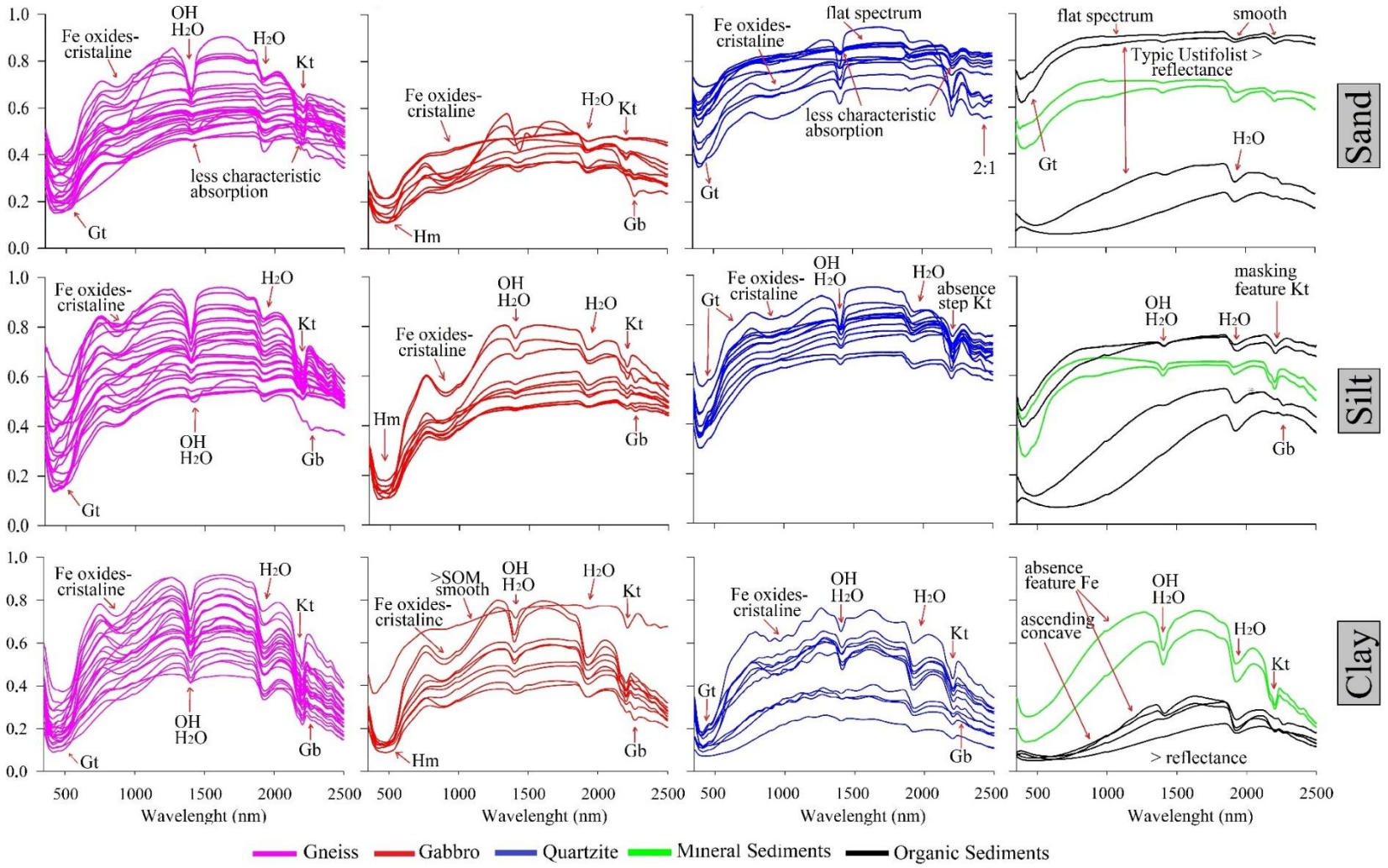
Fe oxides-cristaline
OH H2O
H2O
Kt
less characteristic absorption
Gt
Hm
Gb
flat spectrum
2:1
smooth
Typic Ustifolist > reflectance
absence step Kt
masking feature Kt
>SOM smooth
absence feature Fe
ascending concave
> reflectance
Sand
Silt
Clay
Wavelenght (nm)
Gneiss
Gabbro
Quartzite
Mineral Sediments
Organic Sediments

Fig. 6 - Spectral curves of the sand, silt, and clay fractions of the horizons of the studied soils according to their source materials: gneiss, gabbro, quartzite, mineral sediments, and organic sediments. Kt - Kaolinite, Mc - muscovite, Gb - gibbsite, Gt - goethite, Hm - hematite.

3.4 Correlation between Vis-Nir and X-ray diffraction data

The correlation between the amplitudes of the second derivative of the bands associated with each mineral found in the Vis-Nir spectra and the respective areas of the reflections of these minerals calculated from the XRD was performed via a correlogram (Fig. 7). The areas of Kt-xrd (001 and 002) were positively correlated with the Kt-Vis-Nir amplitudes, especially Kt-Vis-Nir (2160), r = 0.44 and r = 0.49, respectively. Positive correlations were noticed between Gb-xrd (002) and Gb-Vis-Nir (2260) (r = 0.63); between Hm-xrd (012) and Hm-Vis-Nir (535) (r = 0.71); and Hm+Gt-xrd and Hm-Vis-Nir (535) (r = 0.85). Conversely, the correlation between Gt-Vis-Nir (410) and Gt-xrd (110) was negative (r = -0.31) and close to zero with Gt-xrd (111) (r = 0.08). Mc-Vis-Nir (2350) correlated positively with Mc-xrd (r = 0.73), Mc+Kt-xrd (r = 0.82) and with the area of Qz-xrd (110) (r = 0.67). The strong and positive correlations found between the methods indicate the amplitude of the second derivative may help quantify soil minerals. The low accuracy in estimating Gt is associated with overlapping with secondary Hm wavelengths (Scheinost et al., 1998).

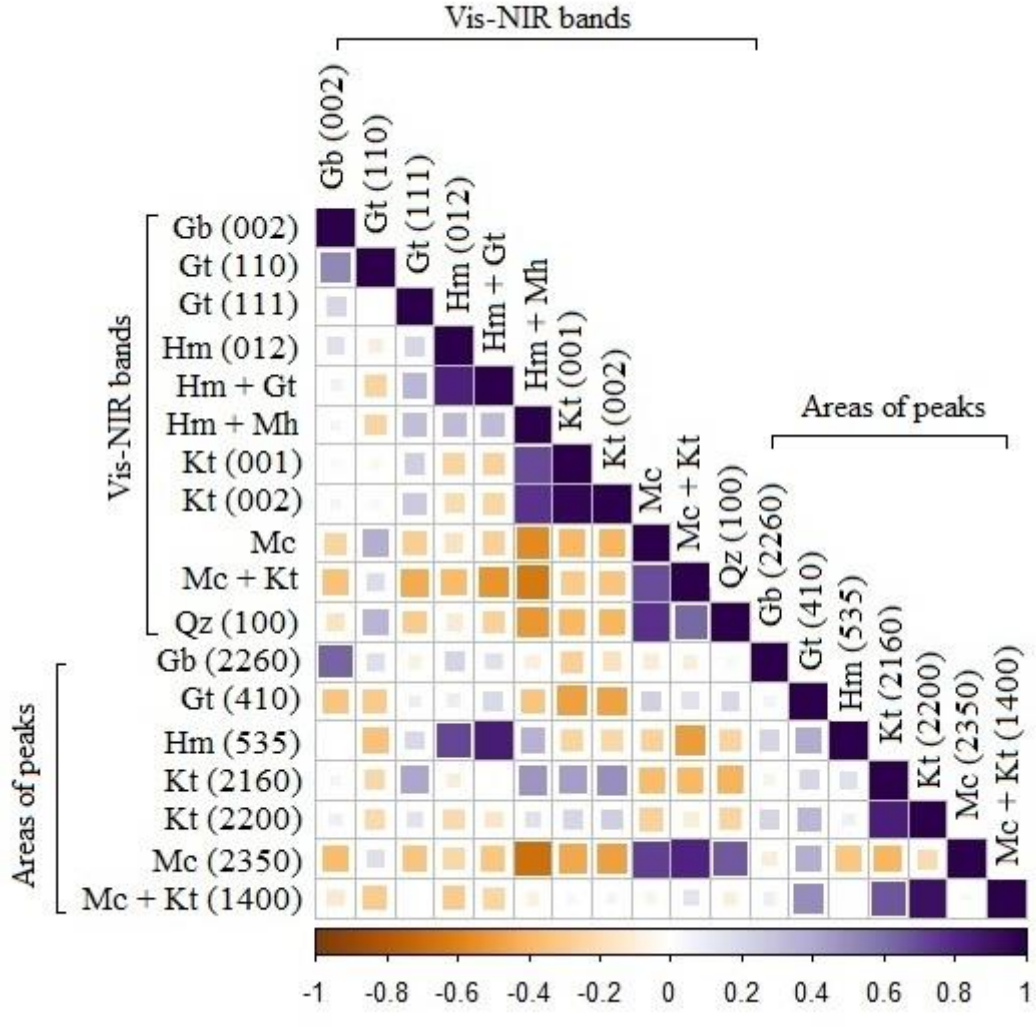

Fig. 7 - Correlograms of the bands associated with each mineral found in the Vis-Nir spectra: Gb (2260); Gt (410); Hm (535); Kt (2160); Kt (2200); Mc (2350); Mc+Kt (1400) and their respective areas in the XRD: Gb (002); Gt (110); Gt (111), Hm (012); Hm+Gt; Hm+Mh; Kt (001); Kt (002); Mc; Mc+Kt; Qz (110). Kt - Kaolinite, Mc - muscovite, Gb - gibbsite, Gt - goethite, Hm - hematite, Qz - quartz. The bluer the square, the greater the positive correlation; the more orange the square, the greater the negative correlation.

3.4 Prediction of minerals of the clay fraction

Table 3 shows the performance of the best models created for predicting the content of minerals identified via XRD. The prediction models presented discrepant RMSE and R^2 values, according to the variables used (pXRF, Vis-NIR, χ, parent material, and texture). It is important to mention that there is some interference between the Hm peaks with Gt (Hm+Gt) and Mh (Hm+Mh) and between Mc and Kt (Mc+Kt) peaks, making it difficult to differentiate between them in the XRD. In addition, for the models that Vis-NIR variables

are present, the amplitude of the second derivative of Kt (~2160) was used, as it performed better than the models using Kt (~2200).

Table 3 - Performance of the best models created to predict the content of minerals determined via X-ray diffraction using the, pXRF, Vis-NIR, parent material (PM), magnetic susceptibility (χ), and texture as predictor variables. RMSE (cps/deg) – Root mean square error. R^2 - coefficient of determination.

Mineral (XRD)	Predictor variables	RMSE (cps/deg)	R^2
Gb (002)	pXRF, Vis-NIR, PM	1.83	0.52
Gt (110)	pXRF, Vis-NIR	0.47	0.15
Gt (111)	pXRF, texture, χ , PM	0.72	0.45
Hm (012)	pXRF, Vis-NIR, texture, χ	0.04	0.60
Hm+Gt	pXRF, Vis-NIR, χ	0.27	0.83
Hm+Mh	χ, PM	0.33	0.74
Kt (001)	pXRF, χ , PM	4.20	0.74
Kt (002)	pXRF, PM	2.46	0.79
Mc (001)	pXRF, PM	0.42	0.71
Mc+Kt	pXRF, PM	0.81	0.78
Qz (100)	pXRF, PM	0.45	0.45

model generated using Kt-Vis-Nir (~2160nm); cps, count per second; deg, degree.

The model created for the prediction of Hm-xrd (012) showed the lowest RMSE = 0.04 cps/deg and R^2 = 0.6; however, when Hm coincides with Gt (Hm+Gt-xrd) and Mh (Hm+Mh-xrd), the values for R^2 increase considerably (RMSE = 0.27 cps/deg and 0.33 cps/deg, R^2 = 0.83 and 0.74, respectively), demonstrating a good performance for their estimation. Reasonable results were found for Gb-xrd (002) (RMSE = 1.83 cps/deg, R^2 = 0.52) and Qz-xrd (100) (RMSE = 0.45 cps/deg; R^2 = 0.45). Un accurate results were found for the prediction of Gt-xrd (110) and Gt-xrd (111) (RMSE = 0.47 cps/deg and 0.72 cps/deg, R^2 = 0.15 and 0.45).

The best prediction models occurred for Kt-xrd (001 and 002) (RMSE = 4.20 cps/deg and 2.46 cps/deg, R^2 = 0.74 and 0.79, respectively), Mc-xrd (RMSE = 0.42 cps/deg, R^2 = 0.71) and Kt+Mc-xrd (RMSE = 0.81 cps/deg, R^2 = 0.78). The presence of pXRF and parent material as predictor variables were essential to the predictions, since the mineralogy of soils is intrinsically linked to the parent material, even for very weathered soils (Curi and Franzmeier, 1987), and the element content obtained by pXRF (Silva et al., 2018).

With intense weathering, the total or partial leaching of silica leads to low Si contents in the clay fraction, which is distributed between the structures of quartz and kaolinite, explaining the low predictive ability of the models for Qz-xrd (110) of the clay fraction. In contrast to Si, Al and Fe are concentrated in the clay fraction and their contents vary among the samples due to differences in the degree of weathering stage and parent materials. The worse performance for predicting Gb-xrd (002) and Gt-xrd (110 and 111) may be related to Al and Fe being also part of the Kt and Hm structures, respectively, which may have confused the models when using pXRF data as prediction variables. Moreover, environment with intense weathering, soil class, parent material and acidic pH that makes Al available, facilitates the substitution of Fe that occurs in greater amounts in Gt than in Hm, (Fitzpatrick and Schwertmann, 1982; Curi and Franzmeier, 1987; Bigham and Fitzpatrick, 2002). Al also influences the intensity and position of the Gt peak in the spectral curves (Jiang et al., 2013), so all these Al-related events may have negatively influenced the Gt prediction models. Regarding the second derivative of Vis-NIR spectra data, were important variables for the prediction of Gt-xrd (110), Hm-xrd (012) and Gb-xrd (002).

In accordance with Fernandes et al. (2004) the amplitude of the spectra can successfully predict the contents of Hm-xrd (R^2 = 0.94) and Gt-xrd (R^2 = 0.63), while the poor capacity of Gt prediction is related to the presence of secondary bands of Hm overlapping the Gt. The same occurs with Gb and Kt, since their absorption bands may be neighboring, very close and overlapping, interfering in the intensity of absorption of Vis-NIR. Even though these interferences occur in the absorption features related to Gt and Gb, the amplitude positively influenced the model. The χ and the pXRF data stood out in the models for predicting Fe oxides.

3.4 Importance Variables

The importance of the variables for the best prediction models are shown in Fig. 8. The greater the value of %IncMSE, the greater the importance of the variable for the prediction model (Gonzalez et al., 2015). For predicting Gb-xrd (002) contents, the Vis-Nir amplitude of Gb-Vis-Nir (2260) was the most important variable. In general, K content obtained by pXRF was very important for the prediction of Gb-xrd (002) and Gt-xrd (110) and Gt-xrd (111). K, as well as Si, present dynamic behavior in soil that can be leached and

correlate negatively with the clay fraction and with Al and Fe oxides (Silva et al., 2022). During weathering, the loss of K and the desilification of Si facilitate the neoformation of Gb and Fe oxides. The Fe and Si contents (mainly), the χ and the amplitude of Hm stood out for the prediction of Hm-xrd (012) and Hm+Gt-xrd. One of the conditions for the formation of Hm in detriment of Gt is the high Fe available contents that correlate positively with χ and negatively with Si.

The amplitude of Hm-Vis-Nir and the content of Fe oxides were important predictors of the Hm-xrd content and the lower accuracy found for the estimation of Gt-xrd through the amplitude was probably due to the interference of the secondary bands of Hm (Fernandes et al., 2004). For Hm+Mh-xrd, a contrary condition to Hm-xrd (012) and Hm+Gt-xrd was observed, since quartzite with low Fe contents and consequently low χ, excelled the degree of importance. The Al, Fe, Si contents and the parent material were important for the prediction of Kt-xrd (001) and Kt-xrd (002).

The combination of the data obtained by pXRF and parent material was adequate for prediction of clay-sized mineral contents, as they appear in most of the models. The models built for kaolinite, hematite and mica presented the best accuracies. These results demonstrate that this data set is able to provide robust predictions for content of some clay-sized minerals.

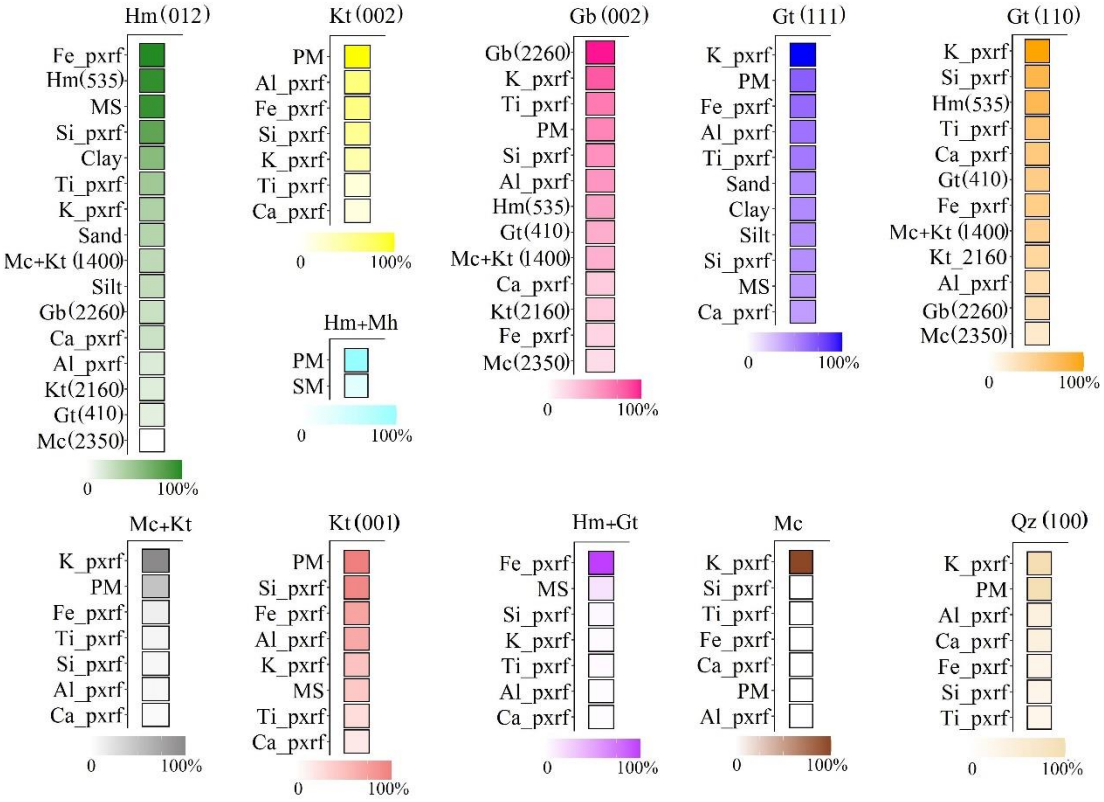

Fig. 8 - The importance of the variables for the best prediction models for the minerals Kt (001); Kt (002); Gb (002); Hm (012); Gt (110); Gt (111); Hm + Mh; Hm + Gt; Mc (002); Mc +Kt and Qz (100), in decreasing order of importance. Kaolinite (Kt), muscovite (Mc), gibbsite (Gb), goethite (Gt), hematite (Hm), quartz (Qz).

4. Conclusions

The studied soils developed from different parent materials have distinct mineralogy, elemental contents and texture. The elemental data of the portable X-ray fluorescence spectrometer and the magnetic susceptibility were able to identify variations of the soil particle size fractions according to the soil parent material. Moreover, the spectral curves of the visible near-infrared spectrometer and the X-ray diffraction were relatable, confirming that the combined use of sensor data and X-ray diffraction enhanced the understanding of the pedogenetic processes related to soil mineralogy.

The best prediction models for the content of minerals were obtained for Hm (012), Hm (104)+Gt (130), Hm (110)+Mh (313), Kt (001), Kt (002), Mc (001) and Kt (020)+Mc (020). The most important variables in almost all models were portable X-ray fluorescence

spectrometer and parent material data, which may drastically reduce the time needed to determine mineral contents in soils. More studies are encouraged to evaluate the prediction of mineral contents, especially regarding silt and sand fractions (not evaluated herein).

References

Alves, M.J.F., Melo, V. de F., Reissmann, C.B., Kaseker, J.F., 2013. Reserva mineral de potássio em Latossolo cultivado com Pinus taeda L. Rev. Bras. Ciência do Solo 37, 1599–1610. https://doi.org/10.1590/S0100-06832013000600016.

Andrade, R., Silva, S.H.G., Weindorf, D.C., Chakraborty, S., Faria, W.M., Guilherme, L.R.G., Curi, N., 2021. Micronutrients prediction via pXRF spectrometry in Brazil: Influence of weathering degree. Geoderma Reg. 27, e00431. https://doi.org/10.1016/j.geodrs.2021.e00431.

Araujo, M.A., Pedroso, A.V., Amaral, D.C., Zinn, Y.L., 2014. Paragenese mineral de solos desenvolvidos de diferentes litologias na região sul de Minas Gerais. Rev Bras Cienc do Solo 38, 11–25. https://doi.org/10.1590/S0100-06832014000100002.

Bahia, A.S.R.d.S., Marques, J., Siqueira, D.S., 2015. Procedures using diffuse reflectance spectroscopy for estimating hematite and goethite in Oxisols of São Paulo, Brazil. Geoderma Reg. 5, 150–156. https://doi.org/10.1016/j.geodrs.2015.04.006.

Balsam, W., Ji, J., Renock, D., Deaton, B.C., Williams, E., 2014. Determining hematite content from NUV/Vis/NIR spectra: Limits of detection. Am. Mineral. 99, 2280–2291. https://doi.org/10.2138/am-2014-4878.

Barbosa, J.Z., Poggere, G., Silva, S.H.G., Mancini, M., Motta, A.C.V., Marques, J.J.G. de S. e. M., Curi, N., 2021. National-scale spatial variations of soil magnetic susceptibility in Brazil. J. South Am. Earth Sci. 108. https://doi.org/10.1016/j.jsames.2021.103191.

Barros and Souza, A., Demattê, J.A.M., Bellinaso, H., Mello, D.C. de, da Silva Lisboa, C.J., de Oliveira Mello, F.A., Marques, K.P.P., de Resende, M.E.B., Reis, J.V., Mancini, M., Silva, S.H.G., Curi, N., 2021. A sensors-based profile heterogeneity index for soil characterization. Catena 207. https://doi.org/10.1016/j.catena.2021.105670.

Benedet, L., Faria, W.M., Silva, S.H.G., Mancini, M., Demattê, J.A.M., Guilherme, L.R.G., Curi, N., 2020. Soil texture prediction using portable X-ray fluorescence spectrometry and visible near-infrared diffuse reflectance spectroscopy. Geoderma 376, 114553. https://doi.org/10.1016/j.geoderma.2020.114553.

Benites, V.M., Schaefer, C.E.G.R., Simas, F.N.B., Santos, H.G., 2007. Soils associated with rock outcrops in the Brazilian mountain ranges Mantiqueira and Espinhaço. Rev. Bras. Botânica 30, 569–577. https://doi.org/10.1590/S0100-84042007000400003.

Bigham, J.M., Fitzpatrick, R.W., Schulze, D.G., 2002. Iron Oxides. In: Soil Mineralogy with Environmental Applications. Madison, pp. 323–366. https://doi.org/10.1515/9783110289039.351.

Bócoli, F.A., Santos, W.J.R. dos, Silva, S.H.G., Teixeira, A.F. dos S., Mancini, M., Curi, N., 2021. Study of an abnormal occurrence of Oxisols in strongly undulated relief in the south of Minas Gerais, Brazil, with support of pXRF and geomorphology. Ciência e Agrotecnologia 45. https://doi.org/10.1590/1413-7054202145018121.

Brindley, G.W., Brown, G., 1980. Crystal structures of clay minerals and their X-ray identification. Mineralogical Society of Great Britain and Ireland, London. https://doi.org/10.1180/mono-5.

Camelo, D. de L., Ker, J.C., Fontes, M.P.F., Corrêa, M.M., Da Costa, A.C.S., Melo, V.F., 2017. Pedogenic iron oxides in iron-rich oxisols developed from mafic rocks. Rev. Bras. Cienc. do Solo 41, 1–16. https://doi.org/10.1590/18069657rbcs20160379.

Canton, L.C., Souza Júnior, I.G. de, Silva, L.S., Marques Júnior, J., Costa, A.C.S. da, 2021. Identification and quantification of iron oxides by diffuse reflectance spectroscopy with Praying Mantis accessory and integration sphere. Catena 196. https://doi.org/10.1016/j.catena.2020.104899.

Cervi, E.C., Maher, B., Poliseli, P.C., Souza Junior, I.G., da Costa, A.C.S., 2019. Magnetic susceptibility as a pedogenic proxy for grouping of geochemical transects in landscapes. J. Appl. Geophys. 169, 109–117. https://doi.org/10.1016/j.jappgeo.2019.06.017

Clark, R.N., Roush, T.L., 1984. Reflectance spectroscopy: quantitative analysis techniques for remote sensing applications. J. Geophys. Res. 89, 6329–6340. https://doi.org/10.1029/JB089iB07p06329.

Coblinski, J.A., Inda, A.V., Demattê, J.A.M., Dotto, A.C., Gholizadeh, A., Giasson, É., 2021. Identification of minerals in subtropical soils with different textural classes by VIS–NIR–SWIR reflectance spectroscopy. Catena 203. https://doi.org/10.1016/j.catena.2021.105334.

Curi, N., Franzmeier, D.P., 1987. Effect of parent rocks on chemical and mineralogical properties of some Oxisols in Brazil. Soil Sci. Soc. Am. J. 51, 153–158.

Da Costa, A.C.S., Bigham, J.M., Rhoton, F.E., Traina, S.J., 1999. Quantification and characterization of maghemite in soils derived from volcanic rocks in southern Brazil. Clays Clay Miner. 47, 466–473. https://doi.org/10.1346/CCMN.1999.0470408

Dalmolin, R.S.D., Gonçalves, C.N., Klamt, E., Dick, D.P., 2005. Relação entre os constituintes do solo e seu comportamento espectral. Ciência Rural 35, 481–489. https://doi.org/10.1590/s0103-84782005000200042.

Dantas, A.A.A., Carvalho, L.G. de, Ferreira, E., 2007. Classificação e tendências climáticas em Lavras, MG. Ciência e Agrotecnologia 31, 1862–1866. https://doi.org/10.1590/S1413-70542007000600039.

Dearing, J., 1999. Environmental Magnetic Susceptibility: Using the Bartington MS2 System, second ed. Chi Publishing, Kenilworth.

Deaton, B.C., Balsam, W.L., 1991. Visible spectroscopy; a rapid method for determining hematite and goethite concentration in geological materials. J. Sediment. Res. 61, 628–632. https://doi.org/10.1306/D4267794-2B26-11D7-8648000102C1865D.

Demattê, J.A.M., 2002. Characterization and discrimination of soils by their reflected electromagnetic energy. Pesqui. Agropecu. Bras. 37, 1445–1458. https://doi.org/10.1590/S0100-204X2002001000013.

Demattê, J.A.M., Epiphanio, J.C.N., Formaggio, A.R., 2003. Influência da matéria orgânica e de formas de ferro na reflectância de solos tropicais. Bragantia, v. 62, p. 451–64, 2003.

Demattê, J.A.M., Araújo, S.R., Fiorio, P.R., Fongaro, C.T., Nanni, M.R., 2015. Espectroscopia VIS-NIR-SWIR na avaliação de solos ao longo de uma topossequência em Piracicaba (SP). Rev. Cienc. Agron. 46, 679–688. https://doi.org/10.5935/1806-6690.20150054.

Demattê, J.A.M., Campos, R.C., Alves, M.C., Fiorio, P.R., Nanni, M.R., 2004. Visible-NIR reflectance: A new approach on soil evaluation. Geoderma 121, 95–112. https://doi.org/10.1016/j.geoderma.2003.09.012.

Demattê, J.A.M., Mafra, A.L., Bernardes, F.F., 1998. Comportamento espectral de materiais de solos e de estruturas biogênicas associadas. Rev. Bras. Ciência do Solo 22, 621–630. https://doi.org/10.1590/s0100-06831998000400007.

Fang, Q., Hong, H., Zhao, L., Kukolich, S., Yin, K., Wang, C., 2018. Visible and Near-Infrared Reflectance Spectroscopy for Investigating Soil Mineralogy: A Review. J. Spectrosc. 2018, 1–14. https://doi.org/10.1155/2018/3168974.

Fitzpatrick, R.W., Schwertmann, U., 1982.Al substituted goethite - an indicator of pedogenic and other weathering environments in South Africa. Geoderma 27, 335-347.

Fernandes, R. B. A., Barrón, V., Torrent, J., Fontes, M.P.F., 2004. Quantificação de óxidos de ferro de latossolos brasileiros por espectroscopia de refletância difusa. Rev. Bras. Cienc. do Solo 28, 245–257.

Formaggio, A.R.; Epiphanio, J.C.N.; Valeriano, M.M.; Oliveira, J.B.., 1996. Comportamento espectral (450-2.450 nm) de solos tropicais de São Paulo. Rev. Bras. Cienc. do Solo 20, 467–474.

Gee, G.W., Bauder, J.W., 1986. Particle-size analysis, in: Klut, A. (Ed.), Methods of Soil Analysis. American Society of Agronomy, Madison, pp. 383–412.

González, S., Herrera, F., García, S., 2015. Monotonic random forest with an ensemble pruning mechanism based on the degree of monotonicity. New Gener. Comput. 33, 367–388.

Grauer-Gray, J., Hartemink, A.E., 2018. Raster sampling of soil profiles. Geoderma 318, 99-108. https://doi.org/10.1016/j.geoderma.2017.12.029.

Guimarães, S.T., Lima, H.N., Teixeira, W.G., Neves, A.F., Silva, F.W.R., Macedo, R.S., de Souza, K.W., 2013. Caracterização e classificação de Gleissolos da várzea do rio Solimões (Manacapuru e Iranduba), Amazonas, Brasil. Rev. Bras. Cienc. do Solo 37, 317–326. https://doi.org/10.1590/S0100-06832013000200003.

Hu, P., Jiang, Z., Liu, Q., Heslop, D., Roberts, A.P., Torrent, J., Barrón, V., 2016. Estimating the concentration of aluminum-substituted hematite and goethite using diffuse reflectance spectrometry and rock magnetism: Feasibility and limitations. J. Geophys. Res. Solid Earth 121, 4180–4194. https://doi.org/10.1002/2015JB012635.

Jenny, H., 1941. Factors of Soil Formation: A System of Quantitative Pedology, Soil Science, McGraw Hill book company, New York.

Jiang, Z., Liu, Q., Colombo, C., Barrón, V., Torrent, J., Hu, P., 2013. Quantification of Al-goethite from diffuse reflectance spectroscopy and magnetic methods. Geophys. J. Int. 196, 131–144. https://doi.org/10.1093/gji/ggt377.

Jones, E.J., Singh, B., Mcbratney, A.B., 2019. Checks and Mass Balances for In Situ Quantification of Mineral Composition using Proximal Soil Sensors. Soil Sci. Soc. Am. J. 83, 1253–1262. https://doi.org/10.2136/sssaj2018.11.0440

Kämpf, N., Curi, N., 2012. Formação e evolução do solo (pedogênese), in: Ker, J.C., Curi, N., Schaefer, C.E.G.R., Vidal-Torrado, P. (Eds.), Pedologia - Fundamentos. SBCS, Viçosa, pp. 208–291.

Kämpf, N., Marques, J.J., Curi, N., 2012. Mineralogia de solos brasileiros, in: Ker, J.C., Curi, N., Schaefer, C.E.G.R., Vidal-Torrado, P. (Eds.), Pedologia - Fundamentos. SBCS, Viçosa, pp. 81–146.

Kämpf, N., Curi, N., Marques, J.J., 2016a. Intemperismo e ocorrência de minerais no ambiente do solo, in: Melo, V.F., Alleoni, L.R.F. (Eds.), Química e mineralogia do solo. Viçosa, pp. 333–380.

Kämpf, N., Curi, N., Marques, J.J., 2016b. Óxidos de alumínio, silício, manganês e titânio, in: Melo, V.F., Alleoni, L.R.F. (Eds.), Química e mineralogia do solo. Viçosa, pp. 574–599.

Kokaly, R.F., Clark, R.N., Swayze, G.A., Livo, K.E., Hoefen, T.M., Pearson, N.C., Wise, R. A., Benzel, W.M., Lowers, H.A., Driscoll, R.L., Klein, A.J., 2017. USGS Spectral Library Version 7, U.S. Geological Survey Data Series 1035. https://doi.org/ 10.3133/ds1035.

Kuhn, M., 2008. Building Predictive Models in R Using the caret Package. J. Stat. Softw. 25, 1-26. https://doi.org/10.18637/jss.v028.i05.

Lima, W. de, Mancini, M., Avanzi, J.C., Silva, S.H.G., Acuña-Guzman, S.F., Demattê, J.A.M., Curi, N., 2023. Tracing the origin of deposited sediments: A study applying proximal sensing in a drainage subbasin. J. South Am. Earth Sci. 123. https://doi.org/10.1016/j.jsames.2023.104241.

Liu, L., Zhang, K., Fu, S., Liu, B., Huang, M., Zhang, Z., Zhang, F., Yu, Y., 2019. Rapid magnetic susceptibility measurement for obtaining superficial soil layer thickness and its erosion monitoring implications. Geoderma 351, 163–173. https://doi.org/10.1016/j.geoderma.2019.05.030

Madeira Netto, J. S., Baptista, G. M., 2000. Reflectância espectral de solos. Embrapa Cerrados. Planaltina.

Malengreau, N., Muller, J.P., Calas, G., 1995. Spectroscopic approach for investigating the status and mobility of Ti in kaolinitic materials. Clays Clay Miner. 43, 615–621. https://doi.org/10.1346/CCMN.1995.0430511.

Mancini, M., Silva, S.H.G., Hartemink, A.E., Zhang, Y., de Faria, Á.J.G., Silva, F.M., Inda, A.V., Demattê, J.A.M., Curi, N., 2021. Formation and variation of a 4.5 m deep Oxisol in southeastern Brazil. Catena 206, 105492. https://doi.org/10.1016/j.catena.2021.105492.

Mello, D., Demattê, J.A.M., Silvero, N.E.Q., Di Raimo, L.A.D.L., Poppiel, R.R., Mello, F.A.O., Souza, A.B., Safanelli, J.L., Resende, M.E.B., Rizzo, R., 2020. Soil magnetic susceptibility and its relationship with naturally occurring processes and soil attributes in pedosphere, in a tropical environment. Geoderma 372, 114364. https://doi.org/10.1016/j.geoderma.2020.114364.

Melo, V.F., Schaefer, C.E.G.R., Singh, B., Novais, R.F., Fontes, M.P.F., 2002. Propriedades químicas e cristalográficas da caulinita e dos óxidos de ferro em sedimentos do grupo barreiras no município de Aracruz, estado do Espírito Santo. Rev. Bras. Ciência do Solo 26, 53–64. https://doi.org/10.1590/s0100-06832002000100006.

Melo, V.F., Castilho, R.M.V., Pinto, L.F.S., 2016. Reserva Mineral do Solo, in: Melo, V.F., Alleoni, L.R.F. (Eds.), Química e mineralogia do solo. Viçosa, pp. 251–332.

Mendes, W. de S., Demattê, J.A.M., Bonfatti, B.R., Resende, M.E.B., Campos, L.R., Costa, A.C.S. da, 2021. A novel framework to estimate soil mineralogy using soil spectroscopy. Appl. Geochemistry 127, 104909. https://doi.org/10.1016/j.apgeochem.2021.104909.

Pearlshtien, D.H., Ben-Dor, E., 2020. Effect of organic matter content on the spectral signature of iron oxides across the VIS-NIR spectral region in artificial mixtures: An example from a red soil from Israel. Remote Sens. 12. https://doi.org/10.3390/rs12121960.

Poggere, G.C., Inda, A.V., Barrón, V., Kämpf, N., de Brito, A.D.B., Barbosa, J.Z., Curi, N., 2018. Maghemite quantification and magnetic signature of Brazilian soils with contrasting parent materials. Appl. Clay Sci. 161, 385–394. https://doi.org/10.1016/j.clay.2018.05.014.

Poppiel, R.R., Lacerda, M.P.C., Demattê, J.A.M., Oliveira, M.P., Gallo, B.C., Safanelli, J.L., 2019. Pedology and soil class mapping from proximal and remote sensed data. Geoderma 348, 189–206. https://doi.org/10.1016/j.geoderma.2019.04.028.

Quemenéur, J.J.G., Ribeiro, A., Trow, R.A.J., Paciullo, F.V.P., Helibron, M., 2002. Geology of Lavras Sheet, South of Minas Project, Phase I. COMIG-UFMG-UFRJ-UERJ.Belo Horizonte.

Ramos, P.V., Inda, A.V., Barrón, V., Siqueira, D.S., Marques Júnior, J., Teixeira, D.D.B., 2020. Color in subtropical brazilian soils as determined with a Munsell chart and by diffuse reflectance spectroscopy. Catena 193, 104609. https://doi.org/10.1016/j.catena.2020.104609

R Core Team, 2020. R: A language and environment for statistical computing. R Foundation for Statistical Computing, Vienna, Austria.

Rodríguez, J.M.F., Fernández, J.A.F., 2005. Application of the second derivative of the Kubelka-Munk function to the semiquantitative analysis of Roman paintings. Color Res. Appl. 30, 448–456. https://doi.org/10.1002/col.20157.

Savitzky, A., Golay, M.J.E., 1964. Smoothing and differentiation of data by simplified least squares procedures. Anal. Chem. 36, 1627–1639. https://doi.org/10.1021/ac60214a047.

Schaefer, C.E.G.R., Fabris, J.D., Ker, J.C., 2007. Minerals in the clay fraction of Brazilian Latosols (Oxisols): a review. Clay Miner. 43, 137–154. https://doi.org/10.1180/claymin.2008.043.1.11.

Scheinost, A.C., Chavernas, A., Barron, V., Torrent, J., 1998. Use and Limitations of Second-Derivative Diffuse Reflectance Spectroscopy in the Visible to Near-Infrared Range to Identify and Quantify Fe Oxide Minerals in Soils. Clays Clay Miner. 46, 528–536. https://doi.org/10.1346/CCMN.1998.0460506.

Scheinost, A.C., Schwertmann, U., 1999. Color identification of iron oxides and hydroxysulfates: Use and limitations. Soil Sci. Soc. Am. J. 63, 1463-1471.

Sellitto, V.M., Fernandes, R.B.A., Barrón, V., Colombo, C., 2009. Comparing two different spectroscopic techniques for the characterization of soil iron oxides Diffuse versus bi-directional reflectance.pdf. Geoderma 149, 2–9. https://doi.org/https://doi.org/10.1016/j. geoderma.2008.11.020.

Silva, S.H.G., Ribeiro, B.T., Guerra, M.B.B., Carvalho, H.W.P., Lopes, G., Carvalho, G.S.,Guilherme, L.R.G., Resende, M., Mancini, M., Curi, N., Rafael, R.B.A., Cardelli, V.,Cocco, S., Corti, G., Chakraborty, S., Li, B., Weindorf, D.C., 2021. Chapter one –

pXRF in tropical soils: methodology, applications, achievements and challenges. Advances in Agronomy. 167, 1-62. https://doi.org/10.1016/bs.agron.2020.12.001.

Silva, F.M., Weindorf, D.C., Silva, S.H.G., Silva, E.A., Ribeiro, B.T., Guilherme, L.R.G., Curi, N., 2019. Tropical Soil Toposequence Characterization via pXRF Spectrometry. Soil Sci. Soc. Am. J. 83, 1153–1166. https://doi.org/10.2136/sssaj2018.12.0498.

Silva, F.M., Silva, S.H.G., Acuña-Guzman, S.F., Silva, E.A., Ribeiro, B.T., Fruett, T., Inda, A.V., Teixeira, A.F. dos S., Mancini, M., Guilherme, L.R.G., Curi, N., 2021. Chemical and mineralogical changes in the textural fractions of quartzite-derived tropical soils, along weathering, assessed by portable X-ray fluorescence spectrometry and X-ray diffraction. J. South Am. Earth Sci. 112, 103634. https://doi.org/10.1016/j.jsames.2021.103634.

Silva, F.M., Silva, S.H.G., Teixeira, A.F. dos S., Inda, A.V., Fruett, T., Weindorf, D.C., Guilherme, L.R.G., Curi, N., 2022. Using proximal sensors to assess pedogenetic development of Inceptisols and Oxisols in Brazil. Geoderma Reg. 28, e00465. https://doi.org/10.1016/j.geodrs.2021.e00465.

Silva, S.H.G., Hartemink, A.E., Teixeira, A.F. dos S., Inda, A.V., Guilherme, L.R.G., Curi, N., 2018. Soil weathering analysis using a portable X-ray fluorescence (PXRF) spectrometer in an Inceptisol from the Brazilian Cerrado. Appl. Clay Sci. 162, 27–37. https://doi.org/10.1016/j.clay.2018.05.028.

Soil Survey Staff, 2014. Keys to soil taxonomy, 12th ed. USDA-NRCS.

Souza Junior, I.G., da Costa, A.C.S., Vilar, C.C., Hoepers, A., 2010. Mineralogy and magnetic susceptibility of iron oxides of b horizon of Paraná state soils. Cienc. Rural 40, 513–519. https://doi.org/10.1590/s0103-84782010000300003.

Stevens, A., Ramirez-Lopez, L., 2014. An introduction to the prospectr package [WWW Document]. R Packag. Vignette. URL https://cran.r-project.org/web/packages/ prospectr/ vignettes/prospectr-intro.pdf.

Stockmann, U., Cattle, S.R., Minasny, B., McBratney, A.B., 2016. Utilizing portable X-ray fluorescence spectrometry for in-field investigation of pedogenesis. Catena 139, 220–231. https://doi.org/10.1016/j.catena.2016.01.007.

Szalai, Z., Kiss, K., Jakab, G., Sipos, P., Belucz, B., Németh, T., 2013. The use of UV-VIS-NIR reflectance spectroscopy to identify iron minerals. Astron. Nachrichten 334, 940–943. https://doi.org/10.1002/asna.201211965.

Taboada, T., Cortizas, A.M., García, C., García-Rodeja, E., 2006. Particle-size fractionation of titanium and zirconium during weathering and pedogenesis of granitic rocks in NW Spain. Geoderma 131, 218–236. https://doi.org/10.1016/j.geoderma.2005.03.025.

Vidal-Torrado, P., Ferreira, T.O., 2017. Solos de restingas e áreas úmidas costeiras, in: Pedologia: Solos Dos Biomas Brasileiros. Sociedade Brasileira de Ciência do Solo, Viçosa, pp. 597.

Viscarra Rossel, R.A., Behrens, T., Ben-Dor, E., Brown, D.J., Demattê, J.A.M., Shepherd, K.D., Shi, Z., Stenberg, B., Stevens, A., Adamchuk, V., Aïchi, H., Barthès, B.G., Bartholomeus, H.M., Bayer, A.D., Bernoux, M., Böttcher, K., Brodský, L., Du, C.W., Chappell, A., Fouad, Y., Genot, V., Gomez, C., Grunwald, S., Gubler, A., Guerrero, C., Hedley, C.B., Knadel, M., Morrás, H.J.M., Nocita, M., Ramirez-Lopez, L., Roudier, P., Campos, E.M.R., Sanborn, P., Sellitto, V.M., Sudduth, K.A., Rawlins, B.G., Walter, C., Winowiecki, L.A., Hong, S.Y., Ji, W., 2016. A global spectral library to characterize the world's soil. Earth-Science Rev. 155, 198–230. https://doi.org/10.1016/j.earscirev.2016.01.012.

Viscarra Rossel, R.A., Chen, C., 2011. Digitally mapping the information content of visible-near infrared spectra of surficial Australian soils. Remote Sens. Environ. 115, 1443–1455. https://doi.org/10.1016/j.rse.2011.02.004.

Walkley, A., Black, I.A., 1934. An examination of the degtjareff method for determining soil organic matter, and a proposed modification of the chromic acid titration method. Soil Sci 37, 29–38. https://doi.org/10.1097/00010694-193401000- 00003.

Wei, T., Simko, V., Levy, M., Xie, Y., Jin, Y., Zemla, J., 2017. Package "corrplot". R Dev. Core Team. Available at:https://github.com/taiyun/corrplot%0Ahttps://cran.r-project.org/web/packages/corrplot/corrplot.pdf.

Weindorf, D.C., Chakraborty, S., Herrero, J., Li, B., Castañeda, C., Choudhury, A., 2016. Simultaneous assessment of key properties of arid soil by combined PXRF and Vis-NIR data. Eur. J. Soil Sci. 67, 173–183. https://doi.org/10.1111/ejss.12320.

White, K., Walden, J., Drake, N., Eckardt, F., Settle, J., 1997. Mapping the iron oxidecontent of dune sands, Namib Sand Sea, Namibia, using Landsat thematic mapper data. Remote Sens Environ 62, 30–39. https://doi.org/10.1016/S0034-4257(97)00068-0.

ARTIGO 3 - Variação de atributos de Latossolos e Cambissolos desenvolvidos de diferentes materiais de origem com auxílio de sensores próximos

Resumo

Compreender a pedogênese e a variabilidade do solo, assim como a sua caracterização física, química e mineralógica e seu respectivo material de origem nem sempre é uma tarefa simples e direta, especialmente nas regiões tropicais, onde solos poligenéticos são comumente encontrados. Com os avanços tecnológicos, metodologias e ferramentas como a fluorescência de raios-X portátil (pXRF) e a espectroscopia de refletância difusa no espectro visível e infravermelho próximo (Vis-NIR DRS) associadas a Difração de raios - X foram empregadas na caracterização de Cambissolos e Latossolos, buscando aumentar a eficiência e reduzir os custos. Assim, o objetivo desta pesquisa foi utilizar o pXRF, Vis-NIR e a DRX para caracterizar química, física e mineralogicamente cinco perfis de solos com graus de intemperismo semelhantes, mas desenvolvidos de diferentes materiais de origem encontrados em áreas relativamente próximas (117 ha) e identificar possíveis descontinuidades nos materiais de origem formadores desses solos através das relações Ti/Zr, Si/Al, areia fina /areia grossa (AF/AG) e mineralogia das frações areia, silte e argila. Foram descritos morfologicamente e coletados cinco perfis de solo; Cambissolo Flúvico (CY), Cambissolo Háplico (CX), Latossolo Amarelo (LA), Latossolo Vermelho Amarelo (LVA) e Latossolo Vermelho (LV). O total des 96 amostras foram coletadas, sendo 3 amostras por horizonte (composta), seguindo um grid regular de 15 x 15 cm na parede dos perfis, que foram analisadas via pXRF. As amostras de solos compostas de cada horizonte foram separadas nas frações areia, silte e argila e submetidas a análises mineralógicas via DRX. As análises via Vis-NIR foram realizadas em duas profundidade de acordo com cada perfil de solo. O pXRF revelou a diversidade da composição elementar de cada perfil de solo em profundidade e na sua distribuição espacial, evidenciando de que maneira cada material de origem imprimiu suas características distintivas em cada um desses perfis. As relações Ti/Zr e a análise mineralógica das frações areia, silte e argila foram capazes de identificar as descontinuidades presentes nos materiais de origem. Os dados de Vis-NIR correlacionaram com a textura e a mineralogia dos solos estudados.

1. Introdução

Compreender a pedogênese e a variabilidade do solo, assim como a sua caracterização física, química e mineralógica e seu respectivo material de origem nem sempre é uma tarefa simples e direta. De acordo com Moniz et al. (1982), é frequente encontrar solos poligenéticos nos trópicos, ou seja, que podem ser desenvolvidos a partir do intemperismo direto das rochas (autóctones), ou a partir da erosão e deposição de materias pré-intemperizados ou não, provenientes de outras áreas (alóctones). Diante disso, depara-se com uma dificuldade em estabelecer a associação entre o solo e seu respectivo material de origem. As adversidades também residem na ausência de afloramentos rochosos

próximos que possam ser relacionados, bem como na falta de detalhamento nas escalas dos mapas geológicos disponíveis, o que compromete a obtenção de um diagnóstico preciso dos materiais de origem.

Uma abordagem utilizada para identificar descontinuidades consiste na análise da relação Ti/Zr, uma vez que esses elementos são componentes de minerais de alta estabilidade no solo, como o rutilo e o zircão, respectivamente (GRAUER-GRAY et al., 2018; MANCINI et al., 2023). Sendo assim, o solo deve apresentar uniformidade ou pouca variação de Ti/Zr com a profundidade do solo para que o material de origem seja considerado homogêneo (ANDA et al., 2009). Além da relação Ti/Zr, as relações entre areia fina e areia grossa (AF/AG) são também empregadas em estudos de similaridade de material de origem; quando o material de origem for homogêneo essa relação permanece uniforme ao longo do perfil (KUZILA, 1995). Por outro lado, a relação Si/Al é utilizada para identificar solos com diferentes graus de intemperismo (NOVAES FILHO et al., 2012). A quantidade de Si diminui à medida que o grau de intemperismo se intensifica, enquanto o Al aumenta, em virtude de sua presença na composição dos argilominerais e nos óxidos de alumínio residuais no solo (STOCKMAN et al.,2016). Além disso, a análise mineralógica, juntamente com a análise morfológica do perfil, também é empregada na identificação de descontinuidades do solo (LAGES et al., 2008).

Com os avanços tecnológicos, surgiram diversas ferramentas e metodologias empregadas na caracterização dos solos, buscando aumentar a eficiência e reduzir os custos das análises. Além disso, a obtenção de resultados antes dificilmente conseguidos tem possibilitado novas discussões e conhecimentos sobre solos. Entre essas ferramentas, destacam-se a fluorescência de raios-X portátil (pXRF) e a espectroscopia de refletância difusa no espectro visível e infravermelho próximo (Vis-NIR), que permitem, respectivamente, identificar os elementos químicos presentes nos solos (SUN et al., 2020) e determinar as interações entre a radiação eletromagnética e os atributos dos solos através da reflectância difusa da luz emitida pelo equipamento (SOUZA et al., 2021).

Por um lado, as informações obtidas pelo pXRF já foram empregadas com sucesso para auxiliar no monitoramento da poluição por metais e determinação de elementos potencialmente tóxicos como As, Cd, Cr, Cu e Hg (CAPORALE et al., 2018; XU et al., 2020). Na avaliação da fertilidade do solo (ANDRADE et al., 2021; SHARMA et al., 2015), análise da textura do solo (BENEDET et al., 2020; ZHU et al., 2011); estudos de pedogênese (STOCKMAN et al., 2016; SILVA et al., 2022) e pesquisas geológicas (MANCINI et al.,

2019; POTTS et al., 2006). Ainda é possível espacializar os dados elementares evidenciando as diferenças existentes ao longo do perfil do solo (BENEDET et a., 2022; SILVA et al., 2018).

Quanto ao Vis-NIR, a técnica em questão tem sido empregada na caracterização e diferenciação de classes de solos (TERRA et al., 2018; DEMATTÊ et al., 2015), medição indireta de atributos físicos, como textura e umidade (PEREIRA et al., 2019; HOBLEY ; PRATER, 2019; CHANG et al., 2005), atributos químicos e carbono orgânico (DEMATTÊ et al., 2017; BUDAK et al., 2016; JI et al., 2015; VISCARRA ROSSEL et al., 2015), além da identificação e quantificação de minerais comparativas com resultados provenientes da difratometria de raios-X, como observado recentemente por Fang et al. (2018), Coblinsk et al. (2021) e Fernandes et al. (2004). Nos últimos anos, a integração das duas técnicas revelou-se complementar para detalhar a caracterização de solos (TEIXEIRA et al., 2022; SILVA et al., 2022; MANCINI et al., 2023; GOZUKARA et al., 2021).

Assim, o objetivo deste trabalho foi utilizar pXRF, Vis-NIR e a DRX para: i) caracterizar química, física e mineralogicamente perfis de Latossolos e Cambissolos desenvolvidos de diferentes materiais de origem encontrados em áreas relativamente próximas (117 ha); ii) verificar descontinuidades nos materiais de origem formadores desses solos através das relações Ti/Zr, Si/Al, AF/AG e mineralogia das frações areia, silte e argila. Nossa hipótese é que os resultados provenientes do pXRF, em conjunto com a análise por DRX, sejam capazes de evidenciar as diferenças entre os solos com base em seus materiais de origem específicos, bem como identificar descontinuidades litológicas não identificadas nas análises morfológicas, caso existam.

2. Materiais e métodos

2.1 Localização e amostragem

A área de estudo localiza-se na Fazenda Palmital pertencente à Universidade Federal de Lavras – Minas Gerais, no Município de Ijaci (Fig. 1a). Em termos geológicos, de acordo com Quemenéur et al. (2002) na região ocorre uma depressão constituída por metacalcários cobertos por uma espessa camada de alteração intempérica (Fig. 1b). Os metacalcários situam-se sobre um embasamento arqueano formado por charnockitos, monzonitos, enderbitos (metatonalito) e rochas máficas do tipo gabro e intrusões graníticas, em grande parte metamorfizadas. Além dessas rochas ocorrem lamitos intercalados com arenitos ricos

em feldspatos e depósitos aluvionares inconsolidados do Quaternário, compostos por seixos, cascalhos, areia, siltes (estratificados) e sedimentos pelíticos (NALINI JÚNIOR et al., 2007). Essa grande diversidade reportada é devido à menor escala de detalhes do mapa geológico existente para a região e a possibilidade de sobreposição de materiais geológicos contrastantes.

De acordo com a classificação de Köppen, o clima local é designado como Cwa, caracterizado como um clima subtropical, com invernos secos, com temperaturas abaixo de 18ºC, e verões quentes com temperaturas acima de 22ºC (DANTAS et al., 2007). Os perfis de solos representativos da área e suas respectivas localizações na paisagem são os seguintes: Cambissolo Flúvico (CY) contendo grandes quantidades de frações granulómetricas entre 2 – 19 mm e frações > 19 mm, localizado no terço médio da paisagem, mas com indícios de ter sido formado em ambiente fluvial; Cambissolo Háplico (CX) e Latossolo Vermelho (LV) localizados no terço superior, Latossolo Amarelo (LA) que ocupa uma microdepressão localizada e Latossolo Vermelho Amarelo (LVA) localizado no terço inferior da paisagem. Quanto ao uso e ocupação atual dos solos, os CY, LA e LVA encontram-se sob culturas anuais, LV sob silvicultura (plantio de *Pinus* sp.) e CX está coberto por vegetação nativa.

Nos perfis de Latossolos, realizou-se uma escavação de aproximadamente 2 metros de profundidade, enquanto para os Cambissolos, os perfis foram abertos até o horizonte C. A descrição morfológica foi realizada de acordo com SANTOS et al. (2018).

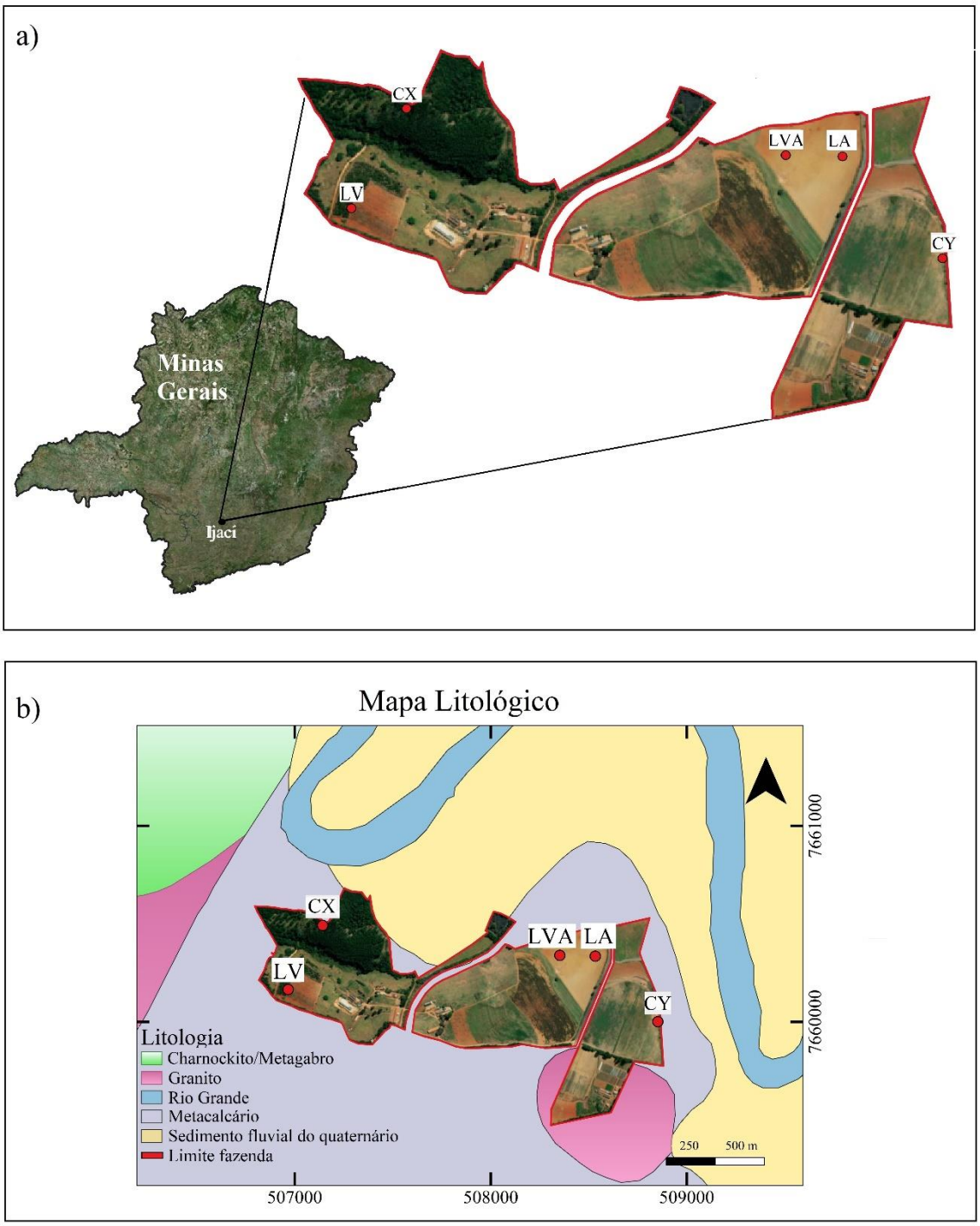

Fig. 1. a) Localização e limite da fazenda Palmital; b) Mapa Litológico da região e localização dos perfis de solos estudados: Cambissolo Flúvico (CY), Cambissolo Háplico (CX); Latossolo Amarelo (LA); Latossolo Vermelho Amarelo (LVA); Latossolo Vermelho (LV).

No total, nos 5 perfis, foram coletadas 96 amostras, sendo 3 amostras por horizonte morfogenético, seguindo um grid regular de 15 x 15 cm na parede dos perfis, com exceção do horizonte C1 do Cambissolo Flúvico onde foram coletadas apenas 2 amostras devido a impedimentos físicos. No horizonte C2 do Cambissolo Flúvico optou-se por coletar 4 amostras para melhor caracterização. As amostras coletadas foram secas ao ar e peneiradas (< 2 mm) (terra fina seca ao ar - TFSA). Para os dois Cambissolos e o Latossolo Vermelho-Amarelo observou-se a presença de frações grosseiras com diâmetro superior a 2 mm (TFSA), que foram separadas em frações entre 2 mm – 19 mm e frações > 19 mm. Para a realização das análises químicas e físicas as amostras foram agrupadas por profundidade, constituindo amostras compostas. Em seguida, foram submetidas a análise de textura pelo método da pipeta modificado (GEE; BAUDER, 1986); pH em água; $Ca^{2+,}$ Mg^{2+} e Al^{3+} trocáveis extraídos com 1 mol L^{-1} KCl (MCLEAN et al., 1958); teores de K^{+} e P extraídos por Mehlich (MEHLICH, 1953); H^{+} + Al^{3+} pelo extrator de SMP (SHOEMAKER et al., 1961); carbono orgânico pelo método Walkley Black (WALKLEY; BLACK, 1934) e P-rem por adição de solução contendo 60 mg de P (ALVAREZ; FONSECA, 1990). A capacidade de troca catiônica (CEC), soma de bases e saturação por bases foram calculadas a partir dos atributos químicos correspondentes.

As amostras compostas de cada horizonte foram separadas nas frações areia, silte e argila e utilizadas nas análises mineralógicas dessas frações. A dispersão da argila foi realizada com 50 g de TFSA utilizando-se 100 mL 0,1 mol mol^{-1} de NaOH, e agitação por 16 horas. Após agitação, a suspensão foi passada por uma peneira de 53 µm. A fração areia foi retida, enquanto as frações silte e argila foram separadas por sedimentação da fração silte de acordo com a lei de Stokes (GEE; BAUDER, 1986).

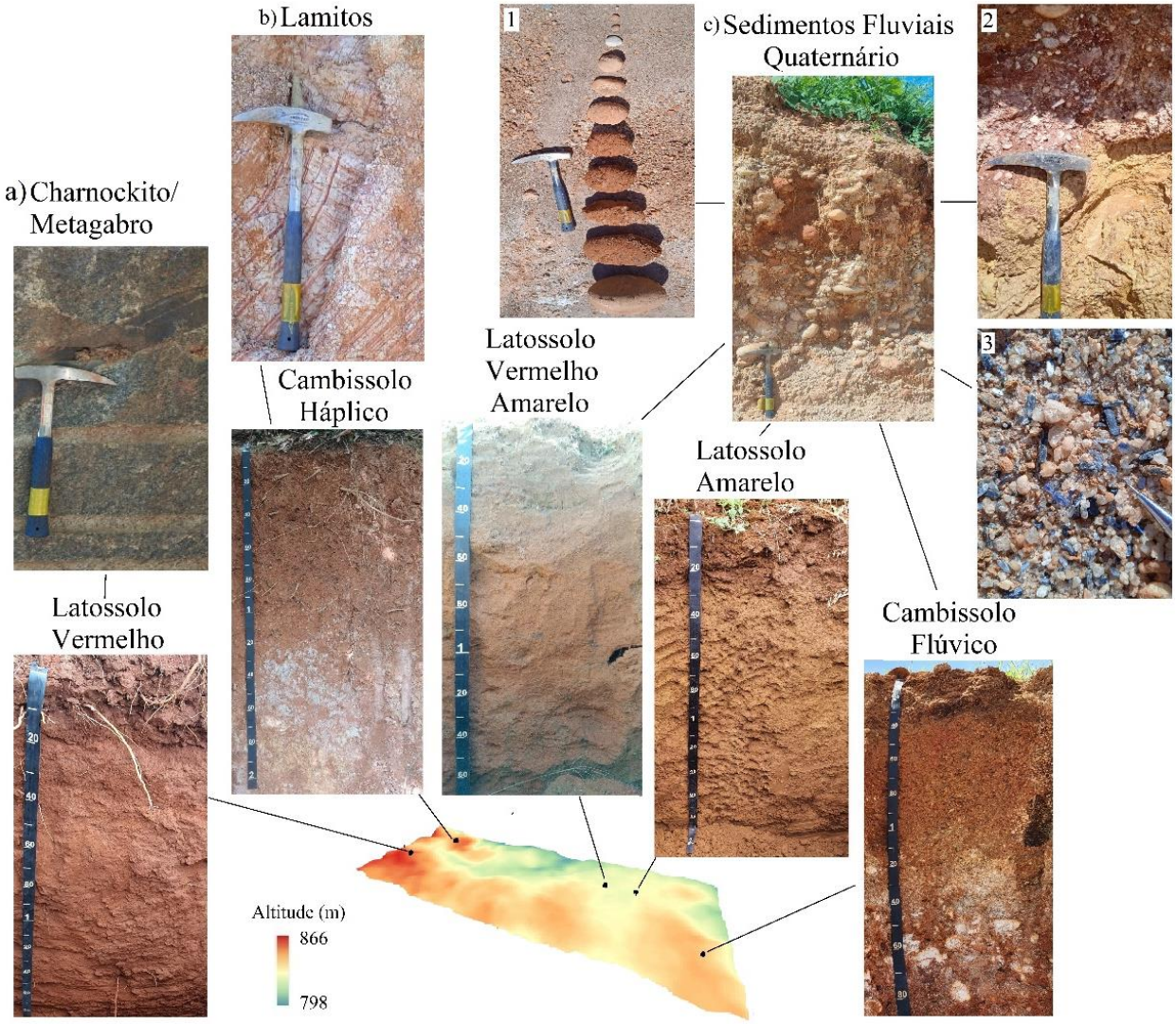

Fig. 2. Localização dos perfis de solos na paisagem e seus respectivos materiais de origem: a) Charnockito com veio de metagabro; b) lamitos com níveis de óxido de Fe; c) sedimentos fluviais do quaternário: 1) detalhe da variação no tamanho e arredondamento dos seixos; 2) transição entre sedimentos finos e grosseiros; 3) detalhe da fração areia constituída por quartzo, cianita e feldspato.

2.2 Análise do solo via sensores próximos e difração de raios-X

As 96 amostras individuais de TFSA e as amostras de areia, silte e argila referentes a cada horizonte foram analisadas usando um pXRF, Bruker (modelo Tracer 5G) contendo um tubo de raios X Rh (4 W, 50 KV e 200 µA) e detector de silício (SDD). As amostras foram analisadas durante 60s na configuração “modo solo”. A calibração do equipamento foi realizada analisando o padrão check-sample (CS) da Bruker®. Os elementos avaliados

neste estudo foram: Al, Ca, Fe, Mg, Si, Ti, e Zr. O resultado das análises elementares das amostras compostas foram obtidos através da média entre as leituras das amostras individuais coletadas em cada horizonte. As análises a partir do Vis-NIR foram realizadas na profundidade 1 e profundidade 2 respectivamente: CY: 0 – 10 cm e 40 - 60 cm; CX: 0 – 20 cm e 45 – 65 cm; LA: 0 – 10 cm e 40 – 60 cm; LVA: 0 – 10 cm e 40 – 60 cm; LV: 0 – 10 cm e 40 – 80 cm utilizando-se um espectrômetro portátil Vis-NIR DRS PSR-3500 (Spectral Evolution, EUA) com faixa espectral de 350 a 2500 nm, intervalo de amostragem de 2 nm e resolução espectral de 3, 5, 10 e 7 nm de 350 a 1000, 1500 e 2100 nm. As análise foram realizadas em laboratório, onde as amostras de cada perfil foram distribuídas homogeneamente em placas de Petri com a sonda de digitalização colocada verticalmente sobre as amostras. Cada amostra foi escaneadas três vezes, girando 90° entre cada varredura, compondo 10 varreduras internas por 1,5 segundo. A calibração do equipamento ocorria após a digitalização de 5 amostras por meio do escaneamento de um painel de radiação rastreável NIST de 12,7 por 12,7 cm. A curva espectral foi obtida pela média das três varreduras em cada amostra.

Para determinar a mineralogia das frações areia, silte e argila, utilizou-se a difração de raios-X por meio de um difratômetro Bruker D2 PHASER, equipado com módulo linear rápido LYNXEYE^{TM} e operado com software DIFFRAC.SUITE. As análises foram realizadas nas amostras dos horizontes A, B e C em pó e não orientadas, irradiadas de 2 a 70° 2Θ s^{-1} durante períodos de 0,02° 2Θ s^{-1} com radiação CuKα de l = 1,541838 Å, filtro de Ni, voltagem de 30 kVA e intensidade de corrente de 10 mA. O software Diffract Suite Eva produziu os difratogramas de raios-X, que foram foram interpretados com o auxílio de tabelas descritas por BRINDLEY e BROWN (1980).

2.3 Análise estatística

Para a espacialização dos teores elementares do pXRF em cada perfil, utilizou-se o método multilevel B-Spline da extensão SAGA GIS (CONRAD et al., 2015) contida no software livre QGIS 3.16 (QGIS).

3. Resultados e Discussões

3.1 Morfologia e fertilidade dos perfis de solo

3.1.1 Cambissolos

Os maiores teores de argila (46%) e silte (7%) observados em CY, ocorreram no horizonte Bi (Tab.1). A partir do horizonte BC observa-se o aumento nos teores de areia (> 69%). A presença de fragmentos de 2 e 19 mm foi constatada em todos os horizontes e fragmentos maiores que 19 mm nos horizontes A, BC e C2. Nos depósitos grosseiros aluvionares inconsolidados do quaternário, ambiente típico de ocorrência do CY foram encontrados seixos de variadas dimensões (centímetros a decímetros), litologias (quartzito, granito, arenito ferruginoso) e mineralogia (quartzo leitoso), arredondados a sub-arredondados suportados por uma matriz arenosa mais avermelhada (Fig. 2). A matriz arenosa é praticamente constituída por quartzo, mica, feldspato, cianita e minerais opacos. Esse material de origem de textura variada conferiu menor profundidade ao CY e maior quantidade de fragmentos grosseiros (Tab. 1). Os maiores teores de argila observados no horizonte A e Bi são consequência de um material de origem mais fino que o restante do perfil. Nos horizontes BC, C e C2, os teores de areia elevados, evidenciam a natureza grosseira do material de origem.

As diferenças acima mencionadas originam-se na distinção da granulometria entre os sedimentos transportados, que ocorreram possivelmente em eventos distintos de sedimentação com variação na intensidade do fluxo de transporte. A intensidade do fluxo teria sido maior na base do perfil, em vista do tamanho e arredondamento dos seixos. Portanto a relação AF/AG não pode ser considerada como descontinuidade no material de origem, em virtude do caráter flúvico inerente ao solo. Estudos realizados por Novaes Filho et al., (2002) demonstraram mudanças significativas na relação AF/AG e Zr/Ti a partir de 3 metros de profundidade para um Latossolo Vermelho Amarelo situado em encosta, indicando descontinuidades no material de origem. Os autores também ressaltaram a importância de analisar em conjunto as relações indicadoras.

CX exibiu o menor teor de areia (< 11%) e o maior teor de argila (> 67%) (Tab. 1) quando comparado aos demais perfis de solo. Adicionalmente apresentou elevada variabilidade no teor de silte com presença de fragmentos grosseiros (2-19 mm) apenas nos horizontes A, BC, C1 e C2. A maior profundidade de CX e a textura argila ocorre devido os lamitos serem constituídos por argilominerais, muitas vezes impregnados por óxido de ferro e intercalados com níveis mais arenosos ricos em feldspato (Fig. 2). As diferenças na granulometria no material de origem refletiram no solo, com o horizonte A apresentando

maior teor de areia, enquanto os horizontes AB, Bi e BC maior teor de argila. Conforme esperado, os horizontes menos intemperizados seguiram o mesmo fundamento. Os horizontes C1 e CR2 estariam localizados em um nível mais lamítico do que os horizontes C2 e CR1. De acordo com Kämpf e Curi (2012) as características do material de origem são mais pronunciadas nos horizontes menos intemperizados, uma vez que nos solos mais jovens ocorre uma relação mais direta com o material de origem. O padrão observado na relação AF/AG é resultado da natureza do material de origem, que consiste em uma combinação de camadas de lamito e arenito. CX, apresentou coloração variegada composta por N1 com mosquedos abundantes e médios 2.5YR 5/8 no horizonte CR e coloração variegada composta de N1 com mosqueados 2,5 YR 5/8 e 10YR 7/6 no horizonte CR2 (Tab. 2).

CY apresenta acidez média a fraca e o CX acidez elevada conforme paramêtros agronômicos definidos por Alvarez et al. (1999) (Tab.2). Em razão da faixa do pH (5,4 a 6,6) observada em CY, o alumínio trocável está praticamente precipitado e a saturação por alumínio é baixa e por vezes nula. Entretantro o pH mais baixo em CX (< 4,6) aumenta a solubilidade do Al, o que acarreta nos altos valores de Al^{+} trocável e saturação por Al (Tab. 2). O Al provém do intemperismo dos minerais primários e minerais secundários como a caulinita, segundo Ronquim et al. (2010) quanto maior o teor de caulinita no solo, maior o teor Al.

Os teores de Ca^{2+}, Mg^{2+}, K^{+}, SB, V% e CTC, observados no horizonte superficial de ambos os Cambissolos está associada a MOS. No entanto, em maiores profundidades são influenciados pelos minerais primários presentes no solo (Fig. 6). O valor mais alto de P disponível no horizonte A relaciona-se ao P orgânico. Os menores valores de P-rem acompanham o aumento no teor de argila. De acordo Prezotti et al. (2003) a disponibilidade de P depende da textura, matéria orgânica e mineralogia.

3.1.2 Latossolos

Entre os latossolos destaca-se os altos teores de argila em LV e LA, principalmente no horizonte Bw (> 55%). No LVA os teores de argila são menores (< 44%), entretanto o teor de areia é alto (> 50%) e ocorre frações granulométricas com tamanhos entre 2 e 19 mm em todos os horizontes (Tab. 1). O LA e o LVA assim como o Cambissolo Flúvico, encontram-se sobre o domínio dos sedimentos inconsolidados do quaternário. O LA situa-

se em uma fase mais lamítica, enquanto o LVA pertence a uma fase mais rica em areia e fragmentos grosseiros, o que justifica a textura encontrada para esses solos. O elevado teor de argila encontrado em LV é reflexo do metagabro, material de origem composto por uma alta concentração de minerais primários ferromagnesianos suscetíveis ao intemperismo. O horizonte BC e CB de LA com 7,5YR 5/8 e 10YR 5/8 respectivamente apresentam mosqueados comuns, pequenos e distintos 2YR 4/8. Com base na variação da relação AF/AG, não foi possível identificar a presença de descontinuidade no material de origem dos Latossolos.

O pH acima de 6.4 observado em LA e LVA não é característico para esta classe de solo (Tab. 2). Os valores mais altos de pH, teores dos cátions básicos, P disponível, CTC, SB e V% nos horizontes superficiais são resultado das práticas de manejo da fertilidade adotadas na área e da MOS. Em profundidade os teores mais elevados desses atributos são presumivelmente provenientes do material de origem. A acidez trocável é praticamente nula, e a baixa saturação por alumínio pode indicar o predomínio do alumínio na forma precipitada Al $(OH)_3$. Os Latossolos apresentam alto poder de fixação de P devido a sua mineralogia constituída por óxidos de ferro e alumínio (KER, 1997). A combinação da textura argilosa com a mineralogia oxídica justifica os menores teores de P-rem no solo.

Tabela 1- Textura e distribuição das frações granulométricas em tamanhos menores que < 2mm, entre 2 – 19 mm e > 19 mm, em seus respectivos horizontes no Cambissolo Flúvico, Cambissolo Háplico, Latossolo Amarelo, Latossolo Vermelho Amarelo, Latossolo Vermelho.

Classe de Solo	Hor	Argila	Silte	Areia	Areia Grossa	Areia Fina	Areia Fina/ Areia Grossa	< 2 mm	2 – 19 mm	> 19 mm
						%				
Cambissolo Flúvico	A	44	3	53	38	15	0,4	27,7	67,8	4,5
	Bi	46	7	47	31	16	0,5	31,7	68,3	0,0
	BC	28	3	69	52	17	0,3	31,0	68,4	0,6
	C1	26	1	73	55	18	0,3	36,3	63,7	0,0
	C2	24	2	74	59	15	0,3	41,8	51,7	6,5
Cambissolo Háplico	A	67	22	11	5	6	1,2	79,2	20,8	0,0
	AB	76	15	9	4	5	1,3	0,0	0,0	0,0
	Bi	73	18	9	4	5	1,3	0,0	0,0	0,0
	BC	75	16	9	4	5	1,3	63,8	36,2	0,0
	C1	79	14	7	3	4	1,3	43,7	56,3	0,0
	C2	75	20	5	2	3	1,5	97,2	2,8	0,0
	CR1	75	22	3	1	2	2,0	0,0	0,0	0,0
	CR2	79	18	3	1	2	2,0	0,0	0,0	0,0

Latossolo Amarelo	A	53	15	32	20	12	0,6	0,0	0,0	0,0
	BA	58	7	35	22	13	0,6	0,0	0,0	0,0
	Bw1	55	11	34	20	14	0,7	0,0	0,0	0,0
	Bw2	58	11	31	17	14	0,8	0,0	0,0	0,0
	BC	57	15	28	15	13	0,9	0,0	0,0	0,0
	CB	60	13	27	16	11	0,7	0,0	0,0	0,0
Latossolo Vermelho Amarelo	A1	40	3	57	37	20	0,5	84,6	15,4	0,0
	A2	40	3	57	38	19	0,5	85,6	14,4	0,0
	AB	42	3	55	37	18	0,5	79,2	20,8	0,0
	BA	42	5	53	33	20	0,6	81,9	18,1	0,0
	Bw1	46	4	50	34	16	0,5	82,7	17,3	0,0
	Bw2	44	6	50	32	18	0,6	100,0	0,0	0,0
	Bw3	44	6	50	35	15	0,4	77,9	22,1	0,0
Latossolo Vermelho	A	59	17	24	12	12	1,0	0,0	0,0	0,0
	AB	67	11	22	11	11	1,0	0,0	0,0	0,0
	BA	72	6	22	11	11	1,0	0,0	0,0	0,0
	Bw1	74	5	21	10	11	1,1	0,0	0,0	0,0
	Bw2	72	7	21	10	11	1,1	0,0	0,0	0,0
	Bw3	69	10	21	11	10	0,9	0,0	0,0	0,0

Tabela 2. Caracterização química e morfológica dos perfis de solos: Cambissolo Flúvico, Cambissolo Háplico, Latossolo Amarelo, Latossolo Vermelho Amarelo e Latosssolo Vermelho da Fazenda Palmital.

Classe de solo	Hor	Profundidade	Cor úmida	pH	K	P	Na^+	Ca^{2+}	Mg^{2+}	Al^{3+}	H^+Al^{3+}	SB	t	T	V	m	M,O,	P-Rem
		cm	(Munsell)		---------mg/dm³--------			---------- $cmol_c/dm^3$----------							------%-----		dag/kg	mg/L
Cambissolo Flúvico	A	0 – 30	5YR 3/3	6,6	207,5	1,9	6,0	0,7	0,6	0,2	1,6	1,8	2,0	3,4	52,9	10,1	1,5	24,6
	Bi	30 - 68	5YR 5/8	5,4	74,6	0,3	4,0	1,9	0,4	0,1	3,9	2,5	2,6	6,4	39,1	3,9	0,9	11,0
	BC	68 - 95	5YR 5/8	6,2	23,2	0,2	3,0	1,1	0,2	0,0	1,0	1,4	1,4	2,4	58,0	0,0	0,3	18,2
	C1	95 - 125	5YR 6/6	6,6	17,8	0,3	3,0	1,0	0,2	0,0	0,8	1,2	1,2	2,0	60,0	0,0	0,1	27,7
	C2	125 +	2,5YR 5/8	6,4	19,3	0,2	3,0	0,8	0,2	0,1	0,8	1,0	1,1	1,8	54,8	9,4	0,0	23,9
Cambissolo Háplico	A	0 - 16	5YR 4/6	4,2	97,5	8,0	6,0	1,1	0,4	1,7	11,2	1,7	3,4	12,9	13,5	49,4	3,7	25,0
	AB	16 - 22	5YR 5/8	4,2	48,0	4,0	4,0	0,4	0,2	2,1	9,6	0,7	2,8	10,3	6,4	76,4	2,3	19,4
	Bi	22 - 43	5YR 5/6	4,4	34,1	2,3	4,0	0,3	0,1	1,9	8,1	0,5	2,4	8,6	5,5	80,2	2,0	19,2
	BC	43 - 60	5YR 5/8	4,5	29,8	1,6	3,0	0,2	0,1	1,7	6,6	0,3	2,0	6,9	4,6	84,2	1,1	20,5
	C1	60 - 98	5YR 5/8	4,5	30,1	1,2	3,0	0,3	0,1	1,4	4,0	0,5	1,9	4,5	11,4	72,9	0,8	22,5
	C2	98 - 120	5YR 5/8	4,6	20,4	0,9	3,0	0,3	0,1	1,3	4,4	0,5	1,8	4,9	9,3	74,3	0,6	21,2
	CR1	120 - 160	N1	4,5	10,8	0,6	2,0	0,1	0,0	1,6	6,2	0,1	1,7	6,3	2,2	92,0	0,0	16,8
	CR2	160 – 200 +	N1	4,5	13,1	0,5	3,0	0,1	0,1	1,4	3,4	0,2	1,6	3,6	6,2	86,4	0,1	15,2
Latossolo Amarelo	A	0 – 23	7,5YR 4/4	6,5	95,6	8,3	3,0	1,0	0,3	0,1	2,0	1,6	1,7	3,6	43,5	6,1	3,1	11,0
	BA	23 – 54	7,5YR 4/6	6,4	57,4	0,3	3,0	0,9	0,4	0,0	1,7	1,5	1,5	3,2	46,1	0,0	2,2	3,1
	Bw1	54 – 96	7,5YR 5/8	6,5	33,5	0,2	4,0	2,4	0,8	0,1	1,5	3,3	3,4	4,8	68,6	3,0	1,8	2,2
	Bw2	96 – 125	7,5YR 5/8	6,8	17,1	0,6	4,0	1,2	0,3	0,2	1,4	1,6	1,8	3,0	53,0	11,3	1,0	1,3
	BC	125 – 210	7,5YR 5/8	6,8	12,8	0,1	4,0	0,8	0,3	0,1	1,3	1,1	1,2	2,4	46,8	8,1	0,9	1,2
	CB	210 +	10YR 5/8	6,9	12,5	0,1	3,0	1,2	0,3	0,1	1,2	1,5	1,6	2,7	56,3	6,1	0,5	1,0
Latossolo Vermelho Amarelo	A1	0 – 12	7,5YR 4/4	8,1	111,2	83,2	6,0	6,4	0,6	0,2	0,9	7,3	7,5	8,2	89,0	2,7	1,8	26,6
	A2	12 – 32	7,5YR 3/4	8,2	115,5	12,0	5,0	6,0	0,5	0,2	0,9	6,9	7,1	7,8	88,3	2,8	1,4	19,4
	AB	32 – 53	7,5YR 4/4	7,8	57,9	0,2	4,0	4,7	0,3	0,1	1,1	5,2	5,3	6,3	82,4	1,9	0,9	16,4

	BA	53 – 65	7,5YR 5/8	7,8	39,8	0,0	4,0	4,1	0,3	0,1	0,9	4,5	4,6	5,4	83,4	2,2	0,8	9,7
	Bw1	65 – 88	7,5YR 5/8	7,9	38,1	0,0	4,0	3,9	0,2	0,1	1,1	4,2	4,3	5,3	79,0	2,4	0,7	6,7
	Bw2	88 – 127	7,5YR 5/8	7,2	36,2	2,3	5,0	3,7	0,2	0,1	1,5	4,0	4,1	5,5	72,8	2,4	0,4	3,7
	Bw3	127 +	7,5YR 5/8	6,5	24,6	0,0	4,0	3,3	0,1	0,1	0,8	3,4	3,5	4,2	80,9	2,9	0,3	2,2
	A	0 – 19	7,5R 3/3	5,1	30,4	21,3	3,0	2,1	0,4	0,1	4,8	2,6	2,7	7,4	34,8	3,8	3,1	20,0
	AB	19 – 27	7,5R 3/6	4,8	15,2	1,2	3,0	1,8	0,2	0,1	5,0	2,1	2,2	7,1	29,1	4,7	2,1	10,9
Latossolo	BA	27 – 51	7,5R 2,5/4	5,0	9,1	0,4	3,0	1,8	0,1	0,1	3,6	1,8	1,9	5,4	33,6	5,2	1,7	7,2
Vermelho	Bw1	51 – 89	7,5R 3/6	5,5	8,9	0,3	3,0	1,7	0,0	0,1	2,7	1,7	1,8	4,4	38,7	5,6	1,4	5,2
	Bw2	89 – 136	7,5R 3/8	5,6	8,2	0,2	3,0	4,4	1,8	0,1	2,5	6,2	6,3	8,7	71,1	1,6	0,9	2,6
	Bw3	136 – 200 +	7,5R 2,5/8	5,6	8,0	0,1	4,0	2,4	1,8	0,1	2,1	4,2	4,3	6,3	66,8	2,3	0,8	2,1

3.2. Caracterização dos solos via pXRF

3.2.1 Cambissolos

Em CY o teor de Si aumenta em profundidade enquanto o teor de Fe diminui (Fig. 3 e 4). Partes com coloração esbranquiçada ocorrem em profundidade, devido a presença de seixos de quartzo parcialmente intemperizados, justificando os maiores teores de Si. Além do quartzo, outro mineral primário e fonte de Si observado em campo encontrado em grande concentração na fração areia foi a cianita (Al_2SiO_5). O Al concentra-se no horizonte mais intemperizado e mais argiloso enquanto os maiores teores de Fe concordam com as crostas ferruginosas encontradas em superfície. O aumento no teor de K na base do perfil, destaca-se entre os outros horizontes, devido a granulometria mais grosseira e a presença dos principais minerais portadores de K (mica e feldspato) (Fig. 6). De acordo com Melo et al. (2001) existe uma relação positiva entre as frações grosseiras do solo e o teor de K.

O comportamento concordante do Al e Si em CX, com maiores teores nas partes de coloração esbranquiçada do perfil (Fig. 2, 3 e 4) ocorre em razão dos horizontes menos intemperizados, com maior concentração de minerais primários como o quartzo e a mica e argilominerais secundários como a caulinita (Fig. 6). As partes mais vermelhas do perfil, indicam maior teor de Fe no material de origem e o seu enriquecimento relativo.

A diversidade na composição mineralógica do material de origem dos Cambissolos, resulta na variação e distribuição dos teores de Ti e Zr. Enquanto a liberação de Ca, Mg e K da estrutura dos minerais pelo intemperismo, sua mobilização e ciclagem pelas plantas são os responsáveis pela distribuição desses elementos (CORINGA et al., 2014).

A relação Si/Al varia entre 2,17 a 2,69 em CY e entre 1,98 e 2,36 em CX, a diferença entre os valores refletem além do intemperismo, o material de origem (STOCKMAN et al., 2016). O menor valor da relação Si/Al no horizonte Bi de CY e CX (Fig. 3) é indicativo de um aumento na intensidade do intemperismo. Enquanto os valores encontrados na base do perfil de CY está de acordo com a granulometria mais grosseira, com maior concentração de quartzo, portanto maiores teores de Si. Em CX, o maior teor de argila, resulta em um aumento equivalente no teor de Al, uma vez que este elemento integra a composição dos argilominerais, provocando a diminuição da relação Si/Al. A variação da razão Ti/Zr para CY ocorre devido a seu carater flúvico, em CX decorre das camadas de argilominerais e arenitos que constituem o material de origem.

3.2.2 Latossolos

O maior teor de Si em superfície e no LVA (Fig. 3 e 4), deve-se ao maior teor de areia constituída principalmente por quartzo e a reciclagem biológica (CORNELIS e DELVAUX, 2016). Conforme esperado o maior teor de Fe ocorre nos horizontes mais intemperizados e com maior teor de argila (Fig. 3 e 4). Segundo César de Mello et al. (2020) a fração argila apresenta alta correlação com o Fe (r = 0,86), além disso o maior teor desse elemento em LV decorre do seu material de origem, constituído por minerais ferromagnesianos. A ciclagem biológica e a adição de fertilizantes e corretivos são os responsáveis pelos teores e variação de Ca, Mg e K, visto o estágio avançado de intemperismo dessa classe de solo.

Em LA até o horizonte Bw2 os elementos Ti e Mg seguem o mesmo padrão de distribuição (Fig. 3), o qual horizontes com maior teor de argila apresentaram também maiores teores de Mg e Ti. De acordo com Mancine et al. (2023) o acúmulo de Mg pode ocorrer na fração argila devido a sua movimentação mais lenta. O Ti correlaciona-se positivamente (r = 0,81) com a fração argila, o elemento seria assimilado pela argila e/ou translocado, após ser liberado pelo intemperismo dos minerais primários (AHR et al., 2012) A diminuição de Ti e Zr nos horizontes BC e C indica a menor concentração desses elementos nos sedimentos formadores de LA. Sendo assim esse contraste na relação Ti/Zr não pode ser considerado uma descontinuidade no material de origem, mas sim como resultado dos processos de meteorização e redistribuição do Ti no solo. Além disso, a relação Si/Al varia entre 1,41 e 1,5, indicando que os sedimentos a partir dos quais esse solo se desenvolveu apresentam um alto grau de intemperismo.

A composição elementar do horizonte AB de LVA, contrasta com a composição predominante do solo (Fig. 3 e 4), ocorrendo o empobrecimento de Si, Al, Fe, Ca, K e Ti concomitante ao aumento no teor de argila. Isto associado as variações significativas encontradas na relação Ti/Zr entre os horizontes A1, A2, AB, BA, Bw1 e Bw3 indicam a presença de descontinuidades nos sedimentos depositados e formadores desse solo. O menor valor para relação Si/Al ocorre no horizonte Bw3 (1,84) e o maior no horizonte AB (2,58) denotando o estágio avançado de intemperismo e o aumento no teor de argila nesses horizontes, respectivamente.

As proporções identificadas nas relações Si/Al e Ti/Zr entre LA e LVA ressaltam a distinção existente entre os materiais de origem de ambos os solos. Apesar de desenvolvidos a partir de sedimentos quaternários, é notório que tais sedimentos apresentam características

diferentes. STOCKMAN et al. (2016) comprovou por meio da relação SiO_2/Al_2O_3 e Ti/Zr que um Vertissolo e um Luvissolo evoluíram de basalto e lamitos, respectivamente e que a razão Ti/Zr apresentava maior variabilidade em profundidade. Tal variabilidade pode estar relacionada a mineralogia do solo, visto que o Ti pode fazer parte de minerais como a mica e ilmenita, menos resistente ao intemperismo que o zircão, além disso a mobilidade da argila pode influenciar redistribuição desses elementos (MAYNARD, 1992).

O material de origem de LV apresenta como minerais acessórios a biotita, biotita titanífera, titanita e zircão, o que explica os teores de Zr e Ti nesse solo (QUEMENÉUR et al., 2002). A relação Ti/Zr no horizonte Bw2 exibe um contraste significativo. Existem duas hipóteses que podem ser consideradas para justificar essa observação. A primeira é que o aumento nos teores de Ti e Zr resulta da presença de minerais portadores desses elementos nessa parte específica do perfil durante a cristalização da rocha. A segunda hipótese é que ocorreu movimentação dos elementos no perfil do solo. Embora o Ti e o Zr sejam considerados elementos imóveis, em solos tropicais sujeitos a um intemperismo intenso, pode ocorrer perda ou movimentação do Ti no solo (CORNU et al., 1999). Quanto ao Zr, ele pode ser liberado por dissolução da estrutura do mineral zircão em condições de elevada acidez do solo e posteriormente, precipitar em camadas mais profundas ou ser lixiviado do perfil (KURTZ et al., 2000; SMITH; CARSON, 1978). Assim como nos outros Latossolos, os menores valores de Si/Al foram observados nos horizontes Bw2 e Bw3. Consequentemente, pode-se deduzir que esse perfil não sofreu influência de materiais de origem externa, mas sim evoluiu mediante um processo de intemperismo de longa duração no metagabro.

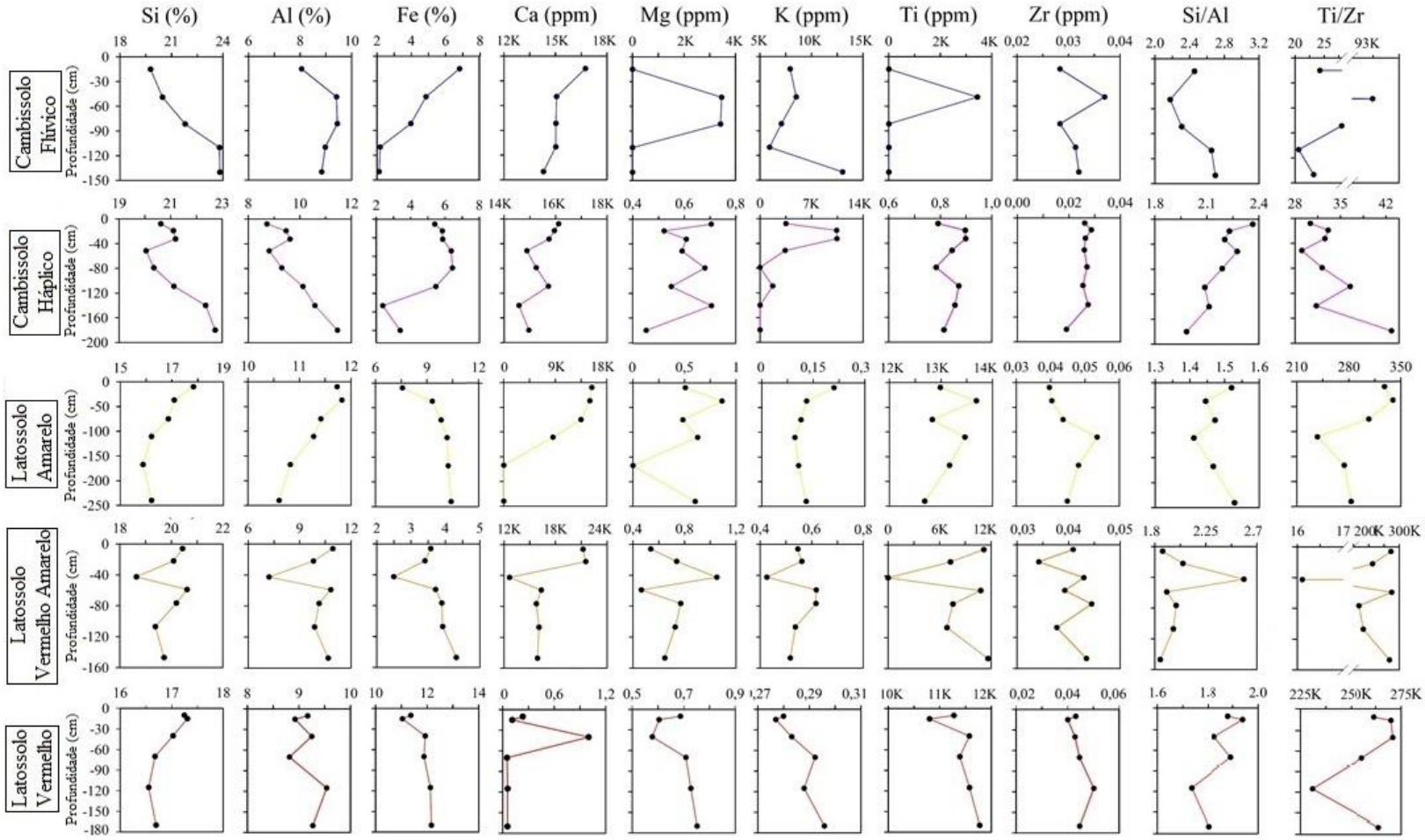

Fig. 3. Teores dos elementos químicos na terra fina seca ao ar obtidos via fluorescência de raios-X portatil para os perfis de solos estudados. K = 1000.

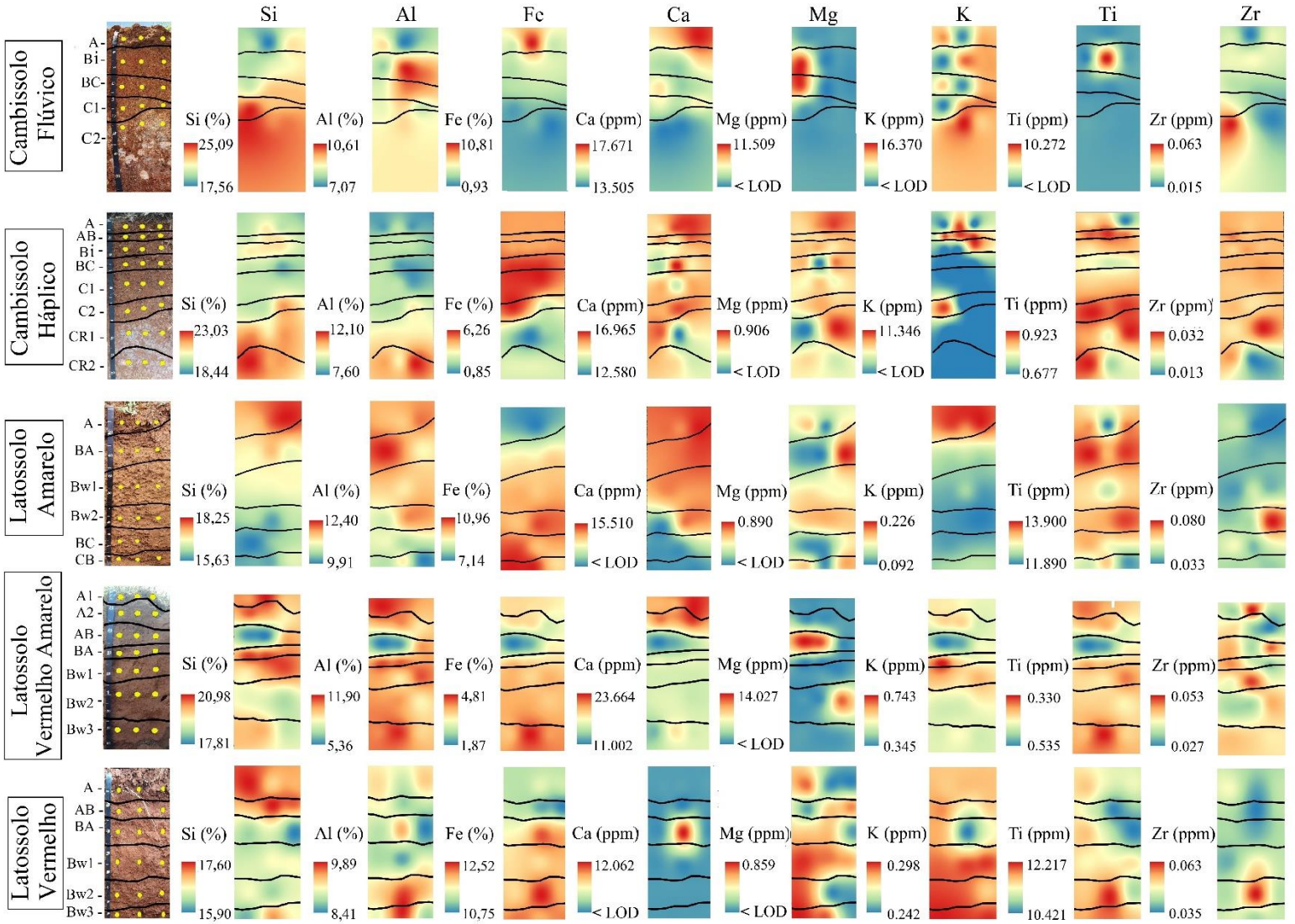
Si
Al
Fe
Ca
Mg
K
Ti
Zr
Cambissolo Flúvico
A
Bi
BC
C1
C2
Si (%) 25,09 17,56
Al (%) 10,61 7,07
Fe (%) 10,81 0,93
Ca (ppm) 17.671 13.505
Mg (ppm) 11.509 < LOD
K (ppm) 16.370 < LOD
Ti (ppm) 10.272 < LOD
Zr (ppm) 0.063 0.015
Cambissolo Háplico
A
AB
Bi
BC
C1
C2
CR1
CR2
Si (%) 23,03 18,44
Al (%) 12,10 7,60
Fe (%) 6,26 0,85
Ca (ppm) 16.965 12.580
Mg (ppm) 0.906 < LOD
K (ppm) 11.346 < LOD
Ti (ppm) 0.923 0.677
Zr (ppm) 0.032 0.013
Latossolo Amarelo
A
BA
Bw1
Bw2
BC
CB
Si (%) 18,25 15,63
Al (%) 12,40 9,91
Fe (%) 10,96 7,14
Ca (ppm) 15.510 < LOD
Mg (ppm) 0.890 < LOD
K (ppm) 0.226 0.092
Ti (ppm) 13.900 11.890
Zr (ppm) 0.080 0.033
Latossolo Vermelho Amarelo
A1
A2
AB
BA
Bw1
Bw2
Bw3
Si (%) 20,98 17,81
Al (%) 11,90 5,36
Fe (%) 4,81 1,87
Ca (ppm) 23.664 11.002
Mg (ppm) 14.027 < LOD
K (ppm) 0.743 0.345
Ti (ppm) 0.330 0.535
Zr (ppm) 0.053 0.027
Latossolo Vermelho
A
AB
BA
Bw1
Bw2
Bw3
Si (%) 17,60 15,90
Al (%) 9,89 8,41
Fe (%) 12,52 10,75
Ca (ppm) 12.062 < LOD
Mg (ppm) 0.859 < LOD
K (ppm) 0.298 0.242
Ti (ppm) 12.217 10.421
Zr (ppm) 0.063 0.035

Fig. 4. Distribuição espacial dos conteúdos elementares obtidos por pXRF nos perfis de solos. As linhas tracejadas são os limites dos horizontes identificados. Os pontos são os locais de amostras coletadas com intervalo de 15 cm em cada horizonte e LOD, limite de detecção.

3.3 Teor dos elementos via pXRF e mineralogia via DRX das frações areia, silte e argila

3.3.1 Cambissolos

Os maiores teores de Si na fração areia dos Cambissolos ocorrem devido a predominância do quartzo e pequenas quantidades de mica, feldspato e caulinita (Fig. 5 e 6). A resistência do quartzo e das micas ao intemperismo, em conjunto com a caulinita neoformada resulta nos teores de Si e Al na fração silte e principalmente no horizonte C menos intemperizado. Além disso o aparecimento de caulinita e gibbsita na fração silte pode estar associada à meteorização e liberação das mesmas de pseudomorfos de feldspato e mica, como consequencia da evolução da pedogênese (BUOL; WEED, 1991; SEQUEIRA BRAGA et al., 2002). O material de origem de CX, apresenta niveis arenosos ricos em feldspatos, que sob clima tropical podem se intemperizar em micas e esmectitas em condições mal drenadas, em caulinita, haloisita e gibbsita em condições de boa drenagem e fluxo intenso (KÄMPF et al., 2016). Isso explicaria a ausência do feldspato nas frações grosseiras desse solo e nos horizontes com maior teor de areia.

Os maiores teores de K na fração silte concordam com os picos mais intensos de mica em razão da sua presença na estrutura cristalina desse mineral. De acordo com Melo et al. (2001) em solos mais jovens o menor intemperismo dos minerais primários das frações grosseiras mantêm o K e o Mg em sua estrutura. Além da mica, o feldspato também é responsável pelos teores de K e Ca nas frações grosseiras, enquanto os teores de Ca e Mg na argila indicam sua adsorção.

Na fração argila a concentração de Si é menor, contrapondo-se as altas concentrações de Al, que está relacionada a presença reduzida de mica, e a predominância de gibbsita e caulinita em CY e CX respectivamente.

O maior teor de Fe na fração argila e na superfície de CY condiz com os picos mais intensos da hematita e goethita e com as crostas ferruginosas encontradas. Entretanto em direção a base do perfil de CX, nas frações argila e silte, os picos de goethita diminuem

consideravelmente e os de hematita não foram observados. A ausência de minerais portadores de ferro na fração areia reflete a pobreza do material de origem nessa parte do perfil de CX, que corresponde as maiores concentrações de caulinita e coloração esbranquiçada (Fig. 2). O rutilo herdado do material de origem concentra-se na fração silte enquanto o anatásio, neoformado encontra-se na fração argila dos horizontes mais intemperizados. O zircão é o principal mineral portador de Zr e tende a predominar nas frações mais grosseiras do solo, o mesmo não foi detectado pelo DRX (TABOADA et al., 2006). A diferença na mineralogia encontrada entre os horizontes dos Cambissolos reflete a a heteorogeneidade dos respectivos materiais de origem.

3.3.2 Latossolos

Os teores de Si concordam com os difratogramas, uma vez que o maior teor ocorre na fração areia, seguida da fração silte e o principal mineral encontrado é o quartzo (Fig 5 e 7). Ainda na fração areia, a gibbsita foi encontrada em LA, e minerais primários como a olivina, feldspato e mica em LVA, algo incomum tratando-se dessa classe de solo. Uma das razões para os maiores teores de Ca, K e Mg concentrarem-se nas frações grosseiras do solo pode estar relacionada à presença de minerais primários que não foram detectados nos difratrogramas e aos que ainda resistem ao intemperismo como em LVA.

A caulinita ocorre de forma residual na fração silte, e a predominância dos reflexos da gibbsita indica uma grande quantidade desse óxido sendo formado em detrimento da caulinita, principalmente em LA e LV, justificando os teores de Al nessa fração.

Na fração argila, os maiores teores de Al são atribuídos à predominância da gibbsita sobre a caulinita. O Fe, concentra-se na forma de goethita e hematita e a cor amarela de LA esta relacionada a maior presença de goethita, único óxido de ferro detectado pelo DRX (Fig. 7). Embora a cor vermelha da hematita seja predominante em LV, a presença da goethita foi constatada em todos os horizontes.

Os teores de Ti coincidem com o domínio do rutilo na fração silte e anatásio na fração argila. O zircão não foi detectado por mais que os maiores teores se encontrem na fração silte.

Os sedimentos resultantes do intemperismo das rochas durante o período quaternário não apresentaram tempo suficiente para a formação de Latossolos tão intensamente intemperizados. Sendo assim o LA parece ter se desenvolvido de sedimentos intemperizados

pré-existentes, que foram posteriormente retrabalhados pelas condições ambientais que ocorreram durante o período quaternário até o momento.

A análise mineralógica da fração areia e silte de LVA mostram significativas alterações entre seus horizontes. Observa-se picos mais intensos da mica, feldspato e quartzo na fração areia do horizonte A1 em relação ao A2. Isso é um indicativo de descontinuidade, uma vez que é esperado maior intensidade dos picos em profundidade quando comparado a superfície. Se o horizonte A2 e AB fossem desenvolvidos do mesmo material de origem, teriam que apresentar a mesma mineralogia, o que não foi observado, admitimos assim, outra descontinuidade. Os minerais presentes no horizonte BA, são os mesmos encontrados no horizonte A1, o que apoia a suposição de que eles tenham a mesma fonte de material de origem. A mineralogia dos horizontes Bw1 e Bw2 é semelhante, indicando que ambos se desenvolveram a partir do mesmo sedimento. A distinção entre os horizontes Bw1 e Bw2 em relação ao horizonte Bw3, indica a existência de outra descontinuidade nessa região do perfil do solo. KUZILLA (1995) pesquisando solos em Nebraska identificou a partir de 80 cm de profundidade um aumento na intensidade dos picos de montimorillonita, essa alteração em conjunto com o aumento na CTC da fração argila na mesma profundidade, representava descontinuidade nos sedimentos aluviais que deram origem a esses solos.

O mesmo raciocínio pode ser aplicado à fração silte, a qual evidencia as descontinuidades no perfil do LVA. É importante ressaltar que a origem dos sedimentos relacionados aos horizontes A1, A2 e BA sugere que eles foram diretamente intemperizados a partir da rocha, devido à presença da olivina, um mineral facilmente intemperizável. Por outro lado, os demais horizontes parecem ter se desenvolvido a partir de sedimentos que passaram por estágios prévios de intemperização. Essas observações sugerem que há múltiplas descontinuidades no LVA, indicadas pela mineralogia da fração areia e confirmadas na fração silte.

Nenhuma descontinuidade foi observada em LA e LV com base na análise mineralógica.

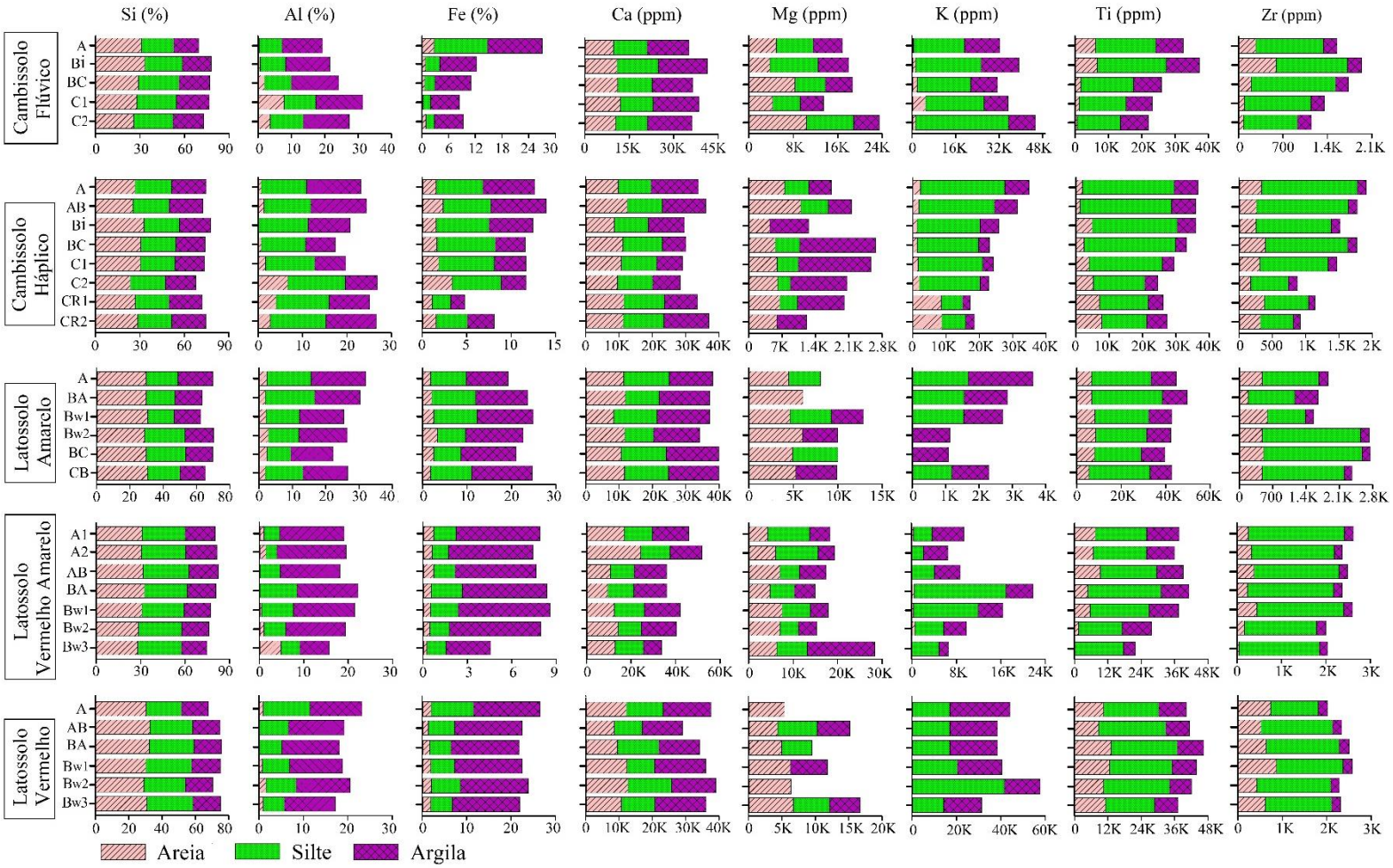

Fig. 5. Teores elementares via pXRF nas frações areia, silte e argila dos perfis de solo estudados. K = 1000.

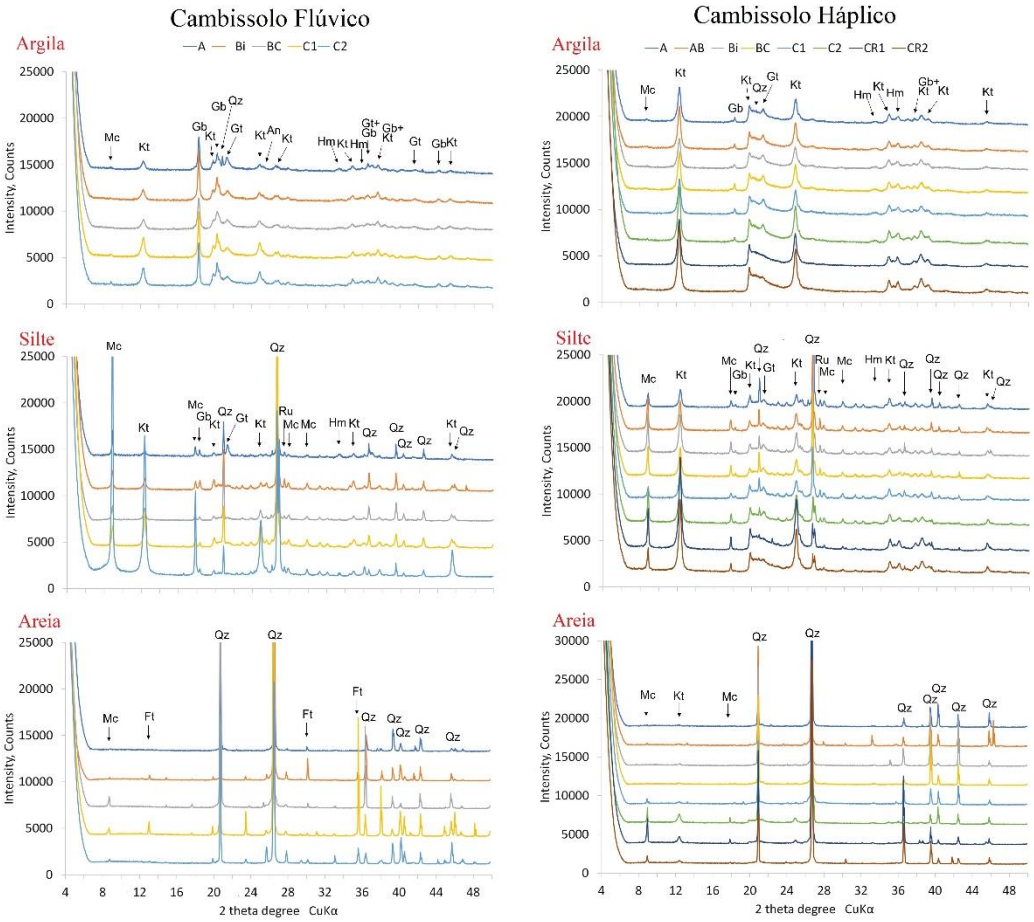

Fig. 6. Difratogramas das frações areia silte e argila referentes ao Cambissolo Flúvico e Cambissolo Háplico. Qz, quartzo; Kt, Caulinita; Gb, gibbsita; Hm, hematita; Gt, goethita; An, anatásio; Ru, rutilo; Mc, Mica; Ft, feldspato.

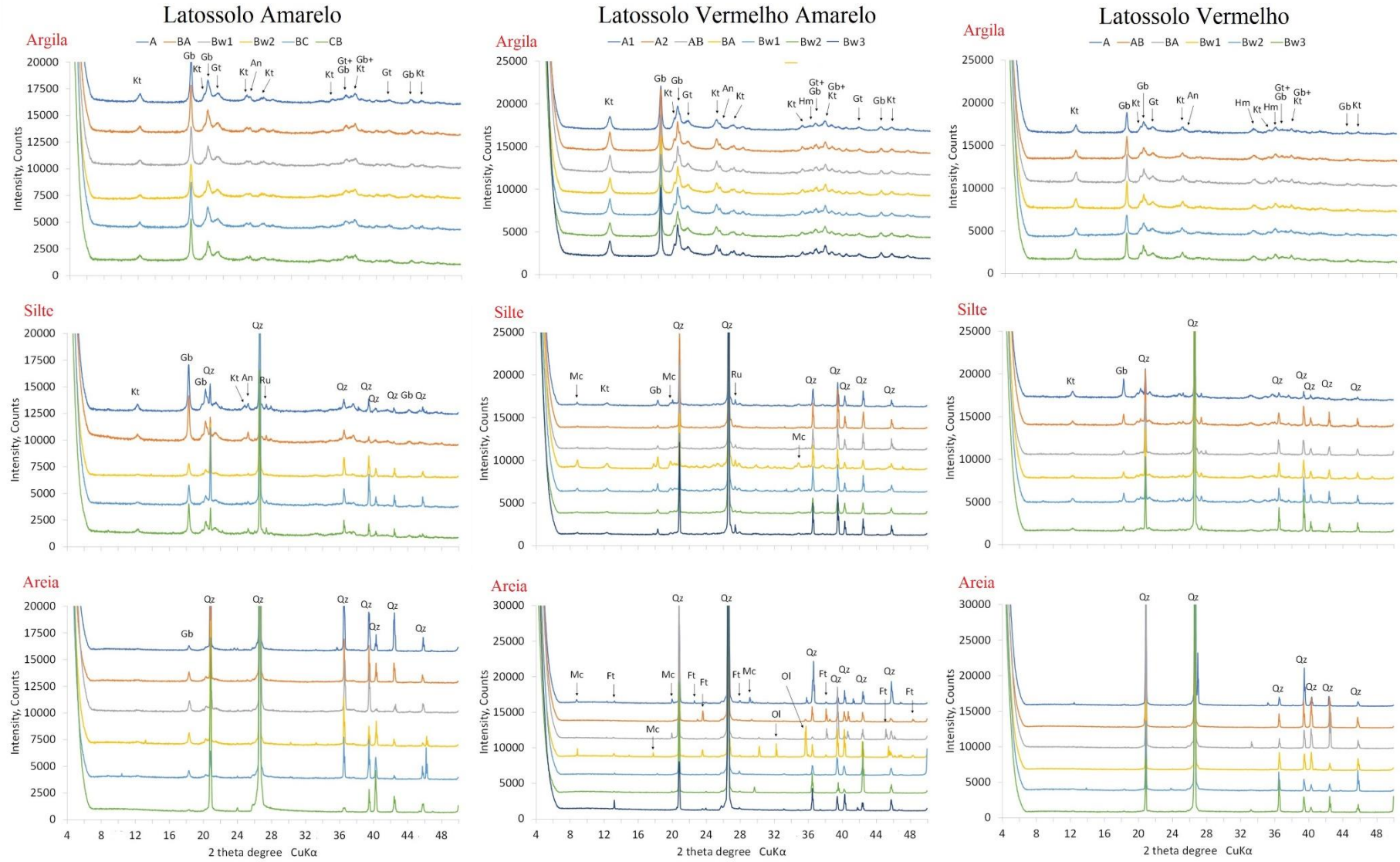
Latossolo Amarelo
Latossolo Vermelho Amarelo
Latossolo Vermelho
Argila
Silte
Areia
A
BA
Bw1
Bw2
BC
CB
A1
A2
AB
Bw3
Intensity, Counts
2 theta degree CuKα
Kt
Gb
Gt
An
Hm
Gt+
Gb+
Qz
Mc
Ru
Ft
Ol

Fig. 7. Difratogramas das frações argila, silte a areia referentes ao Latossolo Amarelo, Latossolo Vermelho Amarelo e Latossolo Vermelho. Qz, quartzo; Kt, Caulinita; Gb, gibbsita; Hm, hematita; Gt, goethita; An, anatásio; Ru, rutilo; Mc, Mica; Ft, feldspato; Ol, Olivina.**** A análise do horizonte Bw1 na fração silte do Latossolo Amarelo não foi realizada devido à escassez de amostra disponível.

3.4. Caracterização do solo via Vis-NIR

3.4.1 Cambissolos

Os espectros obtidos via Vis-NIR nas duas profundidades exibem forma e valores de refletância diferentes. Os valores de reflectância em superficie são maiores que em profundidade (Fig. 8).

A baixa absorção de CY para as os espectros nas duas profundidades é resultado dos maiores teores de areia, portanto maior concentração de quartzo, que apresenta alta reflectância (Fig. 8) (DEMATTÊ et al., 2002). A diminuição da MOS no espectro de 40 – 60 cm de profundidade intensifica a caracteristica de absorção dos óxidos de ferro entre os comprimentos de onda 750 e 1000 nm (GALVÃO; VITORELLO, 1998). Segundo Demattê et al. (2003) a diminuição no teor de MOS tem uma influência maior na absorção em solos com maior teor de areia, como é evidenciado em CY. A presença da goethita pode ser confirmada pela característica de absorção acentuada em 410 e 480 nm, bem como pela suave concavidade entre 600 e 750 nm. As características de absorção referentes aos óxidos de ferro são encontradas no intervalo de comprimento de onda entre 400 e 1000 nm, por outro lado, a presença de matéria orgânica impacta a absorção ao longo de todo o espectro (VISCARRA ROSSEL et al., 2011). As feições de absorção situadas em 1400 e 1900 nm deve-se à vibração molecular da água, em 2200 nm é atribuída a vibração da hidroxíla e alumínio (caulinita), enquanto a feição em 2265 e 2350nm refere-se a gibbsita e minerais 2:1 respectivamente (DALMOLIN et al., 2005; FORMAGGIO et al., 1996; MATHIAN et al., 2018). A característica de absorção menos pronunciada da caulinita revela seu baixo teor no solo, enquanto a gibbsita é o mineral predominante na fração argila.

Em CX, observa-se que o maior teor de argila resulta em uma diminuição na reflexão nos espectros nas duas profundidades (Fig. 8). Além disso, a presença de um maior teor de argila contribui para uma concavidade acentuada em torno de 917 nm, nas duas curvas

espectrais. Destaca-se que a goethita é predominante em CX, e uma de suas características é deslocar a concavidade do espectro entre 750 e 1000 nm para a direita, conforme mencionado por Madeira Neto (2000) e Scheinost e Schwertmann (1998). A absorção mais intensa nos comprimentos de onda de 1400 e 1900 nm indica uma maior presença de minerais 2:1 nesse solo, corroborada pela presença de mica (Fig. 8) (CLARK et al.,1990). Já a absorção em 2200 nm revela um degrau à esquerda, evidenciando o predomínio da caulinita nesse perfil.

3.4.2 Latossolos

O LA apresenta as maiores reflexões entre os Latossolos para as duas profundidades analisadas (Fig. 8). As feições relacionadas aos óxidos de Fe em torno de 750 e 1000 nm também são mais acentuadas em profundidade, além disso, as características de absorção da goethita e gibbsita são evidentes, indicando que esses óxidos predominam nesse solo.

As curvas espectrais do LVA demonstram um padrão semelhante às do LA. A maior absorção ao longo do espectro de LVA é atribuída à presença de minerais como hematita e olivina (Fig. 7), os quais apresentam maior capacidade de absorção. No entanto, é a goethita que prevalece no LVA devido às suas características espectrais bem marcadas. A presença de mica também contribui para uma absorção mais intensa nos comprimentos de onda de 1400 e 1900 nm, adicionalmente a gibbsita predomina sobre a caulinita.

Devido ao material de origem, o LV apresenta maior proporção de minerais opacos e maior teor de óxidos de Fe que combinados a sua textura argilosa conferem sua menor reflectância. Como o teor de argila e ferro entre as duas profundidades são bem próximos, as curvas também não são distantes uma da outra, como observado nos outros perfis. As bandas de absorção menos acentuadas em 1.400 e 1.900 nm ocorre devido a baixa concentração de caulinita, uma vez que esse solo não apresenta minerais 2:1 (Fig. 7). O domínio da gibbsita em relação a caulinita ocorre pelo destaque da sua feição de absorção. A menor reflexão, a concavidade mais larga entre 400 e 550 nm e a ausência da característica de absorção entre 410 e 480 nm, indicam que em LV a hematita é o óxido de Fe dominante.

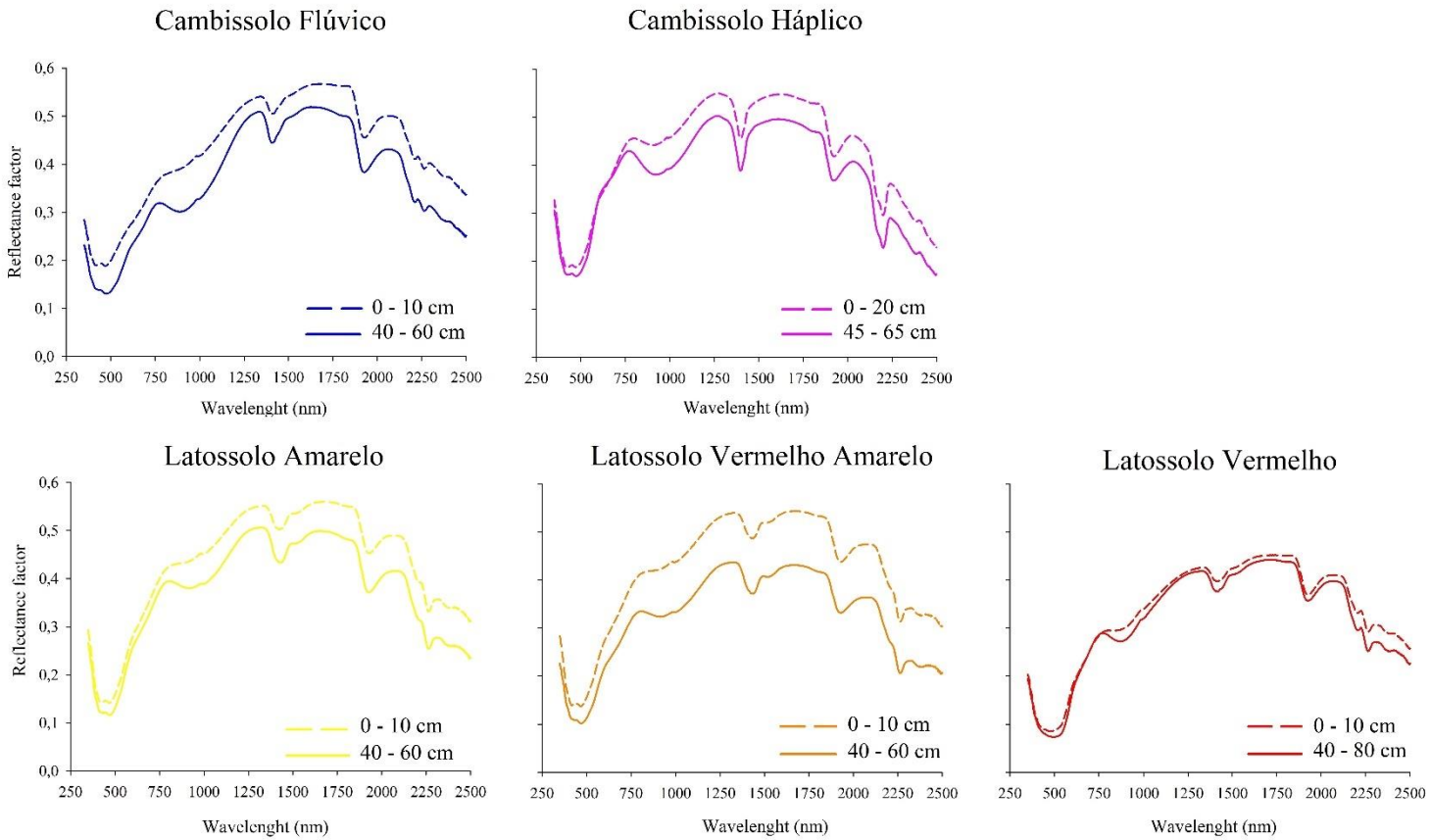

Fig. 9. Espectros obtidos por espectroscopia Vis-NIR em duas profundidades nos perfis de solos estudados.

4. Conclusões

Os resultados obtidos demonstram claramente que o material de origem exerceu uma influência significativa nos atributos químicos, físicos e mineralógicos dos solo estudados. Os dados elementares obtidos pelo espectrômetro de fluorescência de raios-X portátil, revelaram diferenças em termos de distribuição espacial e em profundidade dentro de cada perfil de solo.

As relações Ti/Zr, Si/Al e a análise mineralógica das frações areia e silte foram capazes de identificar as descontinuidades presentes no material de origem de LVA, bem como a natureza flúvica de CY e os diferentes níveis que compõem os lamitos de CX. A espectroscopia de reflectância difusa no infravermelho próximo exibiu a textura argilosa de CX, LA e LV, enquanto os solos CY e LVA apresentaram maior teor de areia. Adicionalmente confirmou-se o predomínio de hematita e gibbsita em LV, de goethita e gibbsita em LA, CY e LVA, e de goethita e caulinita em CX, esses resultados estão em concordância com as informações obtidas pela análise de difração de raios-X.

A combinação dos métodos resultou em uma avaliação abrangente e precisa, fornecendo uma análise completa da influência do material de origem nas características dos solos estudados. A relação Ti/Zr obtida pela fluorescência de raios-X portátil em conjunto com a mineralogia identificaram as descontinuidades no material de origem, presente apenas em LVA.

REFERÊNCIAS

ALVAREZ, V.H.; FONSECA, D.M. Definição de doses de fósforo para a determinação da capacidade máxima de adsorção de fosfato e para ensaios de casa de vegetação. **Revista Brasileira de Ciência do Solo**, v. 14, p. 49–55, 1990.

ALVAREZ, V.V.H. et al. Interpretaçãoo dos resultados das análises de solos. In: RIBEIRO, A.C., GUIMARÃES, P.T. G., ALVAREZ, V.H. **Recomendações Para o Uso de Corretivos e Fertilizantes Em Minas Gerais - 5◦ Aproximação**. Viçosa, p 25–32, 1999.

ANDA, M.; CHITTLEBOROUGH, D.J.; FITZPATRICK, R.W. Assessing parent material uniformity of a red and black soil complex in the landscapes. **Catena**, v. 78, p. 142–153. 2009. https://doi.org/10.1016/j.catena.2009.03.011

ANDRADE, R. et al. Micronutrients prediction via pXRF spectrometry in Brazil: Influence of weathering degree. **Geoderma Regiona**l, v. 27, e00431, 2021.

AHR, S.W.; NORDT, L.C.; DRIESE, S.G. Assessing lithologic discontinuities and parent material uniformity within the Texas sandy mantle and implications for archaeological burial and preservation potential in upland settings. **Quaternary Research**, v. 78, p. 60–71, 2012.

BENEDET, L. et al. Soil texture prediction using portable X-ray fluorescence spectrometry and visible near-infrared diffuse reflectance spectroscopy. **Geoderma**, v. 376, 114553, 2020.

BENEDET, L. et al. Variation of properties of two contrasting Oxisols enhanced by pXRF and Vis-NIR. **Journal of South American Earth Sciences**, v. 115, 103748, 2022.

BRINDLEY, G.W.; BROWN, G. **Crystal structures of clay minerals and their X-ray identification**. London: Mineralogical Society of Great Britain and Ireland, 1980, p. 495.

BUDAK, M.; GUNAL, H. Visible and Near Infrared Spectroscopy Techniques for Determination of Some Physical and Chemical Properties in Kazova Watershed. **Advances in Environmental Biology**, v. 10, p. 61-72, 2016.

BUOL, S.W.; WEED, S.B. Saprolite-soil transformations in the Piedmont and Mountains of North Carolina. **Geoderma**, v. 51, p. 15–28, 1991.

CAPORALE, A.G. et al. Monitoring metal pollution in soils using portable-XRF and conventional laboratory-based techniques: Evaluation of the performance and limitations according to metal properties and sources. **Science of the Total Environment**, v. 643, p. 516–526, 2018.

CÉSAR DE MELLO, D. et al. Soil magnetic susceptibility and its relationship with naturally occurring processes and soil attributes in pedosphere, in a tropical environment. **Geoderma,** v. 372, 114364, 2020.

CHANG, G.W.; LAIRD, D.A.; HURBURGH, G.R Influence of soil moisture on near-infrared reflectance spectroscopic measurement of soil properties. **Soil Science**, v. 170, p. 244 – 255, 2005.

CLARK, R.N. et al. High spectral resolution reflectance spectroscopy of minerals. **Journal of Geophysical Research**, v. 95, n. B8, 1990.

CONRAD, O. et al. System for automated geoscientific analyses (SAGA) v. 2.1.4. Geosci. Model Dev. 8, 1991–2007.

CORINGA, E.A.O.; COUTO, E.G.; TORRADO, P.V. Geoquímica de solos do pantanal norte, Mato Grosso. **Revista Brasileira de Ciência do Solo**, v. 38, p. 1784–1793, 2014.

CORNELIS, J.T.; DELVAUX, B. Soil processes drive the biological silicon feedback loop. **Functional Ecology**, v. 30, p. 1298-1310, 2016.

CORNU, S. et al. Evidence of titanium mobility in soil profiles, Manaus, central Amazonia. **Geoderma**, v. 91, p. 281–295, 1999.

DALMOLIN, R. S. D. et al. Relação entre os constituintes do solo e seu comportamento espectral. **Ciência Rural**, v. 35, p. 481–489, 2005.

DANTAS, A.A.A.; CARVALHO, L.G.; FERREIRA, E. Classificação e tendências climáticas em Lavras, MG. **Ciência e Agrotecnologia**, v. 31, p. 1862–1866, 2007.

DEMATTÊ, J.A.M. Characterization and discrimination of soils by their reflected electromagnetic energy. **Pesquisa Agropecuária Brasileira**, v. 37, p. 1445–1458, 2002.

DEMATTÊ, J.A.M.; EPIPHANIO, J.C.N.; FORMAGGIO, A.R. Influência da matéria orgânica e de formas de ferro na reflectância de solos tropicais. **Bragantia**, v. 62, p. 451–64, 2003.

DEMATTÊ, J.A.M. et al. Espectroscopia VIS-NIR-SWIR na avaliação de solos ao longo de uma topossequência em Piracicaba (SP). **Revista Ciência Agronômica**, v. 46, p. 679–688, 2015.

DEMATTÊ, J.A.M. et al. Chemometric soil analysis on the determination of specific bands for the detection of magnesium and potassium by spectroscopy. **Geoderma**, v. 288, p. 8–22, 2017.

FANG, Q. et al. Visible and Near-Infrared Reflectance Spectroscopy for Investigating Soil Mineralogy: A Review. **Journal of Spectroscopy**, v. 2018, p. 1–14, 2018.

FERNANDES, R.B.A. et al. Quantificação de óxidos de ferro de latossolos brasileiros por espectroscopia de refletância difusa. **Revista Brasileira de Ciência do Solo**, v. 28, p. 245–257, 2004.

FORMAGGIO, A.R. et al. Comportamento espectral (450-2.450 nm) DE SOLOS TROPICAIS DE SÃO PAULO. **Revista Brasileira de Ciência do Solo**, v. 20, p. 467–474, 1996.

GALVÃO, L.S.; VITORELLO, I. Role of organic matter in obliterating the effects of iron on spectral reflectance and colour of Brazilian tropical soils. **International Journal of Remote Sensing**, v. 19, p.1969–1979, 1998.

GEE, G.W.; BAUDER, J.W. Particle-size Analysis. In: Methods of soil analysis: Part 1 - Physical and mineralogical methods. **Soil Science Society of America**, American Society of Agronomy, v. 5, p. 383–411, 1986.

GOZUKARA, G.; ZHANG, Y.; HARTEMINK, A.E. Using vis-NIR and pXRF data to distinguish soil parent materials – An example using 136 pedons from Wisconsin, USA. **Geoderma**, v. 396, 115091, 2021.

GRAUER-GRAY, J.; HARTEMINK, A.E. Raster sampling of soil profiles. **Geoderma**, v. 318, n. January, p. 99–108, 2018.

HOBLEY, E.U.; PRATER, I. Estimating soil texture from vis–NIR spectra. **European Journal of Soil Science**, v. 70, p. 83–95, 2019.

JI, W.; VISCARRA ROSSEL, R.A.; SHI, Z. Improved estimates of organic carbon using proximally sensed vis-NIR spectra corrected by piecewise direct standardization. **European Journal of Soil Science**, v. 66, p. 670–678, 2015.

MAYNARD, J.B., 1992. Chemistry of modern soils as a guide to interpreting Precambrian paleosols. **Journal of Geology**, v.100, p. 279–289, 1992.

NALINI JÚNIOR, H.A.N. et al. **Geologia da Folha Campo Belo** CPRM-SERVIÇO GEOLÓGICO DO BRASIL. p. 1-148, 2007.

KÄMPF, N.; CURI, N. Formação e evolução do solo (pedogênese), in: Ker, J.C. et. al. **Pedologia - Fundamentos**. SBCS, Viçosa, p. 208–291, 2012.

KÄMPF, N.; CURI, N.; MARQUES, J.J. Intemperismo e ocorrência de minerais no ambiente do solo, in: Melo, V.F.; Alleoni, L.R.F. **Química e mineralogia do solo**. Viçosa, p. 333–380, 2016.

KER, J.C. Latossolos Do Brasil: Uma Revisão. **Geonomos**, v. 5, n. 1, p. 17–40, 1997.

KURTZ, A.C. et al. Refractory element mobility in volcanic soils. **Geology**, v. 28, p. 683–686, 2000.

KUZILA, M.S. Identification of multiple loess units within modern soils of Clay County, Nebraska. **Geoderma**, v. 65, p. 45–57. 1995.

LAGES, S.; OLIVEIRA. C.V.; BRITO, V. Análise pedológica aplicada à identificação de descontinuidades estratigráficas: vertentes do Córrego do Quebra: depressão de Gouveia. MG. **Geografias**, v. 4, p. 77-86, 2008.

MADEIRA NETTO, J. DA S.; BAPTISTA, G. M. DE M. **Reflectância espectral de solos**. Planaltina, DF: Embrapa Cerrados, 2000.

MANCINI, M. et al. Digital morphometrics and genesis of soils with buried horizons and lithological discontinuities in southeastern Brazil. **Geoderma Regional**, v. 32, e00612, 2023.

MANCINI, M. et al. Parent material distribution mapping from tropical soils data via machine learning and portable X-ray fluorescence (pXRF) spectrometry in Brazil. **Geoderma**, v. 354, 113885, 2019.

MATHIAN, M. et al. Identifying the phyllosilicate minerals of hypogene ore deposits in lateritic saprolites using the near-IR spectroscopy second derivative methodology. **Journal of Geochemical Exploration**, v. 186, p. 298–314, 2018.

MCLEAN, E. O. et al. Aluminium in soils: I. Extraction methods and magnitud clays in Ohio soils. **Soil Science Society of America**, v. 22, p. 382–387, 1958.

MEHLICH, A**. Determination of P, Ca, Mg, K, Na and NH4 by North Carolina Soil Testing Laboratories**. Raleigh, University of North Carolina. 1953, p. 4.

MELO, V. F. et al. Chemical and Mineralogical Properties of Kaolinite-Rich Brazilian Soils. **Soil Science Society of America Journal**, v. 65, p. 1324–1333, 2001.

MONIZ, A. C.; BUOL, S. W.; WEED, S. B. Formation of an Oxisol-Ultisol Transition in São Paulo, Brazil: II. Lateral Dynamics of Chemical Weathering. **Soil Science Society of America Journal**, v. 46, p. 1234–1239, 1982.

NOVAES FILHO, J. P. et al. Indicativos de descontinuidade litológica de regolitos derivados de granitos em uma microbacia sob floresta Amazônica, em Juruena - MT. **Revista Brasileira de Ciência do Solo**, v. 36, p. 317–324, 2012.

PEREIRA, G. E. et al. VIS-NIR spectral reflectance for discretization of soils with high sand content. **Semina:Ciências Agrarias**, v. 40, p. 99–112, 2019.

POTTS, P. J. et al. Effects of weathering on in situ portable X-ray fluorescence analyses of geological outcrops: Dolerite and rhyolite outcrops from the Preseli Mountains, South Wales**. X-Ray Spectrometry**, 2006.

PREZOTTI, L. C.; GUARÇONI M, A. **Guia de interpretação de análise de Solo E Foliar**, 2013.

QUEMÉNEUR, J.J.G. et al. **Geologia da Folha Lavras. Projeto Sul de Minas**, Etapa I. COMIG, UFMG, UFRJ, v. Capítulo 7, p. 259–319, 2002.

RONQUIM, C. C. **Conceitos de fertilidade do solo e manejo adequado para as regiões tropicais**. Embrapa Monitoramento por Satélite, Campinas, 2010, p. 26.

SANTOS, H.G. et al. **Sistema brasileiro de classificação de solos, 5th, revista e ampliada ed. Embrapa Solos, Brasília**. 2018, p. 356.

SCHEINOST, A.C.; CHAVERNAS, A.; BARRÓN, V. et al. Use and Limitations of Second-Derivative Diffuse Reflectance Spectroscopy in the Visible to Near-Infrared Range to Identify and Quantify Fe Oxide Minerals in Soils. **Clays Clay Miner**, v. 46, p. 528–536, 1998.

SEQUEIRA BRAGA, M.A.; PAQUET, H.; BEGONHA, A. Weathering of granites in a temperate climate (NW Portugal): Granitic saprolites and arenization. **Catena**, v. 49, p. 41–56, 2002.

SHARMA, A. et al. Geoderma Characterizing soils via portable X-ray fl uorescence spectrometer : 4 . Cation exchange capacity (CEC). **Geoderma**, v. 239–240, p. 130–134, 2015.

SHOEMAKER, H.E.; MCLEAN, E.O. & PRATT, P.F. Buffer methods for determining lime requeriment of soils with appreciable amounts of extractable aluminium. **Soil Science Society of America Journal**, v. 25, p. 274-277, 1961.

SILVA, F. M. et al. Using proximal sensors to assess pedogenetic development of Inceptisols and Oxisols in Brazil. **Geoderma Regional**, v. 28, p. 1–10, 2022.

SILVA, S. H. G. et al. Soil weathering analysis using a portable X-ray fluorescence (PXRF) spectrometer in an Inceptisol from the Brazilian Cerrado. **Applied Clay Science**, v. 162, p. 27–37, 2018.

SMITH, I.C., CARSON, B.L., 1978. **Trace Metals in the Environment**, vol. 3: Zirconium. Ann Arbor Science, MI, 1978, p. 405.

STOCKMANN, U. et al. Utilizing portable X-ray fluorescence spectrometry for in-field investigation of pedogenesis. **Catena**, v. 139, p. 220–231, 2016.

SOUZA, A. et al., 2021. A sensors-based profile heterogeneity index for soil characterization. **Catena**, v. 207, 2021.

SUN, F. et al. Enhanced soil profile visualization using portable X-ray fluorescence (PXRF) spectrometry. **Geoderma**, v. 358, 2020.

TABOADA, T. et al. Particle-size fractionation of titanium and zirconium during weathering and pedogenesis of granitic rocks in NW Spain. **Geoderma**, v. 131, n. 1–2, p. 218–236, 2006.

TEIXEIRA, A. F. DOS S. et al. Proximal sensor data fusion for tropical soil property prediction: Soil fertility properties. **Journal of South American Earth Sciences**, v. 116, 2022.

TERRA, F.S.; DEMATTÊ, J.A.M.; VISCARRA ROSSEL, R.A. Proximal spectral sensing in pedological assessments: vis–NIR spectra for soil classification based on weathering and pedogenesis. **Geoderma**, v. 318, p. 123–136, 2018.

VISCARRA ROSSEL, R.A. et al. On the soil information content of visible-near infrared reflectance spectra. **European Journal of Soil Science**, v. 62, p. 442–453, 2011.

VISCARRA ROSSEL, R.A.; HICKS, W.S. Soil organic carbon and its fractions estimated by visible-near infrared transfer functions**. European Journal of Soil Science**, v. 66, p. 438–450, 2015.

WALKLEY, A.; BLACK, I. A. An examination of the Degtjareff method for determining soil organic matter and a proposed modification of the chromic acid titration method. **Soil Science,** p. 29–38, 1934.

XU, D. et al. Using Portable Spectrometers. **Environmental Pollution**, v. 263, p. 114649, 2020.

ZHU, Y.; WEINDORF, D.C.; ZHANG, W. Characterizing soils using a portable X-ray fluorescence spectrometer: 1. Soil textureämpf. **Geoderma**, v. 167–168, p. 167–177, 2011.